Relating Macroscopic Measures of Brain Activity to Fast Dynamic Neuronal Interactions

by

Dave Chawla, B.Sc.

Submitted for the degree of Doctor of Philosophy (Ph.D.)

Wellcome Department of Cognitive Neurology, Institute of Neurology, University College London, University of London, 12 Queen Square, London WC1N 3BG

Abstract

The aim of this thesis was to find a systematic relationship between neuronal synchrony and firing rates, that would enable us to make inferences about one given knowledge of the other. Functional neuroimaging techniques, such as functional magnetic resonance imaging (fMRI), are sensitive to changes in overall population synaptic activity, that can be interpreted in terms of rate coding for a particular stimulus or task. Characterising the relationship between synchrony and firing rates would facilitate inferences about fast neuronal interactions on the basis of macroscopic measures such as those obtained by fMRI. In this thesis, we used computer simulations of neuronal networks and fMRI in humans to investigate the relationship between mean synaptic activity and fast synchronous neuronal interactions. We found that the extent to which different neurons engage in fast dynamic interactions is largely dependent on the neuronal population firing rates and *vice versa. i.e.* as one metric changes (either activity or synchrony), so does the other. Additionally, as a result of the strong coupling between overall activity and neuronal synchrony, there is also a robust relationship between background activity and stimulus-evoked activity: Increased background activity increases the gain of the neurons, by decreasing effective membrane time constants, and enhancing stimulus-evoked population activity through the selection of fast synchronous dynamics. In concluding this thesis, we tested and confirmed, with fMRI in humans, that this mechanism may account for attentional modulation. *i.e.* the change in baseline neuronal firing rates associated with attention, in cell assemblies selectively responding to an attended sensory attribute, enhances responses elicited by presentation of that attribute.

This work is dedicated to my mother, my father and my sister, Gita, who always give unconditionally of their love and tolerance.

Acknowledgements

I am indebted to my primary supervisor, Professor Karl J. Friston, who has always shown unlimited patience and who has contributed invaluably to my scientific development.

I have much gratitude towards my secondary supervisor, Dr. Erik D. Lumer for his priceless scientific input to this thesis. I am grateful, as well, to Dr. Geraint Rees, Dr. Christian Buechel, Dr. Stewart Shipp, Dr. Mike Oram and Professor Mick Rugg for the valuable time and effort that they spent discussing certain parts of this thesis with me and, to Robin Edwards for programming the visual stimuli that were used in the fMRI experiments in chapter 2. It is also a pleasure to thank the Director of the Functional Imaging Laboratory and Dean of the Institute of Neurology, Professor Richard Frackowiak, who has always taken time out to read my work and make helpful suggestions. I also thank, the radiographers at the Wellcome Department of Cognitive Neurology for their assistance in my fMRI experiments and, all of the fMRI volunteers whose brain activations are shown in this thesis. Finally, I show my appreciation to my friends and colleagues at the F.I.L. and my close friends, 1996 - 1999, who all played a part in making the years working on this thesis pass so quickly.

The work in this thesis was supported by the Wellcome Trust.

Contents

Tables and Figures

Tables

Figures

"The whole universe as we perceive it is a system of relations: we know nothing that is, or can be, unrelated"

Lord Buddha

Introduction

This thesis will focus on the relationship between neuronal population dynamics and macroscopic measures of activity such as integrated mean synaptic activity. This is an important issue for two reasons. First, there is the possibility of relating macroscopic measures of neuronal activity, that are integrated over space and time, such as those provided by functional magnetic resonance imaging (fMRI) and positron emission tomography (PET), to more refined temporal dynamics that can be measured electrophysiologically. Second, it addresses the dialectic between rate and synchrony coding as the language that the brain uses to encode information. Rate coding states that the neuronal activity itself is the important feature while synchrony coding posits the precise relative timing of neuronal firing as the important metric. Finding a link between these two aspects of neuronal dynamics would place them both in a larger context and inform the interpretation of imaging studies.

P1 Functional Imaging

In recent years, fMRI and PET have been established as tools for localising brain activity in particular tasks using the blood oxygenation level dependent response (BOLD signal in functional Magnetic Resonance Imaging, fMRI) and regional cerebral blood flow (rCBF in Positron Emission Tomography, PET). fMRI relies on the fact that protons behave like compass needles when placed in a magnetic field. By manipulating this field, one can align the protons. By applying radio-frequency pulses to the protons, the protons are perturbed and emit detectable radio signals as they realign. As hydrogen nuclei are abundant in the human body, due to the fact that water makes up around three quarters of body tissue, high resolution images of human organs, including the brain, can be constructed: Under an intense magnetic field, hydrogen nuclei in water line up like bar magnets. They are then

perturbed with radio-frequency pulses. The energy of the hydrogen nuclei consequently increases, causing their state to change. Following the radio-pulses, the nuclei relax back to their original state and release the surplus energy in the form of electromagnetic radiation. These signals are picked up by receivers that surround the subject's head. If the nuclei are excited again before full recovery, a smaller signal is obtained. The rate of recovery, depends on the type of tissue containing the relevant water molecules. As this varies according to the type of tissue, *i.e.* grey or white matter and bone or plasma etc., an accurate image of the brain anatomy can be acquired.

The fMRI BOLD signal relies on the fact that deoxygenated haemoglobin is much more paramagnetic than oxygenated haemoglobin. During spurts of synaptic activity, there is a physiological uncoupling between flow and metabolism that may have a number of components at different time-scales. These components include transient increases in perfusion that outstrip the metabolic use of oxygen and, at longer time scales, anaerobic metabolism. Therefore although the blood flow to an active brain region increases, the oxygen demand does not parallel it. The surplus in oxygen that has been delivered returns to the circulation via the capillaries and draining veins in the form of oxygenated haemoglobin. The fMRI BOLD signal is attributed to the changes in local venous blood oxygenation. PET measures blood flow distribution or regional cerebral blood flow (rCBF) in the human brain. PET relies on the intravenous administration of radioactive water. Radioactive water is water that is made up of H_2 and ^{15}O rather than ^{16}O. The ^{15}O molecule is unstable and so decays via positron emmission. In this process, a proton converts to a neutron, resulting in unstable ^{15}O becoming stable ^{15}N. The emitted positrons then anihilate with electrons in brain tissue to form gamma waves which are detected by scintillation detectors that encircle the subjects head. In this way accurate images of cerebral blood distribution can be made. A more detailed account of the physics of PET and fMRI can be found in appendices 1 and 2.

Neuroimaging studies depend on the assumption that changes in BOLD or rCBF are representative of global synaptic activity levels. This is supported by optical imaging studies (Grinvald *et al*, 1984, 1986, Frostig *et al*, 1990). Changes in the light absorption or fluorescence of cortical molecules occur as a result of the transition states of intrinsic chromaphores like haemoglobin, cytochromes or NADH. Optical imaging techniques have been able to show that there is a local coupling between neuronal activity integrated over a few seconds, and the micro-circulation (haemodynamics). More recently, a combination of laser Doppler flow imaging and electrode recordings has shown that there is a coupling between regional cerebral blood flow (rCBF), as measured in PET, and local field potentials or global synaptic activity (Mathiesen *et al*, 1998). PET and fMRI measure overall levels of neuronal activity that are integrated over space and time. However, this tells us nothing about the precise timing of spikes, in relation to inputs from other neurons, as has been measured by electrophysiologists for many years. A robust relationship between global neuronal firing rate and neuronal interactions on a millisecond time scale would greatly inform the interpretation of neuroimaging data.

P2 Rate and Synchrony Coding

The two dominant theories of neural coding, the language that the brain uses to convey information, are rate and synchrony coding. There is much evidence in support of both. Rate coding proposes that brain cells code for stimuli through varying their firing rates. It has been shown repeatedly that neurons increase their firing rates subsequent to the stimulation of the cell's receptive field. For instance, primary visual cortex cells fire when objects are introduced to a particular portion of the visual field (Hubel and Wiesel, 1962, 1965, 1968, 1977). There are also specialised visual areas whose neurons increase their firing rate for particular colour combinations (visual area V4, located in the fusiform gyrus) (Daw, 1972, Zeki *et al*, 1983, 1985) and particular speeds and directions of motion (area V5, located in the posterior region of the inferior temporal gyrus and sulcus) (Rodman *et al*, 1987, Cheng *et al*, 1994). In addition, cells in the auditory cortex (located in the superior temporal sulcus) (Brugge, 1973, Kaas *et al*, 1998) have been shown to fire in response to particular auditory tones (Brugge, 1973, Rauschecker, 1998) and cells in the olfactory bulb, in response to particular odours (Meredith and Moulton, 1978).

Although certain neurons, or neuronal populations have been shown to rate code for particular attributes of the external world, how are these attributes linked to form a coherent internal real world representation? This is the problem of perceptual synthesis. For example, an object may be coloured red and be moving left at 10 °/s across a subjects visual field. There are many cells in different brain areas that increase their firing for colour and motion, but how does the subject perceive that the colour and motion belong to the same object? This is a simple example but serves to illustrate the point. The answer is likely to be through the functional integration among neurons or neuronal populations. Functional integration is a term used to describe the concept that neurons must somehow "speak to each other" in order to share information. Over the years, physiological investigations into functional integration have established neuronal synchrony as an important aspect of integrative or synthetic processing.

Synchrony coding states that it is not the neuronal firing rate that is important, but the precise temporal patterns of firing among different neurons. In the brain, synchronization may reflect the direct, reciprocal exchange of signals between two populations, whereby the activity in one population affects the activity in the second, such that the dynamics become entrained and mutually reinforcing, leading to synchronous discharges. In this way, the binding of different features of an object may be accomplished, in the temporal domain, through the transient synchronization of neuronal responses (Milner *et al*, 1974, von der Malsburg,1981, Sporns *et al*, 1991). Physiological evidence has, in general, been compatible with this theory (Engel *et al*, 1991). It has been shown that synchronization of oscillatory responses occurs within as well as between visual areas (Frien *et al*., 1994), for example between homologous areas of the left and right hemispheres and between remote areas in the same hemisphere at different levels of the visuo-motor pathway (Gray *et al*, 1990, Engel *et al*, 1991, Konig *et al*,

1995, Roelfsema *et al*, 1997). Synchronization in the visual cortex appears to depend on stimulus properties such as continuity, orientation similarity and motion coherency (Gray *et al*, 1989, Engel *et al*, 1990, Freiwald *et al*, 1995). Synchronous dynamics among cortical areas is also characteristic of other sensory modalities, suggesting that it represents a fundamental property of cortical interactions. For instance, Nicolelis *et al* (1995) have found synchronous dynamics across different levels of the rat somatosensory cortex. It seems as though synchrony coding may provide a mechanism that underlies perceptual binding and feature linking of particular objects or sounds.

In short, stimulus specific representations in the brain have been found to be coded through both changes in neuronal firing rate and neuronal synchronization. It would, therefore, be extremely important to find a link between these two metrics of neuronal dynamics, as this would enable us to make inferences about one given knowledge of the other. For example, PET and fMRI measure overall changes in firing rates and one can interpret neuroimaging results in terms of rate coding for a particular stimulus or task. However, one cannot make inferences about synchrony coding on the basis of neuroimaging results. Demonstrating a link between these two coding metrics would facilitate these inferences. In this thesis we use computer simulations of neuronal networks and functional imaging in humans to investigate the relationship between mean synaptic activity and fast synchronous interactions in simulated and real neuronal populations. These interactions are the basis of functional integration in the brain.

P3 Simulations of Neurobiology

This thesis is in two sections, each incorporating three chapters. The first chapter embodies a detailed characterization of neuronal dynamics at the single cell level. The next two chapters show through detailed simulations of neuronal populations, using neuronal dynamics as explained in chapter 1, what can be inferred about fast neuronal interactions on the basis of fMRI results.

In this section, we provide the reader with a brief overview of the use of computational modelling in neurobiology as well as an outline of the range of models that theoreticians have used in trying to answer neuroscientific questions. This overview is followed by the motivation for the models that we chose to use in the studies described in this thesis.

In using simulations to make inferences about how the brain works, a plethora of different model types have been used. On the one hand, many neuronal simulations have used small-scale detailed descriptions of single cells, such as cable theory models (Rall, 1995, Traub *et al*, 1991, also see Chapter 1 of this thesis) and multi-compartmental models (Koch *et al*, 1982, Rall and Segev, 1987, also see Chapter 1) to large scale networks of simplified neurons (Lumer *et al*, 1997, Aertsen *et al*, 1994, 1991) that exhibit various types of collective

dynamics. It should be noted that the use of cable theory or multi-compartmental neurons is extremely computationally expensive. As we wanted to study the behaviour of large cell ensemble dynamics, in the context of different activity levels, we have used the simpler, single-compartmental formulation, in two models, where each model involves two different and complementary levels of complexity in the cell dynamics. The first model was a purely phenomological model, of the cell membrane dynamics in which the action potential was implemented whenever the membrane potential exceeded the threshold for firing. Using this simple model allowed us to simulate relatively large populations of interconnected neurons. The second model that we used was also single-compartmental, but was slightly more computationally expensive than the first, incorporating some complex cell behaviour due to the implementation of two realistic ionic membrane channels that generated the cell action potential. Both of these models and the reasons behind our choice of models are described in Chapter 1.

To illustrate the differences in computational processing between our model and the much more complex models that have been used, it is useful to consider an example of the implementation of a multi-compartmental model. Traub *et al*, 1991, developed a 19-compartment model of a guinea pig CA3 pyramidal neuron, with each compartment containing 9 active ionic membrane channels. This model contained 171 ionic channels per neuron whereas the second 'more complex' model that we used, contained only sodium and potassium channels that consisted of only four channels. Our cells are therefore less computationally expensive by a ratio of around 43:1. The implications of this loss in biological detail is discussed at the end of Chapter 1. This study by Traub *et al*, 1991, examined how regulating the different types of membrane channels at different locations of the cell changed the cell conductance and thus conditions for firing. However, it would be computationally infeasible to address such issues at a population level with such complex cell dynamics. Instead, it is easier to simulate the phenomological behaviour of the cell dynamics from empirical observations, using relatively few or even no membrane channels, and simply manipulate the cell parameters so that the cell behaviour conforms to that observed empirically. Indeed, this was the approach adopted by Lumer *et al* (1997). Lumer *et al* (1997), simulated a model consisting of 65,000 spiking single-compartmental neurons to address issues of neuronal population synchrony. This model consisted of two biologically realistic topographically organized thalamocortical areas, where each cortical area was separated into three laminar structures, corresponding to the upper, middle and lower cortical layers; or supragranular layer, layer 4 and infragranular layer. This model also used extremely simple neuronal dynamics, identical to the first neuronal model described in the next chapter. This study was primarily concerned with the role of intra- and inter-area synaptic connections in maintaining fast synchronous population dynamics. By systematically modifying physiological and structural parameters in the model, specific network properties were found to play a major role in the generation of phase-locked activity. For example, fast synchronous dynamics could be sustained autonomously by lateral and interlaminar interactions within and among cortical areas. In addition, these oscillations were

propagated to the thalamus and amplified by corticothalamocortical loops including the thalamic reticular complex. Also, synchronous oscillations were differentially affected by lesioning forward and backward inter-area connections. We actually use the results from this study by Lumer *et al* to test one of the models that we use in this thesis (see p).

Other computational studies (e.g. Boven and Aertsen, 1990, Aertsen and Preiβl, 1991, Aertsen *et al*, 1994) have also addressed the behaviour of neuronal population dynamics as one changes population activity. These studies used simulated neurons that were represented as non-linear systems described by four state variables (equivalent to modelling four channel types). These studies are expanded on more fully in chapter 3, where they are discussed in the context of our studies.

P4 The Neurobiology of Vision

In part two of this thesis, we present an fMRI study in which we study brain activity integrated over many neurons (over roughly several mm^3 of cortex). This fMRI study examines motion-sensitive responses in the human 'visual motion area', V5, as a function of stimulus speed. Consistent with electrophysiological findings, we observed optimal responses at intermediate speeds of around 7 to 30 °/s. The experimental data presented in this chapter is consistent with electrophysiological results showing that V5 cells may code for speed through their activity levels. In the final chapter of this thesis, we test one a specific prediction of our modelling work (derived from part one of this thesis) in the visual cortex of the human brain using fMRI. In this section, it is therefore beneficial for the reader to give a general introduction to the primate visual system. However, it is important to note that this thesis is not in itself about the visual system; it is about the behaviour of neuronal populations. The reason that we test our computational hypothesis, derived from our simulations, on the visual system, is quite simply, because more is known about the functional and anatomical architecture of the visual cortex than about any other part of the brain.

P4.1 The Anatomy of the Macaque Visual System

This section P4.1, represents an extremely concise overview of the macaque monkey visual system. The reason that we discuss the monkey brain here is because the monkey is the closest model that we have to the brain of the human. It is important to note that, as much more is known about the monkey brain than that of the human, it is common for neuroscientists to make inferences about human cortical architecture and brain function from that of the monkey. This is as, it is obviously unethical to explore the human brain, in as much detail and using the same methods, as one does with other animals. Also, we must emphasise that this is a 'concise' version of the visual system. As more is known about the

visual system than any other part of the brain, a full version of the visual system, would probably take up many volumes and is obviously beyond the scope of this thesis. In what follows, we shall describe firstly, the route that visual information takes to reach the visual cortex. Secondly, we overview the functional specialisation of the visual cortex and finally discuss how the human visual system compares to that of the monkey.

Once that visual information enters the eye via the cornea and then the lens, the first stage of visual processing is at the retina. The retina contains three layers of processing. Firstly there are the rods and cones. In the centre, or fovea, of the retina, there are only cones which are sensitive to the colour/wavelength of light and not brightness. Cones are also present throughout the retina, but rods are more abundant in the periphery. Rods are sensitive to luminance or brightness and not wavelength. Rods are the cells that adapt to dim light and are so responsible for night vision. The rods and cones then feed into the next layer which contains horizontal, bipolar and amacrine cells. These cells then feed into the retinal ganglion cells. This is all that we shall say about the retina in this thesis, but for a fuller review of this stage of visual processing, see Hubel, 1988, p36 - 58. Visual information from the ganglion cells of the retina is then carried by the fibres of the optic nerve which then cross over at the optic chiasm, so that information from the nasal part of the retina is represented in the opposite hemisphere of the brain and information from the temporal part of the retina is represented in the same side of the brain. The right hemisphere contains a representation of the visual information from the temporal retina of the right eye and the nasal retina of the left eye. Therefore, each hemisphere of the brain processes the opposite or contralateral field of view.

Fig. P1

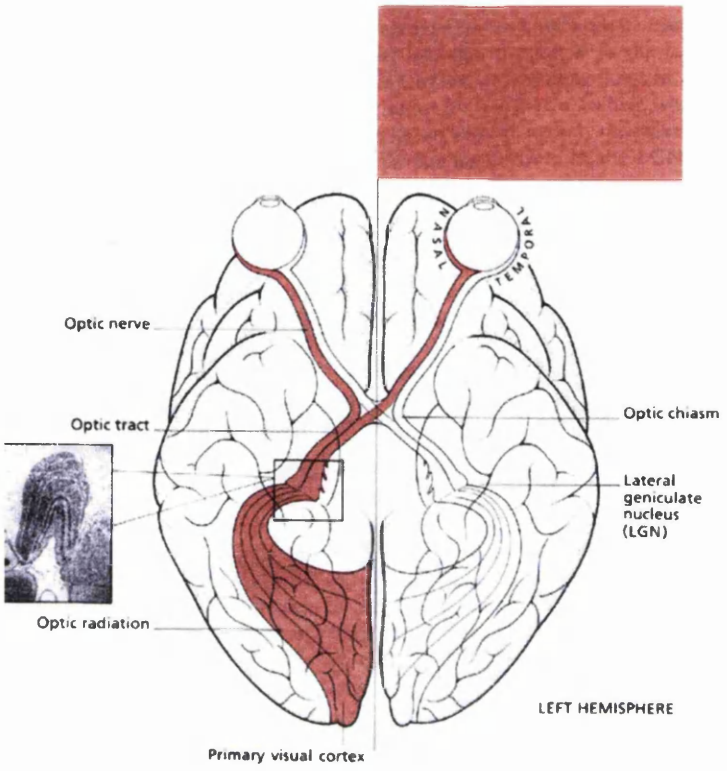

Fig. P1 The connections from the retina to the cerebral hemispheres. Inset to the left shows the multi-layered lateral geniculate nucleus (LGN). (taken from Zeki 1993, A Vision of the brain, p25)

A representation of the layout of the macaque visual system, visualized on a two dimensional sheet, is shown in Figure P2 (Van Essen and Gallant, 1994). The major subcortical areas are the two retinae, the lateral geniculate nucleus, the superior colliculus and the pulvinar complex. In the cortex, 32 distinct areas associated with vision have been identified (see Figure P5), which collectively occupy more than half of the total surface area of the macaque neocortex (Desimone and Ungerleider, 1989, Felleman and Van Essen, 1991). At the earliest stage of cortical processing are the two largest areas, V1 and V2, each of which occupies about 10% of the neocortex. These areas then feed into other cortical areas that are discussed below.

Fig. P2

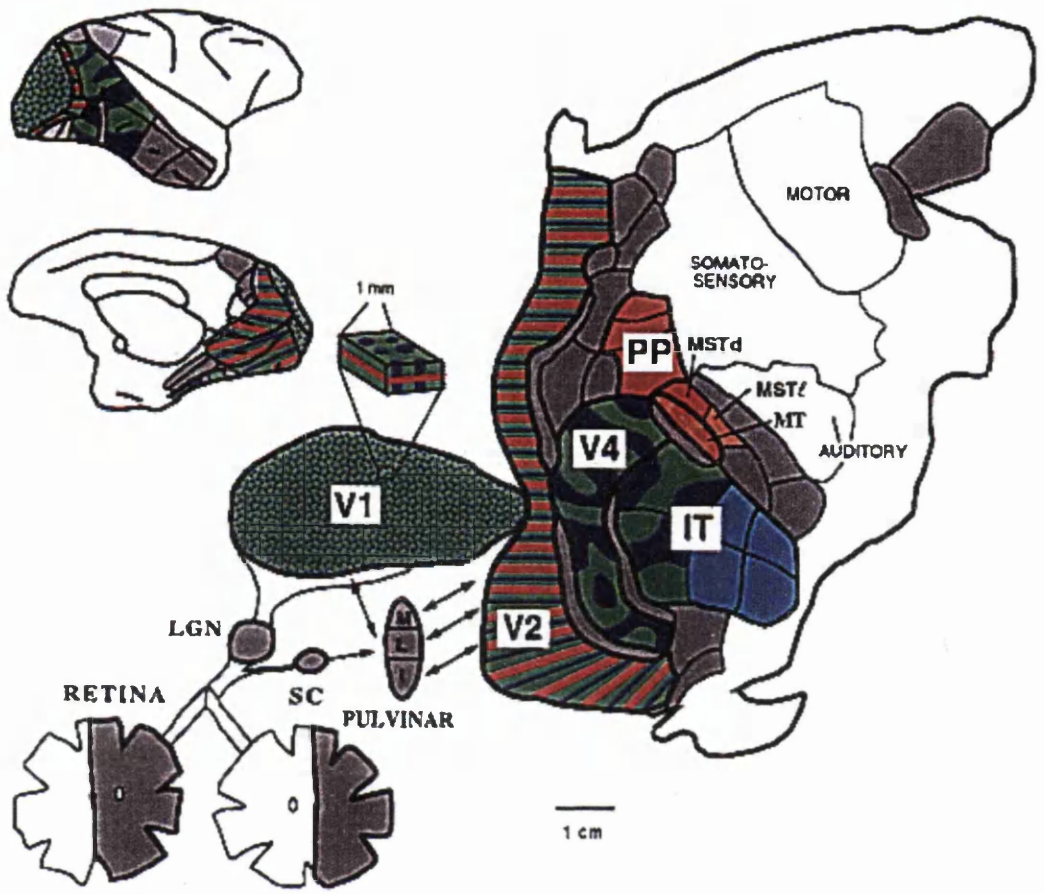

Fig. P2 Two-dimensional map of the cerebral cortex and major subcortical areas in the macaque monkey. The flattened cortical map encompasses the entire right hemisphere. (taken from Van Essen and Gallant, 1994)

After the optic chiasm, the visual pathway becomes the optic tract which relays signals to the LGN. The LGN has six layers which receive a topographic, point to point mapping from the retina. The inputs from the two eyes, to the LGN, are segregated with input from the ipsilateral (same side) eye terminating in layers 2,3, and 5 and that from the contralateral eye terminating in layers 1,4 and 6. The upper four layers of the LGN are the parvocellular (P) layers and the lower two are the magnocellular (M) layers. The layers of the LGN are stacked upon one another in precise registration in terms of retinal representation. Hence, if a cell at a

certain point in one layer corresponds to input from a certain point in the left retina, then a cell directly below in the next layer will receive input from the same point in the right retina. The two magno and parvocellular streams are thought to analyze colour and luminance autonomously and process these attributes in striate and extrastriate cortex. Wavelength information is relayed by the Pß ganglion cells of the retina to the upper four parvocellular layers of the lateral geniculate nucleus (LGN). The P-cells have comparatively small receptive fields, a slow conduction velocity and are wavelength selective. From the P layers of the LGN, the pathways are relayed to layers 2 and 3 of V1 (striate cortex) where they feed the blobs (*colour pathway*) and interblobs (*form from colour*). These two subdivisions are relayed to V4 (extrastriate cortex) through the thin and interstripe structures of V2 respectively. This stream's cells are not as finely tuned to luminance contrast and do not have the temporal resolution of the magnocellular pathway. Magnocellular cells have a high conduction velocity, large receptive fields and are sensitive to luminance contrast. This pathway is fed through the Pα ganglion cells of the retina which project to the lower two layers of the LGN and then to layer 4B of V1 and the thick stripes in V2. These M pathways can then be regarded as undergoing a second bifurcation, sending efferents to the motion sensitive area V5 (extrastriate cortex) (the *motion pathway*) and V3 (*dynamic form*).

V1 or primary visual cortex/striate cortex is situated in Brodman area 17 of the monkey and is parcellated into ocular dominance columns. These columns receive alternate input from the opposite eyes. V1 also has six layers and has blobs and inter blobs, where a blob is situated in the centre of an ocular dominance column (see Figure P3). Around 50% of the cells in the blobs are wavelength specific and thus receive input from the P pathway. The remaining cells in the blobs are broad band (responsive to light of all wavelengths without being orientation specific). The majority of cells in the inter-blobs are orientation specific without being wavelength coded and thus receive input from the M stream.

Fig. P3

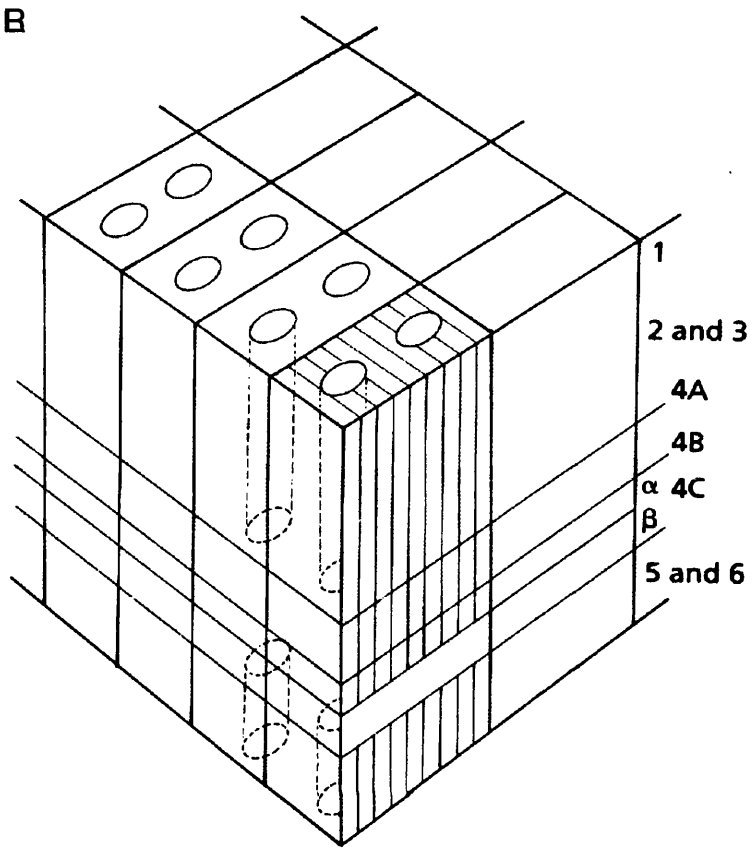

Fig. P3 Diagram of V1 or Primary Visual Cortex (taken form Zeki, 1993, A Vision of the Brain, p201)

It can be seen that V2, situated in Brodman area 18, is a critical point of divergence, representing the last stage of the visual hierarchy that retains a full complement of functionally selective cells (although there are also direct connections from V1 to V3, V4, and V5) (Note that as V5 in the monkey is situated in the middle temporal cortex, it is also widely known as area MT). The physiology of V2 (Hubel and Wiesel 1977, Zeki 1993) shows that V2 contains functionally heterogenous populations of cells, i.e. orientation selective, direction selective and wavelength selective units are all found within its subareas. The thick stripes of V2 receive their input from layer 4B of V1 where orientation and direction cells predominate and project to mediate motion or dynamic form processing through their connections to V5 and V3 respectively. Not surprisingly direction selective cells are concentrated in the thick stripes of V2. The thin stripes of V2 receive their input from the blobs of V1 where the majority of cells are not orientation selective but a lot are wavelength selective. Finally the interstripes receive input from the interblobs and show orientation but not wavelength

selective responses (Shipp and Zeki 1985; De Yoe and Van Essen 1985; Hubel and Livingstone 1987). In summary, thick stripes contain orientation and direction but not wavelength selective units. Thin stripes contain wavelength but not orientation and direction selective units and the interstripes contain orientation but not direction or wavelength selective units.

The explanation given above of the monkey visual cortex is relatively simplified. For example, cells in V4, 'the colour area' have also been shown to be responsive to motion, although they only select for speed and not direction of motion whereas cells in V5 discriminate for both colour and luminance defined visual motion although they are much more sensitive to luminance than colour defined stimulus borders (Cheng *et al*, 1994). Such complications are likely to arise from integration between the P and M visual processing pathways via reciprocal connections (Felleman and Van Essen, 1991).

P4.2 The 'What' and 'Where' pathways

The P and M pathways have been associated with the ventral and dorsal pathways. The ventral or P pathway is also known as the 'what' pathway. The reasons for this are consistent with the above functional characteristics of this visual stream. This stream consists predominantly of colour and orientation cells and as such is thought to code for form or 'what' an object is. Indeed, although V4 is known predominantly as the 'colour area' due to it's large number of colour responsive cells, V4 has also been shown to contain many cells that code for visual form (Schiller *et al* , 1991, Chelazzi *et al* , 1995). There is therefore some controversy as to whether V4 is really a colour or form area (Heywood *et al*, 1995, Cowey *et al*, 1995). In reality, of course it is likely that V4 processes both colour and form as it receives input from both colour and orientation sensitive cells in the blobs of V1 and the thin and inter stripes of V2. V4 actually proceeds to feed input into the inferior temporal area (IT) whose cells have been found to code for complex visual objects. IT cortex is the last visual processing area in the ventral 'what' stream and lesions to this area have been found to impair object recognition and discrimination (Desimone *et al*, 1984, Desimone and Ungerleider, 1989, Tanaka, 1996). The dorsal or M stream is also known as the 'where' pathway as it processes, primarily, visual motion. Area V5 or MT feeds into medial superior temporal area (MST) which has been shown to code for more complex motion than V5, and this area then feeds into the superior temporal polysensory area (STP/parietal cortex). Although, STP is known as the last processing area in the 'where' dorsal pathway, it also receives input from IT in the ventral pathway and is thus one of the few visually responsive areas where the dorsal and ventral pathways converge (Felleman and Van Essen, 1991). Indeed, STP has been found to consist of primarily three sets of cells: those that are responsive to the direction of visual motion (Bruce *et al*, 1981, Hikosaka, *et al*, 1988, Mistlin and Perret, 1990, Oram *et al*, 1993), those that are responsive to form, independently of motion, (Gross *et al*, 1972, Bruce *et al*, 1981, Wachsmuth *et al*, 1994) and those that are responsive to the combination of particular

forms with particular directions of motion (Oram and Perret, 1996). It is also of importance here, that although STP cells may be responsive to motion, unlike V5 cells, they are not sensitive to the speed of motion (Oram *et al*, 1993).

Fig. P4

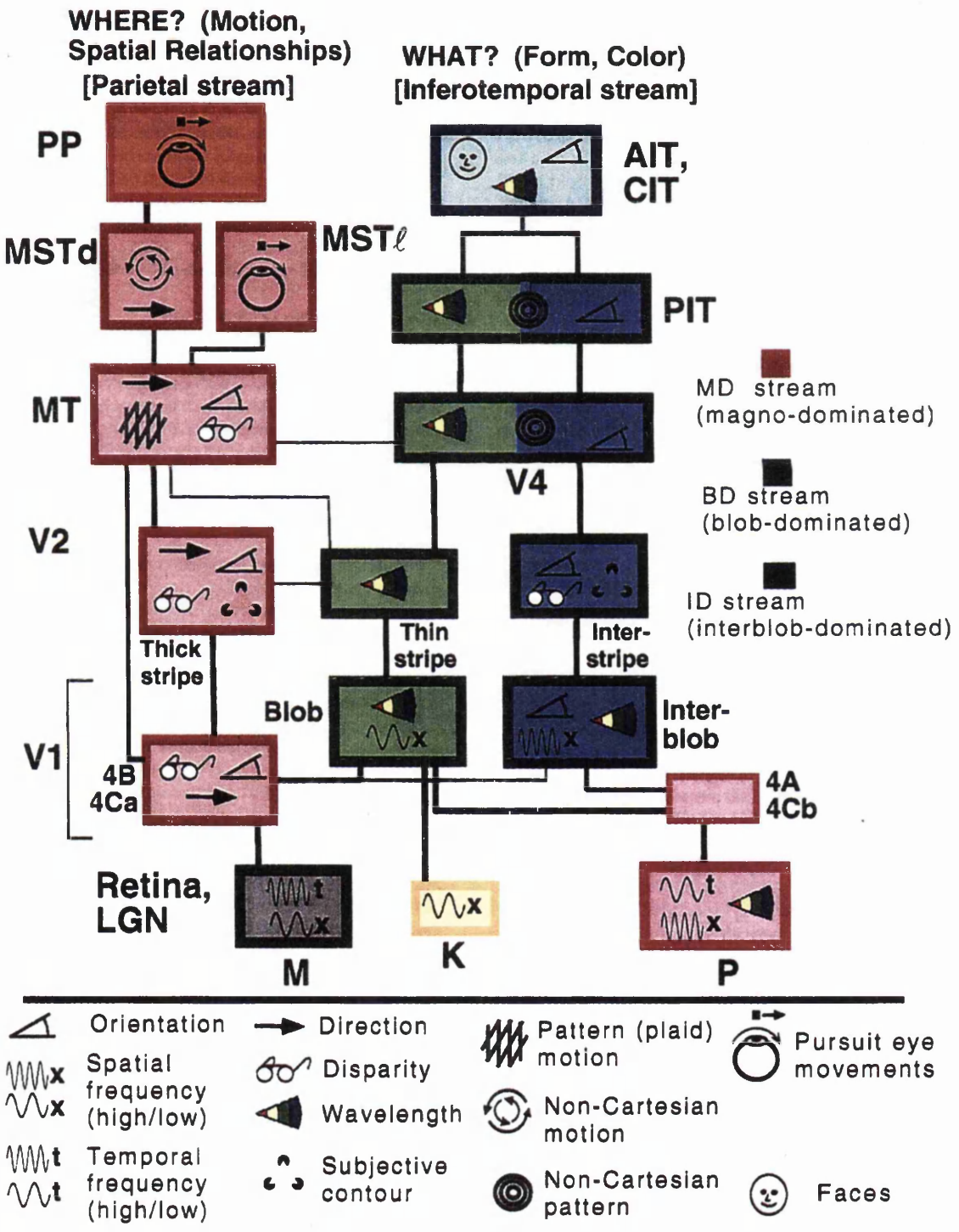

Fig. P4 Hierarchical organization of the ventral (what) and dorsal (where) streams in the monkey. (taken from Van Essen and Gallant, 1994)

P4.3 Human Visual Cortex

So far, we have described the visual system in the monkey but what of the human? As it is obviously unethical to use electrophysiological recordings of single cells in the human brain, inferences about functional architecture in the human has come about largely through functional neuroimaging. Both PET and fMRI have elucidated the 'colour' and 'motion' visual areas, as well as primary visual cortices or V1, in the human. These areas have been largely identified with the use of subtraction procedures. To put it simply, if one measures the rCBF or BOLD response to a visual colour stimulus minus that to an identical black and white stimulus, the area that shows significant activations in the human brain could then be thought to be the 'colour' area and directly analogous to monkey V4. In the human, this area has been found in the fusiform gyrus of occipital cortex and has been labelled 'human V4' (Lueck *et al* , 1989). In the same way, but using motion, 'human V5' has been found to exist in inferior temporal cortex of humans (Watson *et al* 1993, Zeki *et al* 1991). Oddly, this area in the human is still widely referred to as MT even though it is actually in IT of the human. Another area that tends to 'light up' in humans, when viewing 'more complex motion' is an area in the superior part of the middle occipital gyrus that has come to be known as area V3a (Tootell *et al,* 1997). As this area processes more complex motion, such as radial motion, it is likely that this area is directly analogous to area MST in the monkey. Another area that tends to light up in either colour or motion processing is in the calcarine sulcus. This area is thought to be analogous to primary visual cortex/V1. It should be noted as well, that it is extremely difficult to separate V1 and V2 in functional imaging as functional imaging measures integrated responses over large patches of cortex. Therefore, in the final fMRI chapters on vision, in this thesis, when we refer to V1, we mean more specifically V1/V2 complex. Another important point is that, (not withstanding controversies, such as whether V4 is a colour or form area) in our fMRI studies we defined our areas operationally due to either a main effect of colour or motion and so distinguish areas on purely functional grounds. We then test for the effects that we are looking for (in terms of population dynamics) within these areas.

P4.4 Cortical Connectivity

Finally, before concluding this section on the visual system, it may be interesting to say something about the complex connectivities within the visual system. As can be seen, the primate visual system comprises a large number of cortical areas dealing with different

attributes of the visual scene. The 32 visual areas of the macaque are interconnected by more than 300 distinct cortico-cortical pathways (Felleman and Van Essen, 1991). A remarkable feature of the connections among these areas is the fact that they exhibit specific patterns of laminar origin and termination. In a well-known proposal, Felleman and Van Essen organized visual cortical areas in a hierarchy on the basis of these connectivity patterns. Within this hierarchy, ascending connections project from lower to higher-order visual areas and terminate in layer 4. These ascending connections are largely reciprocated by descending projections that terminate outside of layer 4. The organization of visual areas, in levels, on the basis of these connectivity patterns reflects that observed functionally. Neurons in areas at higher levels in the visual hierarchy exhibit larger receptive field sizes and more complex response properties. For example, receptive field sizes of cells in V3, V4 and V5 are known to be much larger than those of cells in V1 and V2 (Tanaka *et al*, 1986). Also, receptive field sizes in IT, MST and STPp are known to be larger still (Bruce *et al*, 1991).

The dense network of ascending and descending connections in the visual hierarchy provides an anatomical basis for the interactions needed to link neuronal processes distributed over widely separated regions into coherent representational states. Indeed, functional specialization depends upon extrinsic and intrinsic connections within and among cortical units, populations and subareas, whose convergent and divergent architectures underlie the segregation of features in the visual field (Zeki 1990). This segregation is reflected in the emergence of distinct spatiotemporal receptive fields of units at various stages of the visual pathways. Interestingly, physiological investigations into types of synaptic arbours (Rockland *et al*, 1996) have shown ascending inputs to be strong and driving and descending inputs to be weak and modulatory. Also, ascending input has been shown to use the type of synaptic arbours that are round and dense while descending connections have extended arbours that are much sparser. Round arbours embody around 100 terminals over an area of diameter of about 100μm while extended arbours incorporate roughly 500 to 1000 terminals over an area of diameter, 1 to 3mm (Crick and Koch, 1998, Rockland *et al*, 1996). Consistent with this synaptic asymmetry, visual area V1 has a strong driving effect on the hierarchically higher area V2, in the sense that visual activation of V2 depends on input from V1 (Schiller and Malpeli, 1977, Sandell and Schiller, 1982). This dependency has been demonstrated by reversibly cooling (deactivating) V1 while recording from the retinotopically corresponding region of V2, during visual stimulation (Schiller and Malpeli, 1977, Girard and Bullier, 1989). In contrast, cooling V2 has a more modulatory effect on V1 unit activity (Sandell and Schiller, 1982). The functional asymmetry between V1 - V2 interactions has now been established in humans using functional magnetic resonance imaging (Friston *et al*, 1995). Additionally, there is evidence that V2 has a strong driving effect on V5 while V5 has a more modulatory effect on V2 (Girard and Bullier, 1989).

Fig. P5

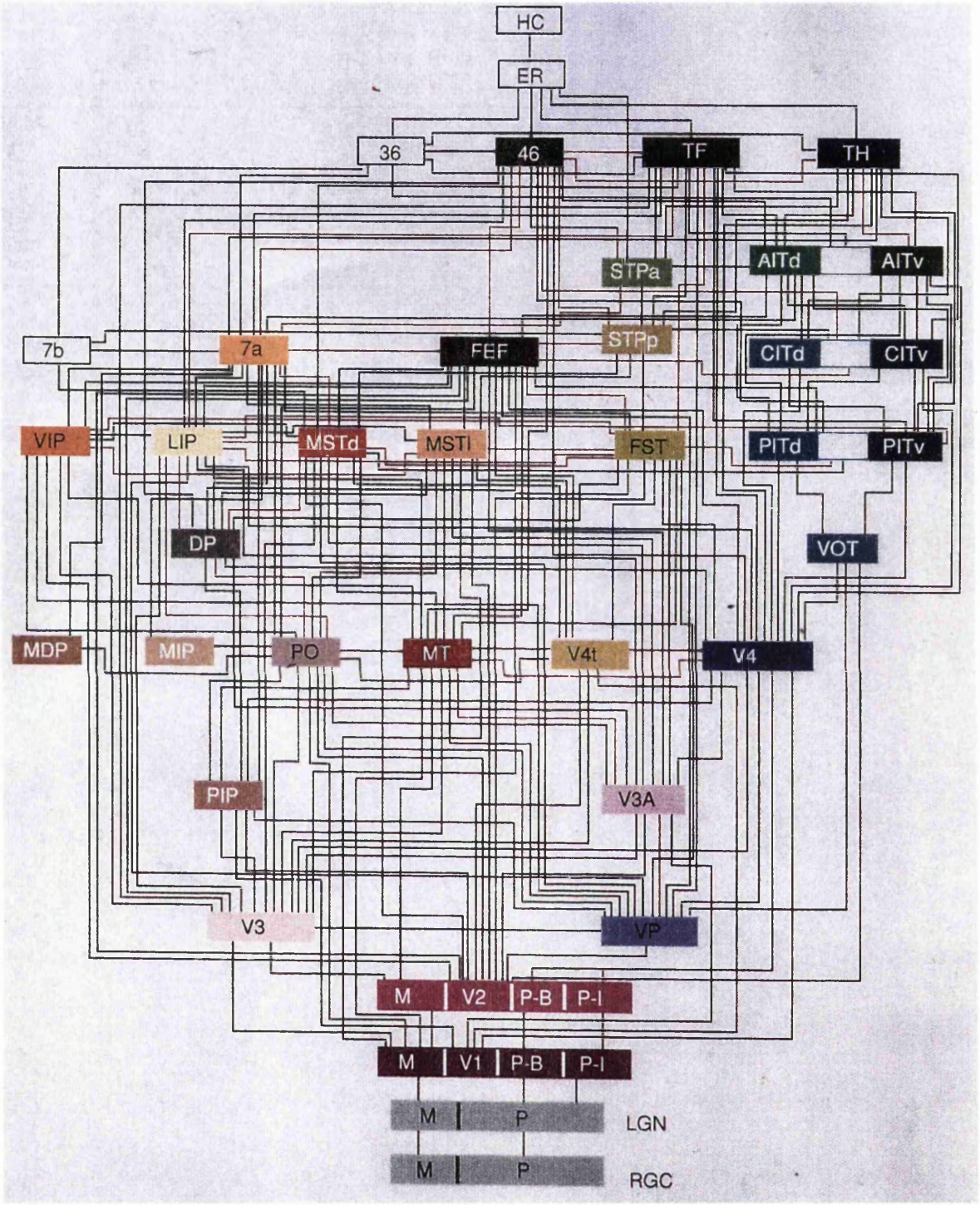

Fig. 5 Diagram of the hierarchical interconnectivity of the 32 visual areas in the monkey. (taken from Felleman and Van Essen, 1991)

Section 1:

Theoretical Investigations

Chapter 1: Modelling Neuronal Dynamics

1.1 Abstract

In this chapter, we describe two synthetic single compartmental neuronal models that, during the course of this thesis, will be used to investigate computational aspects of neuronal coding and functional integration. The first section describes the modelling of Hodgkin-Huxley neuronal dynamics and tests this model to show that it behaves in accordance with real neurophysiological data. Section 2 describes the simpler, integrate and fire, neuronal model. Most of the work in this thesis uses the detailed, Hodgkin-Huxley model. However, in some instances, we also use the simpler, integrate and fire, model, as this allowed us to model much larger neuronal populations without increasing the computational load and thus simulation time.

1.2 Modelling Neuronal Dynamics

Neurons continuously receive pulses, mostly at projections known as dendrites, from thousands of other neurons. These pulses are conveyed at junctions called synapses. Pulses from certain neurons are excitatory, in that they act to increase the membrane potential of the

cell and others are inhibitory, in that they decrease the membrane potential of the cell. The membrane potential fluctuates according to these inputs. If it goes above a certain threshold then an action potential is generated and is propagated down the cell's axon to send a signal to the next cell's dendrite. Action potentials are waves of depolarization, where the membrane potential increases by about 100mV (note that a cell's resting membrane potential is usually around -60mV). Action potentials typically last for around 1 to 3 ms.

Fig. 1

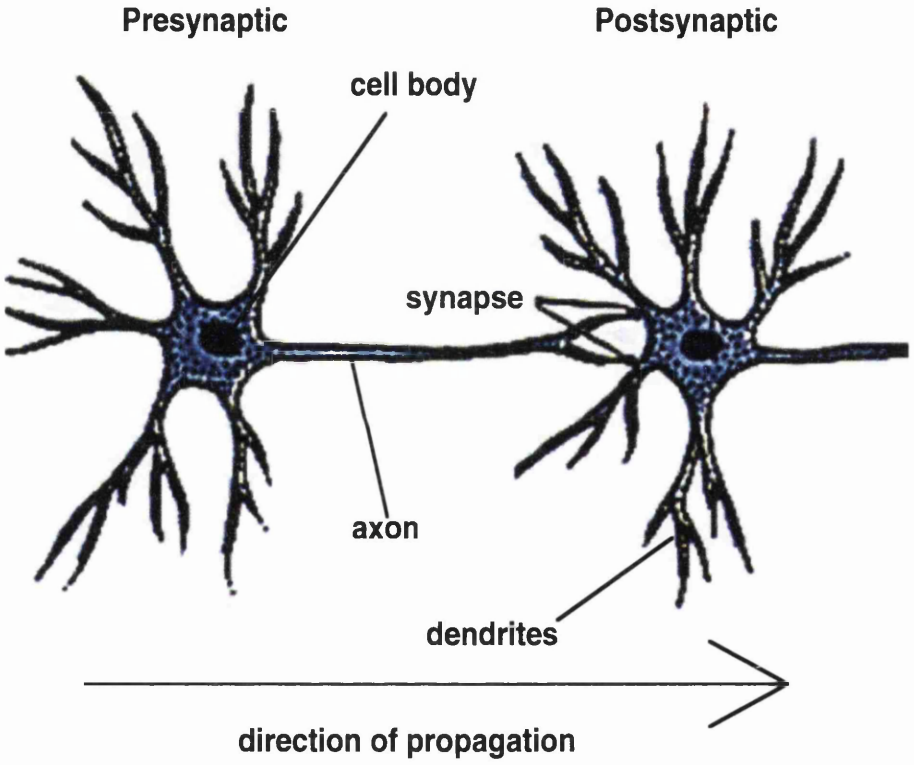

Fig. 1.1 A diagram showing the neuronal axon, dendrite and synapse (taken from Nicholls *et al,* From Neuron to Brain, p26).

1.3 Hodgkin-Huxley Model

The action potential is generated by transient increases in the cell transmembrane sodium (Na^+) and potassium (K^+) currents, which occur when the cell is depolarised above a threshold. The model employed in this thesis uses the Hodgkin-Huxley formalism describing the membrane current properties in the squid giant axon. Hodgkin and Huxley made the following assumptions in describing these membrane currents:

1.) Each channel is able to exist in two states, open and closed.
2.) No current flows through a closed channel.
3.) The total membrane current is dependent on the number of open channels ie. $I = i(V)\, n(V,t)$ where $i(V)$ is the current through one open channel and $n(V,t)$ is the number of channels open.
4.) The number of channels open depends on the Voltage (V) and time (t).
5.) At a given voltage, the current through an open channel is constant.
6.) Changes in membrane potential alter the current through an open channel instantaneously.
7.) Changes in membrane potential also produce a time-dependent change in the number of open channels.

The form of the action potential for a neuron, i, is determined by solving the Hodgkin and Huxley equations (Cronin, 1987). The specific implementation here is based on the equations from the model of the Bullfrog neuron taken from Yamada *et al*, 1989.:

$$dV_i/dt = -1/C_M\{(g_{Na}\, m_i^2\, h_i\, (V_i - V_{Na}) + g_K\, n_i^2 y_i\, (V_i - V_K) + g_{li}\, (V_i - V_l) + g_{ex}(V_i - V_{ex}) + g_{in}(V_i - V_{in})\},$$

$$dm_i/dt = \alpha_{mi}\, (1 - m_i) - \beta_{mi}\, m_i,$$

$$dh_i/dt = \alpha_{hi}\, (1 - h_i) - \beta_{hi}\, h_i,$$

$$dn_i/dt = \alpha_{ni}\, (1 - n_i) - \beta_{ni}\, n_i$$

$$dy_i/dt = \alpha_{yi}\, (1 - y_i) - \beta_{yi}\, y_i$$

$$dg_{ex}/dt = -g_{ex}/\tau_{ex}$$

$$dg_{in}/dt = -g_{in}/\tau_{in}$$

V_i represents the membrane potential of neuron i, C_M represents the membrane capacitance (the capacitance is taken to be constant and to be the same for all neurons), g_{Na} represents the maximum Na^+ channel conductance, g_K represents the maximum K^+ channel conductance, g_l represents the leakage conductance, V_{Na} represents the Na^+ equilibrium potential, V_K

represents the K^+ equilibrium potential, V_l represents the leakage equilibrium potential. m, h, n and y are the fraction of Na^+ and K^+ channel gates that are open (m,h for Na^+ and n,y for K^+). g_{ex} and g_{in} are the conductances of the excitatory and inhibitory synaptic channels respectively. τ represents the excitatory and inhibitory decay time constants. For the purposes of this chapter, we consider pairs of excitatory neurons throughout.

Every iteration, g_{ex} and g_{in} are updated using the equations:

$$g_{ex} = g_{ex} + w_{ji} \quad C1$$

$$g_{in} = g_{in} + w_{ji} \quad C2$$

where w_{ji} represents the synaptic weight between a presynaptic neuron j and a post synaptic neuron i.

As can be seen, Na^+ channels have two sorts of gates, the m and h gates (consistent with Hodgkin-Huxley notation). On membrane depolarisation, the Na^+ current (the sodium current is an inward current and thus causes activation / excitation) initially increases (activation). However, it then shows a slower decay (inactivation / inhibition). The membrane potential is dependent on the activation gate, m raised to the second power (giving the Na^+ activation current an inverted 'U' time course). Conceptually, the Na^+ channels can be thought to have two m gates. As the probability of one gate being open is m, the probability of both gates being open is m^2. On depolarisation, both m gates have to be open before the channel is effectively open. These are assumed to open independently and their rate of opening is given by dm_i/dt (see above).

In the equation, $dm_i/dt = \alpha_{mi} (1 - m_i) - \beta_{mi} m_i$, α_m and β_m are rate constants governing the opening and closing of gates where, $\alpha_{mi} (1 - m_i)$ is the rate of uni-directional movement of the gate from it's closed to open state while $\beta_{mi} m_i$ is the rate of uni-directional movement of the gate from it's open to closed state. The potential is dependent on the inactivation variable, h to the first power (giving the late Na^+ inactivation current an exponential time course). Thus, the Na^+ channels have only one h gate (the h gate is initially open and on depolarisation begins to close). However, the h gate closes much more slowly than the m gates open. The rate of h gates closing is given by dh_i/dt. K^+ channels also have two gates, the n and y gates. Depolarisation opens the n gates and the membrane potential is dependent on n^2 showing that K^+ channels have two n gates. These n gates are initially closed and on depolarisation, begin to open. The K^+ current is an outward current and thus causes inactivation (inhibition). The y gate is an inactivation gate giving the late K^+ inactivation

current an exponential time course.

1.3.1 Interaction between Units

C1, C2 are constants governing the numbers of channels opened in the postsynaptic cell if the presynaptic membrane potential rises above a certain threshold and implicitly releases presynaptic vesicles containing neurotransmitters. If the presynaptic cell is not firing above the threshold, then: C1, C2 = 0. If V_j is above the threshold and if the presynaptic cell has an inhibitory effect, inhibitory synaptic channels are opened rather than excitatory ones and thus C2 > 0 and C1 = 0. If the presynaptic cell has an excitatory effect, excitatory channels are opened and thus C1 > 0 and C2 = 0. This corresponds to the release of excitatory (*eg.* AMPA) or inhibitory (*eg.* GABA) neurotransmitters.

Synaptic transmission is caused by setting C1 or C2 to a non-negative value for the duration of one iteration after the presynaptic cell fires above threshold. The values of C1 and C2 were chosen to be the same as the values of the peak conductances of AMPA and GABA channels taken from Lumer *et al* (1997), as were the values of the reversal potentials and the time constants. The presynaptic input, C1,C2, felt by neuron i from neuron j is only expressed after some propagation delay ($DELAY_{ji}$), which is of the order of a few milliseconds and is constant. g_{Na}, g_K and g_l are positive constants and α_n, β_n, α_m, β_m, α_h, β_h, α_y, β_y are nonnegative functions of V that model voltage-dependent rates of channel configuration transitions:

$\alpha_m = 0.18 (V + 33) / (1 - \exp[-(V + 33) / 3])$

$\beta_m = -0.2 (V + 42)/ (1 - \exp[(V + 42) / 20])$

$\alpha_h = -0.05 (V + 55) /(1 - \exp [(V + 55) / 6])$

$\beta_h = 2.25 / (1 + \exp [- V / 10])$

$\alpha_n = 0.0047 (V + 12) / (\exp[-(V + 12) / 12] -1)$

$\beta_n = \exp-[(V + 147) / 30]$

If V < -25mV:

$\alpha_y = 1 / 6000 (1 + \exp [(V + 25) / 4])$

$\beta_y = (\exp [(V + 25) / 4) / 6000 (1 + \exp [(V + 25) / 4])$

or else:

$$\alpha_y = 1 / 50 (1 + \exp [(V + 25) / 4])$$

$$\beta_y = (\exp [(V + 25) / 4) / 50 (1 + \exp [(V + 25) / 4])$$

When integrating the neuronal equations through each time step, an explicit exponential technique was used due to it's good stability and accuracy statistics (Yamada *et al*, 1989). This rule assumes a first order form for the state equations with constant coefficients A and B over the interval Δt,

$$dy / dt = -By + A$$

then:

$$y_{t + \Delta t} = y_t e^{-B\Delta t} + (A/B) (1 - \exp [-B\Delta t])$$

The values of the parameters in this model are given in Table 1.1, below.

Table 1.1 Values Used in the Model

Membrane Capacitance / C_m	1 microfarad
C1 (AMPA $g_{peak\ (mS)}$)	0.05
C2 (GABA $g_{peak\ (mS)}$)	0.175
time step/dt	0.5 ms
g_{Na}	200 mS
g_K	170 mS
g_l	1 mS

g_{ex}	0.05 mS
g_{in}	0.175 mS
Sodium Equilibrium Potential/Vna	50 mV
Potassium Equilibrium Potential/V_K	-90 mV
Leak Equilibrium Potential/V_l	-60 mV
AMPA Equilibrium Potential/V_{ex}	0 mV
GABA A Equilibrium Potential/V_{in}	-70mV
AMPA decay time constant	3 ms
GABA A decay time constant	7 ms

1.3.2 Simulated Dynamics

If we set the synaptic weights high enough, the coupled neurons resonate (Fig. 1.2). This is because, each time cell i receives a presynaptic impulse, the synaptic weight is sufficiently high that it causes the cell i to fire which in turn causes cell j to fire and so on. In short, each cell repeatedly stimulates the other (with the propagation delay) so that they fire alternately.

Fig. 1.2a b

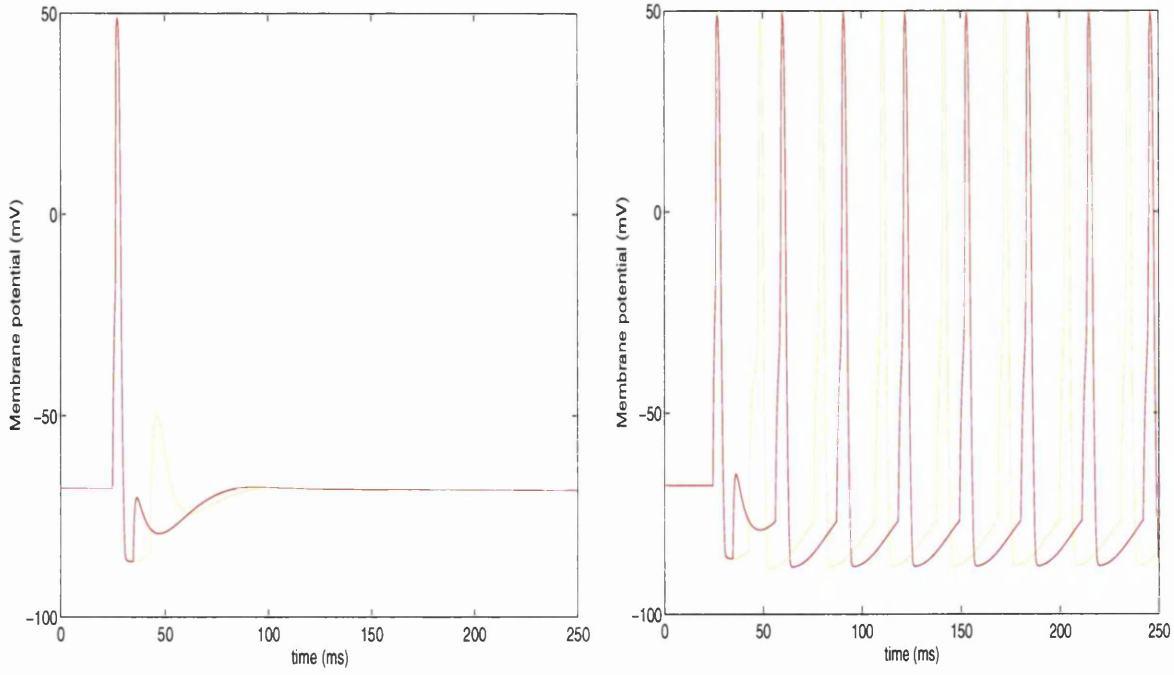

Fig. 1.2 (a) In this example, both synaptic weights w_{ji} and w_{ij} are set to 1. $DELAY_{ij}$ and $DELAY_{ji}$ were set to 8 and 16 ms respectively. (b) the weights were set to 100 with the same delays. Weights of 1 are equivalent to the peak conductance being equal to that for an AMPA channel. Weights with a value of 100 are 100 times bigger than the peak conductance for AMPA and thus (b) is equivalent to the postsynaptic cell receiving inputs from 100 cells simultaneously. In (a) and (b), both cells are stimulated once simultaneously at the beginning of the run.

For each action potential, the initial depolarisation is caused by changes in m, the probability of the Na^+ activation gate increasing while the downward phase is caused by changes in n, the probability of the K^+ gate opening and h, the probability of the Na^+ inactivation gate opens. When, the membrane potential approaches the equilibrium potential again, m and n are decreasing and h is increasing. Note that in the inhibitory case there is a hyperpolarisation below the equilibrium potential following an action potential. This is due to the potassium conductance still being above its resting level.

1.3.3 Refractory Period of the Action Potential

After the peak of the action potential, when n is elevated and h is low, it is not possible, no matter how much the cell is depolarised, to activate enough inward Na^+ current to outweigh the outward K^+ current and initiate an action potential. This period of not being able to activate an action potential is known as the refractory period and is crucial for the model dynamics. After a cell has fired, it cannot fire again for the duration of the refractory period. This phenomenon is implicit in the Hodgkin-Huxley dynamics but is explicitly implemented in the integrate and fire model.

1.3.4 Membrane Capacitance

A critical aspect of cell membrane dynamics is that, as the membrane allows the flow of ionic currents, the membrane accumulates ionic charges on its inner and outer surfaces. It is this charge separation that determines the cells membrane potential. This also makes the membrane analogous to an electrical capacitor that is in parallel with a resistor. Typically, a capacitor consists of two metallic conducting plates separated by a layer of insulating material such as mica or plastic. In a neuron, the ionic fluids on either side of the membrane act as the capacitor plates and the lipoprotein of the membrane acts as the insulating material. In a capacitor, the closer together the plates are, the more charge can be stored. Because the cell membrane is only around 7μm thick, it is capable of storing a relatively large amount of

charge.

The build up of charge in a capacitor is determined by:

$I = dQ/dt = C\,(dV/dt)$.

where, I = current (Amperes), dQ/dt = rate of change of charge stored (Coulombs per second), C = capacitance (Coulombs per Volt) and dV/dt = rate of change of potential difference (Volts per second). Therefore, in a simple circuit, on application of a current, the capacitor will charge linearly as all of the current flows through the capacitor straight away and this is constant (see Fig. 1.3).

Fig. 3

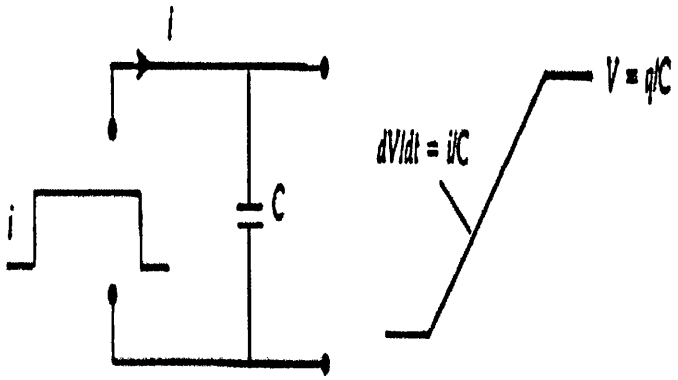

Fig. 1.3 In a purely capacitative circuit, the rate of change of voltage is proportional to the applied current (taken from Nicholls *et al,* From Neuron to Brain, p129).

However, in a circuit comprising a resistor and capacitor in parallel, things become more complicated. Now the current through the capacitor is not constant. Initially all of the current flows through the capacitor and none through the resistor (see Fig. 1.4). However, over time, the current through the resistor increases and that through the capacitor decreases (Fig. 1.4). Eventually, all the current flows through the resistor and none through the capacitor. As a result, on application of the current, the rate of build up of charge stored in the capacitor decreases over time until it reaches a maximum value, and thus the potential across the capacitor increases in the same way, as charge is proportional to potential difference or more specifically,

$Q = CV$

Alternatively, on removal of the current, the capacitor will discharge in the same way.

Fig. 4

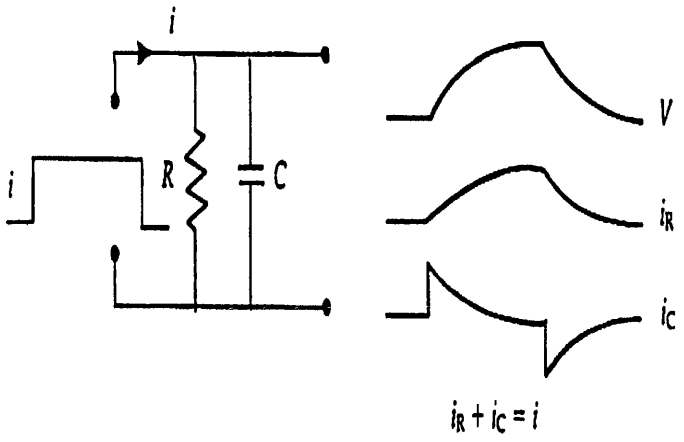

Fig. 1.4 In a combined RC circuit, the initial surge of current is through the capacitor. Finally, all of the current flows through the resistor. Voltage rises to its final value exponentially with time constant, $\tau = RC$ (taken from Nicholls *et al,* From Neuron to Brain, p129).

The time course of the rise of the potential is described by $V = IR\ (1 - e^{-t/\tau})$ where τ is the membrane time constant and is the time for the membrane potential to rise to the fraction (1 - 1/e) or 63% of its maximum value, following an excitatory synaptic input. The capacitance time constant is determined by, $\tau = RC$. In a neuron, the membrane time constant is an extremely important property of the neuron as it determines how fast the membrane potential increases and decreases following an excitatory synaptic input or how fast it decreases and increases following an inhibitory input. This is important because neurons act as temporal integrators that need many excitatory synaptic inputs to cause the membrane potential to increase above the threshold and fire. Therefore, the membrane time constant determines the effective time window over which different synaptic inputs need to arrive in order to have an effect on the postsynaptic cells membrane potential. In a later chapter, we will see how balanced excitatory and inhibitory inputs can dynamically modulate the effective time constants and why this is important for population dynamics.

1.3.5 Testing the Model

a.) To ensure our model reproduces findings from real electro-physiological experiments, we stimulated our cells as described in Markram *et al*, Fig. 1B (1997) :

Fig. 5

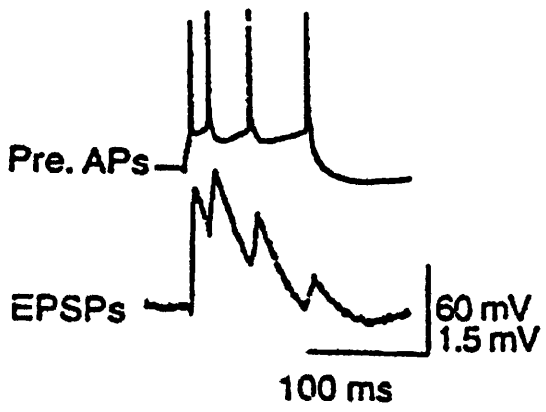

AP = action potential
EPSP = excitatory postsynaptic potential

Fig. 1.5 Physiological results taken from Markram *et al,* Fig. 1B (1997)

Stimulating the postsynaptic cell in the same way as depicted in Fig. 1.5 shows a postsynaptic response as shown in Fig. 1.6. The response shown here is purely due to the dynamics inherent in the Hodgkin and Huxley equations. As can be seen, the results here are consistent with physiological results as shown in Fig. 1.5.

Fig. 1.6

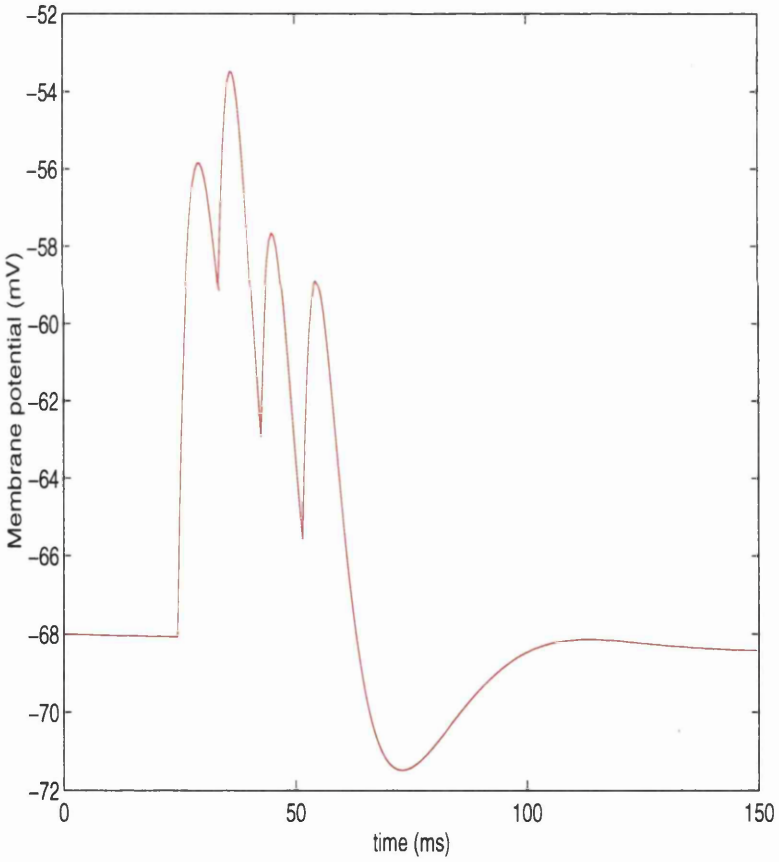

Fig. 1.6 This Figure shows the repeated stimulation of the postsynaptic cell during it's excitatory post synaptic potential (EPSP) as shown in Fig. 1.5.

When we stimulate the presynaptic cell in this way, we see the following response (see Fig. 1.6) in the postsynaptic cell.: The postsynaptic response initially increases and then decreases. This effect of decreasing excitatory postsynaptic potentials (EPSPs), when a cell is repeatedly stimulated during it's EPSP, is thought to occur because of depression due to depletion of neurotransmitters, desensitisation of postsynaptic receptors or the opening of other potassium channels (Magleby, 1987). However, in this model the response as shown in Fig. 1.6 is not due to any learning rule or short term plasticity, but is simply consequent on the Hodgkin and Huxley equations themselves. It can be concluded that some aspects of short term synaptic plasticity are due to nothing other than the Hodgkin-Huxley membrane channel dynamics themselves.

1.4 Integrate and Fire Model

This model does not use detailed Hodgkin-Huxley dynamics and is a simplified neuronal model where the threshold for firing is specified manually, rather than being implemented intrinsically via sodium and potassium channel dynamics. The instantaneous change in membrane potential, V(t), of each model neuron is given by:

$$\tau_m dV / dt = -V + V_0 - \Sigma_j g_j (V - V_j)$$

where τ_m is a passive membrane time constant set at 16ms (8ms) for cortical excitatory (inhibitory) cells and the sum on the right hand side is over synaptic currents. V_0 denotes the passive resting potential that was set to a value of -60mV. V_j are the equilibrium potentials for the jth synaptic type. V is reset to the potassium reversal potential of -90mV, when it exceeds a threshold of -50mV and a spike event is generated for that unit. Synaptic activations of AMPA, GABAa and GABAb receptors are expressed as a change in the appropriate channel conductance, g_j, according to a dual exponential response to single spike events in afferent neurons given by:

$$g = g_{peak}[\exp(-t / \tau_1) - \exp(-t / \tau_2)] / [\exp(-t_{peak} / \tau_1) - \exp(-t_{peak} / \tau_2)]$$

τ_1 and τ_2 are the rise and decay time constants, respectively, and t_{peak}, the time to peak. $t_{peak} = \tau_1 \tau_{2/(\tau_1 - \tau_2)}$. g_{peak} represents the maximum conductance for any particular receptor.

Conductances are implicitly normalized by a leak membrane conductance, so that they are adimensional. Also, in some instances during this thesis, feedback inter-area connections are modelled as modulatory voltage dependent NMDA channels.

The implementation of NMDA channels, was based on Traub *et al* (1991):

$$I_{NMDA} = g_{NMDA}(t)\ M\ (V - V_{NMDA})$$

$$dg_{NMDA}/dt = -g_{NMDA}/\tau_2$$

$$M = 1 / (1 + (Mg^{2+} / 3)(\exp[-0.07 (V - \xi)]))$$

I_{NMDA} is the current that enters linearly into the equation for dV/dt, above. g_{NMDA} is a ligand-gated virtual conductance. M is a modulatory term that mimics the voltage-dependent affinity of the Mg^{2+} channel pore. ξ is -10mV and Mg^{2+} is the external concentration of Mg^{2+} often used in hippocampal slice experiments (2mM). These and other parameters (see Table 1.2) are consistent with experimental data (see Lumer *et al*, 1997 for details).

receptor/channel	$g_{peak\ (mS)}$	τ_1 (ms)	τ_2 (ms)	V_j (mV)
AMPA	0.05	0.5	2.4	0
GABAa	0.175	1	7	-70
GABAb	0.0017	30-90	170-230	-90
NMDA	0.01	0	100	0

Table 1.2 Table showing the parameter values of the integrate and fire model.

1.5 Discussion of the Models used

1.5.1 Modelling the Whole Neuron

As described above, the two models used in this thesis are single-compartmental. However, as mentioned in the introduction, much more complex models that either use cable

theory or multiple compartments are also widely used in theoretical neurobiology. So what exactly are we sacrificing, in terms of neuronal realism, for the sake of lightening the computational load. Before one can answer this one must firstly know exactly what both, cable and multi-compartmental modelling offer the theoretician:

Both, cable theory and multi compartmental modelling allow the modeller to not only simulate the neuronal cell body, but also the neuronal dendrite. Dendrites are the largest component, in both surface area and volume, of the brain and their specific morphology is used to classify neurons into their different classes such as pyramidal, Purkinje, amacrine, stellate and double-bouquet cells. Dendrites are also the cell structures that receive the synaptic pulses from other connected cells and are therefore where temporal integration of synaptic impulses, or indeed 'neuronal computation' takes place. A typical dendritic tree has around ten thousand synapses distributed over it's surface. When activated, these synaptic inputs produce a local conductance change for specific ions at the postsynaptic dendritic membrane, followed by a flow of the corresponding ionic current between the two sides of the membrane. As a result, a local change in membrane potential is generated and then spreads along the dendritic tree. Using cable theory (Rall, 1964), the modeller simulates synaptic impulses as the flow of electrical current into the dendritic tree. Dendrites are effectively thin tubes wrapped with a membrane that is a relatively good electrical insulator compared to the resistance provided by the intracellular core or the extracellular fluid. Because of this difference in membrane vs. axial resistivity, the current inside the core conducter tends to flow parallel to the cylinder axis. This makes the dendrite directly analogous to an electrical cable. For a fuller explanation of the use of cable theory in neuronal simulations, see Bower and Beeman, The Book of Genesis, p53. The other approach, multi compartmental modelling, allows one to overcome some of the assumptions of cable theory, such as assuming a passive membrane that receives it's input as current. This approach involves modelling the dendrite as many functional subunits, directly analogous to the way that we modelled the single compartment neuron (see above). It can be shown that when the dendritic tree is divided into sufficiently small segments (compartments) the solution of the discrete multi-compartmental model converges to that of the continuous cable model. Figure 1.7 shows the differences in how the modeller views the neuron dendrite when using either cable theory or multi-compartmental modelling. Figure 1.8 illustrates a circuit for a 'generic' neuronal multi-compartmental model and shows how the current is propagated along the dendrite.

Fig. 1.7

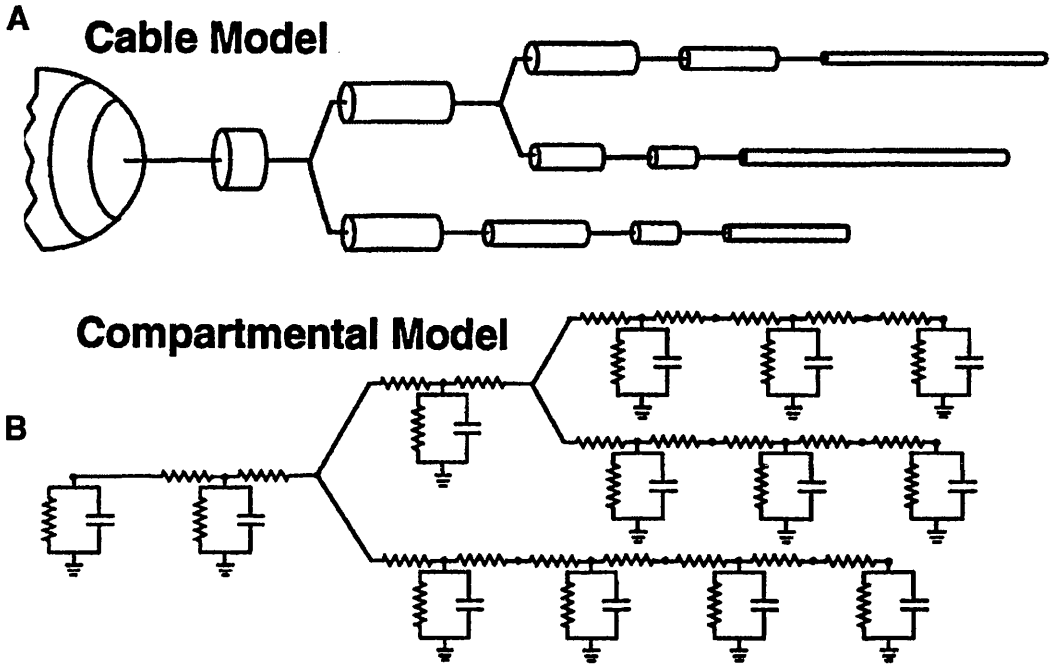

Fig. 1.7 Dendrites are modelled as either a set of cylindrical cables (a) or as a set of discrete R-C compartments (b). (taken from Bower and Beeman, The Book of Genesis, p70)

Fig. 1.8

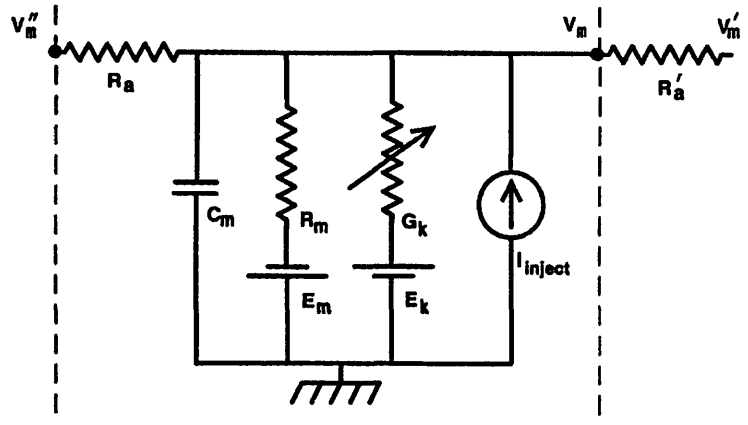

Fig. 1.8. Circuit for a neural compartment. The resistor with the arrow represents one of many possible variable channel conductances which are specific to a particular ion or combination of ions that give individual neurons and neuron types their unique computational properties. Differences in the concentration of the ion between the inside and the outside of the cell result in an osmotic pressure which moves ions along the concentration gradient. The resulting charge displacement creates a potential difference over the cell membrane. (taken from Bower and Beeman, The Book of Genesis, p11)

1.5.2 Modelling other Membrane Channels

So, what are we losing in our simulations by adopting the single-compartment model. One of the differences in behaviour between multi- to single-compartment cells is that the multi-compartments can function as many, almost independent, functional subunits. Each unit can implement a computation (such as local synaptic plasticity) and they can function as semi-autonomous input-output elements (via dendro-dendritic synapses). Also, neurons with slow currents in the dendrites and fast currents in the soma can produce a large repertoire of frequency patterns (Pinsky and Rinzel, 1994). However, from a phenomological point of view, these functions of the dendrites can be implemented via varying the inter-neuron delays and also by varying the number of inter-connected neurons.

The second shortcoming of our models is that they either use no ionic channel dynamics (integrate and fire model) or very few (Hodgkin-Huxley model). Again, many studies use neuron models that have a multitude of different membrane channels that influence the cell behaviour in a different way. For instance, Traub *et al*, 1991, implemented the following in their model of the CA3 pyramidal neuron:

1.) Sodium channels that activate the action potential as in our model.
2.) Calcium channels that act to activate the action potential along with the sodium channels.
3.) Delayed rectified and, after hyperpolarisation, calcium-dependent potassium channels that act as much slower inactivaters of the cell following an action potential (these channel dynamics mimic long-term neuronal adaptation, as has been shown to occur by Calabresi *et al* (1990) and Lorenzon *et al* (1992))
4.) Types a and b potassium channels that inactivate the cell. Type b is calcium-dependent.

The main functional significance of these channels is that they enable the cells to adapt to their firing at different levels and also cause the duration of cell action potentials to vary. However, as can be seen in Figure 1.6, our Hodgkin-Huxley model also shows some short term adaptation due to the use of two membrane channels whose parameters have been manipulated to enable us to make the cells as realistic as possible. Although, our integrate

and fire model does not show such short term adaptation, we do implement, in population models that use these types of cells, a form of long-term self inhibition (see p55) that mimics long-term adaptation. Another key difference between the two models that we use is that the duration of firing is much quicker in the integrate and fire model (one time step or 0.25ms) than the Hodgkin-Huxley model (around 3ms). Therefore, given the two models that we use, we are able to assess the role of spike duration and also different levels of adaptation on the population dynamics investigated. In short, we have been able to minimise our departure from biological realism by selective use of the appropriate complex cell state variables, which enabled us to substantially reduce the computational load of our simulations.

1.6 Synaptic Plasticity

1.6.1 Short term synaptic changes

We did not incorporate a synaptic learning rule in our model. However, for completeness, we discuss synaptic plasticity, because this phenomenon may cause non-linear coupling between cells of a stronger sort than we have described in our single-compartment models. Implementing a learning rule may, therefore, affect the nature of the population dynamics studied in this thesis. As the field of plasticity becomes more fully understood, it may well become an important component of population models in the future. Synaptic potentiation and depression are the processes by which neurons increase or decrease respectively their synaptic efficacy and thus the influence that presynaptic cell firing has on causing the postsynaptic cell to fire. Synaptic plasticity has been observed in electrophysiological recordings in both the short (of the order of seconds and minutes) and the long term (of the order of hours/days/weeks etc.). Short term depression (STD) and thus decreases in synaptic efficacy can arise from desensitisation of postsynaptic receptors or a decreased amount of transmitter release from the presynaptic terminal. There are four different types of short term potentiation (STP) depending on the level of depolarisation in the pre and post synaptic neurons. These are potentiation, augmentation and the first and second components of facilitation. Each of these mechanisms are kinetically and pharmacologically separable in terms of the neurotransmitter release involved. All four STP components cause the postsynaptic activity to build up during repetitive stimulation and then decay with characteristic time courses. This decay may reflect the build up and decay of Ca^{2+}/Na^{+} ions in the postsynaptic cell as well as an increase and decrease of presynaptic neurotransmitter release. STP can be mediated by an increased number of quantal packets of transmitter being released from the synapse when the presynaptic cell fires.

Facilitation has two components with decay time constants of around 50 and 300ms and is known to double transmitter release after a single impulse. Augmentation, which has a decay

time constant of around seven seconds, increases transmitter release by around one percent after a single impulse but can increase release severalfold during long conditioning trains of impulses. Potentiation whose decay time constant is around 30s to minutes, increases transmitter release by around one percent after one impulse but again, severalfold after hundreds of afferent pulses.

1.6.2 Long-term synaptic changes

More intriguing than these short-term changes in synaptic efficacy, are the longer term changes in synaptic efficacy that might underlie learning and conditioning of the sort observed by Pavlov. Pavlov noticed that hungry dogs used to salivate, even when they heard the footsteps of the man bringing them food (before they could smell or see the food). He designed a paradigm in which he coordinated the feeding of a dog with the sound of a bell being rung. He found that eventually the dog salivated even when the bell was rung but did not to any arbitrary stimulus (such as a visual stimulus). Therefore, by the repeated pairing of sound and salivation, he had presumably strengthened synapses in the sound - salivation pathway. Such long term activity-dependent changes in synaptic transmission were first produced experimentally in the neocortex in the 1960s and lasted tens of minutes. Long term potentiation (LTP) of synaptic efficacy in a mono-synaptic pathway (in the dentate region of the hippocampus) was described by Bliss and Lomo (1973) and was observed as an increase in the slope of the extracellular field potential (reflecting the EPSP occurring in neurons) and as an increase in synaptic voltage or current measured intracellularly after repetitive stimulation of the cell. LTP was shown to be both activity-dependent and synapse-specific. Activity-dependent means that the level of LTP depends on the activity (depolarisation) of both the pre and post synaptic cell. Synapse-specific means that only the synapse between the pre and post synaptic cell strengthens. What made this discovery more exciting, however was that it was shown to occur in parts of the brain known to be important for learning such as the neocortex and hippocampus.

It has been found generally, that for LTP to occur, pre and post synaptic cells must both be active (this is known as associativity). i.e. The presynaptic terminal must be releasing glutamate while the postsynaptic cell is depolarised. Associativity has been inferred in a number of ways including depolarising the postsynaptic cell with intracellular current while activating the presynaptic cell with the input being studied (such as the smell of food) or activating the postsynaptic cell with another input (such as ringing a bell) while activating the presynaptic cell with the input being studied (as in Pavlovian conditioning). Markram *et al* (1997) discovered that if the presynaptic cell fires above the threshold to cause an EPSP at the postsynaptic synapse then, for potentiation to occur, an action potential in the soma must be generated within a sufficient amount of time for a feedback signal to be propagated back down its dendrite to the spine, so that its arrival corresponds roughly with the EPSP. They found that if the action potential is generated within a time window of 10 ms after the EPSP

occurs, then LTP arises but if it is generated within a time window of 10 ms before the EPSP occurs, LTD arises. A large rise of Ca^{2+} in the dendritic spines is required for the induction of LTP. The transmitter release during tetanus activates non-NMDA receptors, which causes the postsynaptic membrane to depolarise and thus remove the magnesium block of NMDA receptor channels. Ca^{2+} then flows through NMDA channels into the spines. This rise in intracellular Ca^{2+} may be augmented by Ca^{2+} entry via voltage-sensitive calcium channels (VSCCs) and the activation of glutamate metabotropic receptors (mGluRs) leading to the release of Ca^{2+} from intracellular stores (Frenguelli *et al*, 1993, Bashir *et al*, 1993).

There are many similarities in the conditions required for LTP and long-term depression (LTD), with only the level of depolarisation being different. If the presynaptic target is strongly depolarised, then strong postsynaptic depolarisation produces LTP whereas weaker depolarisation produces LTD. As in LTP, LTD also depends on the levels of intracellular calcium in the postsynaptic cell. LTD occurs with low levels of calcium. However, as LTD has been observed under conditions of NMDA blockage, it is thought that for LTD to occur, Ca^{2+} must enter the postsynaptic cell through some other source. It is probable that while LTP is mediated by Ca^{2+} entry through NMDA channels, LTD is mediated by calcium entry from intracellular stores via mGluRs. Remember that high depolarisation causes the Mg^{2+} block to move from the NMDA channels whereas low depolarisation is sufficient for Ca^{2+} entry via mGluRs. In causing LTP, Ca^{2+} influx through voltage-gated ion channels activates Protein Kinase C to sensitize AMPA receptors. However, in causing LTD, Ca^{2+} influx activates Protein Kinase C to desensitize AMPA receptors.

1.6.3 Retrograde Messengers

The role of retrograde messengers between the postsynaptic and presynaptic cleft, in signalling synaptic changes is central to associative plasticity. Two of the likeliest candidates as this messenger are Arachidonic acid (AA) and Nitric Oxide (NO). AA is released during LTP induction and blocking its release blocks LTP. Moreover, adding exogenous AA increases the synaptic strength. However, the increase of AA release during LTP is only a small fraction of basal release implying that this is probably not the retrograde messenger. It has also been demonstrated that AA potentiates glutamate evoked currents through NMDA channels suggesting that AA may be needed merely to maintain a large calcium influx through NMDA channels, with a different Ca^{2+} dependent enzyme actually producing the diffusible retrograde messenger. NO is released when NMDA channels are opened by glutamate and blocking NO synthase blocks LTP, as does haemoglobin which binds NO. NO-synthase has also been found in the CA1 pyramidal cells that show LTP. Thus NO has emerged as the more likely candidate out of the two. Indeed it is the current view that LTP could be produced by the release of NO from within the cell coupled with depolarisation induced Ca^{2+} entry.

In summary, LTP/LTD are likely to be good experimental models for synaptic plasticity. Therefore, implementation of the phenomological characteristics of these dynamics in a computational model may provide useful insights into the neural substrates of learning and the effects on the behaviour of neuronal population dynamics. However, in this thesis, we are not concerned with learning and only consider short-term plasticity implicit in the model dynamics described earlier in this chapter.

Chapter 2: The Relationship between Synchronization among Neuronal Populations and their Mean Activity Levels.

2.1 Abstract

In the past decade the importance of synchronized dynamics in the brain has emerged from both empirical and theoretical perspectives. Fast dynamic synchronous interactions of an oscillatory or non-oscillatory nature, may constitute a form of temporal coding that underlies feature binding and perceptual synthesis. The relationship between synchronization among neuronal populations and the population firing rates, as measured by functional magnetic resonance imaging (fMRI) in the previous chapter, addresses two important issues: Firstly, the distinction between rate coding and synchronization coding models of neuronal interactions and, secondly, the degree to which empirical measurements of population activity, such as those employed by neuroimaging, are sensitive to changes in synchronization. We examined the relationship between mean population activity and synchronization using biologically plausible simulations. In this chapter, we focus on continuous stationary dynamics. In the subsequent chapter, we address the same issue using stimulus evoked transients. By manipulating parameters, such as extrinsic input, intrinsic noise, synaptic efficacy, density of

extrinsic connections, the voltage sensitive nature of post-synaptic mechanisms, the number of neurons and the laminar structure within the populations, we were able to introduce variations in both mean activity and synchronization under a variety of simulated neuronal architectures. Analyses of the simulated spike trains and local field potentials showed that, in nearly every domain of the model's parameter space, mean activity and synchronization were tightly coupled. This coupling appears to be mediated by an increase in synchronous gain when effective membrane time constants are lowered by increased activity. These observations show that under the assumptions implicit in our models, rate coding and synchrony coding in neural systems with reciprocal interconnections, are two perspectives on the same underlying dynamic. This suggests that, in the absence of specific mechanisms decoupling changes in synchronization from firing levels, indices of brain activity that are based purely on synaptic activity (e.g. fMRI) may also be sensitive to changes in synchronous coupling.

2.2 Introduction

This chapter is about the relationship between fast dynamic interactions among neuronal populations and measures of neuronal activity that are integrated over time (e.g. functional neuroimaging). In particular, we address the question "can anything be inferred about fast coherent or phasic interactions based upon averaged macroscopic observations of population activity?" This question is important because a definitive answer would point to ways in which data from functional neuroimaging might be related to electrophysiological findings, particularly those based on multi-unit electrode recordings of separable spike trains.

The basic hypothesis behind this work is that fast dynamic interactions between two units in distinct populations are a strong function of the macroscopic dynamics of the populations to which the units belong. In other words, the coupling between the two neurons, reflected in their coherent activity over a time-scale of milliseconds, cannot be divorced from the context in which these interactions occur. This context is determined by the population dynamics expressed over thousands of neurons and extended periods of time. More specifically, on the basis of previous theoretical and empirical work (Abeles *et al*, 1982, Aertsen *et al*, 1990, Lumer *et al*, 1997), we conjectured that the degree of phase-locking, or more generally synchronization, between units in two populations, would co-vary with the average activity in both populations. The aim of the present work was to test this hypothesis using biologically plausible simulations over a large range of parameters specifying the physiological and anatomical architecture of the model. In this chapter we report simulations that address the relationship between mean activity and synchronization during relatively steady-state dynamics following the onset of continuous input lasting for a few seconds. In a subsequent chapter we will address the same issue using evoked transients and dynamic correlations at different levels of mean activity.

Many aspects of functional integration and feature linking in the brain are thought to be mediated by synchronised dynamics among neuronal populations. In the brain, synchronization may reflect the direct, reciprocal exchange of signals between two populations, whereby the activity in one population effects the activity in the second, such that the dynamics become entrained and mutually reinforcing leading to synchronous discharges. In this way, the binding of different features of an object may be accomplished, in the temporal domain, through the transient synchronization of oscillatory responses (Milner *et al*, 1974, von der Malsburg,1981, Sporns *et al*, 1991). Physiological evidence has been, in general, compatible with this theory (Engel *et al*, 1991). It has been shown that synchronization of oscillatory responses occurs within as well as between visual areas, for example between homologous areas of the left and right hemispheres and between remote areas in the same hemisphere at different levels of the visuo-motor pathway (Gray *et al*, 1990, Engel *et al*, 1991, Konig *et al*, 1995, Roelfsema *et al*, 1997). Synchronization in the visual cortex appears to depend on stimulus properties such as continuity, orientation similarity and motion coherency (Gray *et al*, 1989, Engel *et al*, 1990, Freiwald *et al*, 1995). It would therefore seem that synchronization provides a suitable mechanism for the binding of distributed features of a pattern and thus contributes to the segmentation of visual scenes and figure-ground segregation. More generally, synchronization may provide a powerful mechanism for establishing dynamic cell assemblies that are characterised by the phase and frequency of their coherent oscillations. Accordingly, the effective connectivity among different populations can be modulated in a context-sensitive way by synchronization-related mechanisms. Taken together, these considerations indicate that synchronization is an important aspect of neuronal dynamics.

The aim of this study was to see if population synchrony bears some relationship to overall activity levels. We used physiologically based neuronal networks comprising two simulated brain areas, to look at how the level of neuronal activity affects the degree of phase locking between the two populations and vice versa. We used two models. The first had a fairly realistic laminar architecture but simplified (integrate and fire) dynamics (see chapter 1). The second had a simple architecture but detailed (Hodgkin-Huxley) dynamics. By modifying different parameters, such as synaptic efficacy, the density of extrinsic connections, the voltage-sensitive nature of post-synaptic mechanisms, the number of neurons and the laminar structure within the neuronal populations, we were able to model a broad range of different architectures. For each architecture, we induced changes in the mean activity and synchronization among simulated populations by manipulating extrinsic input (or equivalently intrinsic noise). Analyses of the simulated spike trains and local field potentials showed that, in almost all regions of the model's parameter space, mean activity and synchronization were tightly coupled.

2.3 Methods

2.3.1 Integrate and Fire Model

The first component of this study looked at the behaviour of two reciprocally connected cortical areas. Each cortical area was divided into three laminae corresponding to the supra and infragranular layers and layer 4 (see Fig. 2.1a). This laminar organization is consistent with known cortical anatomy (Felleman and Van Essen, 1991). Each layer contained 400 excitatory cells and 100 inhibitory cells. Intra-laminar connections had a density of 10% and included both excitatory and inhibitory connections (with AMPA and GABAa synapses respectively). The supragranular cells also expressed modulatory NMDA and slow GABAb synapses. The pattern of inter-layer connections can be seen in Fig. 2.1a. Inter laminar connections were 7.5% and excitatory. GABAb connections were also implemented from the supragranular layer to the other two layers to represent double-bouquet cells (Conde *et al*, 1994, Kawaguchi, 1995). Our ratio of inter-layer/intra-layer connections approximated the 45%/28% ratio reported in the cat striate cortex (Ahmed *et al*, 1994).

Feedforward connections between cortical areas (Fig. 2.1b) were 5%, from the supragranular excitatory cells in the first cortical area to the AMPA synapses of layer 4 cells in the second cortical area. Feedback connections were 5%, from the infragranular excitatory cells of the second cortical area to the modulatory NMDA synapses of supragranular cells in the first cortical area. The synapse to neuron ratio in this model was consistent with experimental findings (Beaulieu *et al*, 1983, 1985). The extrinsic, inter-areal, connections were exclusively excitatory. This is consistent with known neuroanatomy where, in the real brain, long range connections that traverse white matter are almost universally glutaminergic and excitatory. The excitatory extrinsic connections between the neuronal populations targeted both excitatory and inhibitory neurons within each population. These target neurons are randomly allocated to the excitatory afferent in proportion to the percentage of each cell type. This results in extrinsic connections targeting preferentially excitatory cells which is consistent with the empirical data (Domenici *et al*, 1996, Johnson and Burkhalter, 1996). The anatomy used in this model was consistent with Lumer *et al*, 1997 and has been tested against empirical data (Sukov and Barth, 1998).

Fig. 2.1a

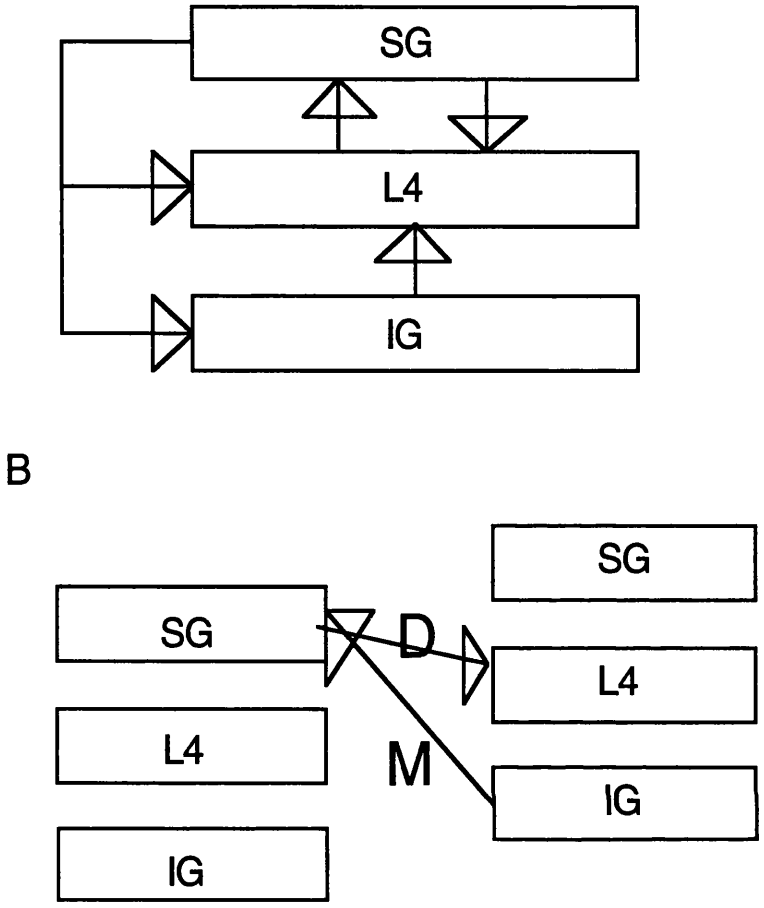

Fig. 2.1 Architecture of the first model. (a) A schematic showing the connectivity structure within one cortical region. (b) Two cortical regions where the first cortical area provides driving input to the second and the second cortical area provides modulatory input to the first. In these diagrams SG, L4 and IG refer to supragranular layers, layer 4 and infragranular layers respectively. D and M refer to driving (AMPA) and modulatory (NMDA) connections respectively.

Individual neurons, both excitatory and inhibitory, were modelled as single-compartment, integrate and fire units (see chapter 1, p30). Synaptic channels were modelled as fast AMPA and slow NMDA for excitatory and fast GABAa and slow GABAb for inhibitory channels (Stern *et al*, 1992, Otis and Mody, 1992, Otis *et al*, 1993). These synaptic influences were modelled using dual exponential functions, with the time constants and reversal potentials taken from the experimental literature (see Lumer *et al*, 1997 for the use and justification of

similar parameters to those used in the present model). Adaptation was implemented in each excitatory cell by simulating a GABAb input from the cell onto itself. Adaptation is an important feature of neocortical cell behaviour and it has been observed consistently that repetitive cell stimulation produces a progressive and reversible decrease of spontaneous depolarizations and a decrease in firing rate (Calabresi *et al*, 1990, Lorenzon *et al*, 1992). Implementing slow GABAb inhibitory inputs from each cell onto itself emulates this effect. Transmission delays for individual connections were sampled from a non central Gaussian distribution. Intra area delays had a mean of 2ms and a standard deviation of 1ms and inter area delays had a mean and standard deviation of 5ms and 1ms respectively. A continuous random noisy input was provided to all units in layer 4 of the first area. Variations in this input were used to induce changes in mean activity and synchronization.

2.3.2 Model based on the Hodgkin-Huxley Formalism

Once we had characterised the relationship between phase-locking and firing rate in the model above, we then tried to replicate our results over a much larger parameter space within the framework of a simpler model consisting of two areas, each containing a hundred cells that were 90% intrinsically connected. Due to the comparatively small number of cells used in this model, such a high connection density gives a similar synapse to neuron ratio as in the previous model. In this second component of our study, individual neurons were modelled as single-compartment units. Spike generation in these units was implemented according to the Hodgkin-Huxley formalism for the activation of sodium and potassium transmembrane channels. This facilitated a more detailed and biologically grounded analysis of effective membrane time constants (see below). Specific equations governing these channel dynamics can be found in chapter 1. In addition, synaptic channels provided fast excitation and inhibition. These synaptic influences were modelled using exponential functions, with the time constants and reversal potentials for AMPA (excitation) and GABAa (inhibition) receptor-channels specified as in the previous model. Cells were 20% inhibitory and 80% excitatory (Beaulieu *et al*, 1992). Reciprocal extrinsic (inter area) connections were all excitatory. Transmission delays for individual connections were sampled from a non central Gaussian distribution with means and standard deviations as given in the first model. A continuous random noisy input was provided to all units in one of the two areas (area one). In some simulations, the mean inter area delay was increased to 8ms to mimic a greater separation between the areas. In other simulations, excitatory NMDA synaptic channels (see chapter 1, p42) were incorporated. These NMDA channels were used only in the feedback connections.

2.3.3 Data Analysis

The neuronal dynamics from both models were analyzed with the cross correlation function

between time series from two areas, after subtraction of the shift predictor (Nowak *et al*, 1995). We used the time-series of the number of cells spiking per millisecond (in each population) as well as the mean membrane potential, analogous to the local field potential, of each population. We ran the model for two seconds of simulated time, eight times. The cross correlation between the first time series (eight runs in order) and a second time series, comprising eight runs in a random order, constituted our shift predictor. The shift predictor reflects phase-locking due only to transients locked to the onset of each stimulation.

As a measure of the level of phase-locking between the two populations, we used the peak cross correlation following correction. This separates stimulus onset related phase-locking from that due purely to neuronal interactions, allowing us to see how phase-locking due to the interactions between the two neuronal populations varied as a function of activity level.

The measure of phase-locking given above is effectively a measure of the functional connectivity between the two areas. Functional connectivity has been defined as the correlation between two neurophysiological time series, whereas effective connectivity refers to the "influence" that one neuronal system exerts over another (Friston *et al*, 1994). In this work, we also examined how mean activity and phase-locking varies with effective connectivity, using the second model. As our measure of effective connectivity we used the probability (averaged over units and time) that a cell in the first population would cause a connected cell in the second population to fire. Furthermore, we tried to elucidate some of the mechanisms that could underlie the relationship between mean activity and synchronization in terms of temporal integration at a synaptic level. Our hypothesis was that high levels of activity would engender shorter membrane time constants. This in turn would lead to the selection of synchronised interactions by virtue of the reduced capacity for temporal integration (Bernander *et al*, 1991). We therefore estimated the effective membrane time constants to see how these varied with mean activity and phase-locking. Details of the simulations can be found in chapter 1 and measurement of effective connectivity and derivation of the effective time constants can be found in appendices 3 and 4.

2.4 Results

We found that increases in the activity level of the network were universally associated with increases in the phase-locking between and within the populations as represented by the peak shift predictor subtracted cross-correlation. This held for large ranges of mean activity with a fall off at very high levels. This was observed regardless of the way that the activity level was varied (*eg.* changing the input to population one, varying the number of connections or manipulating the synaptic efficacies).

Firstly, we used the model incorporating two cortical areas, each comprising three layers (Fig. 2.1b) and manipulated the input activity level (Fig. 2.2) to layer four of the first area. Phase-

locking rose systematically with activity levels with a fall off at very high levels.

Fig. 2.2a b

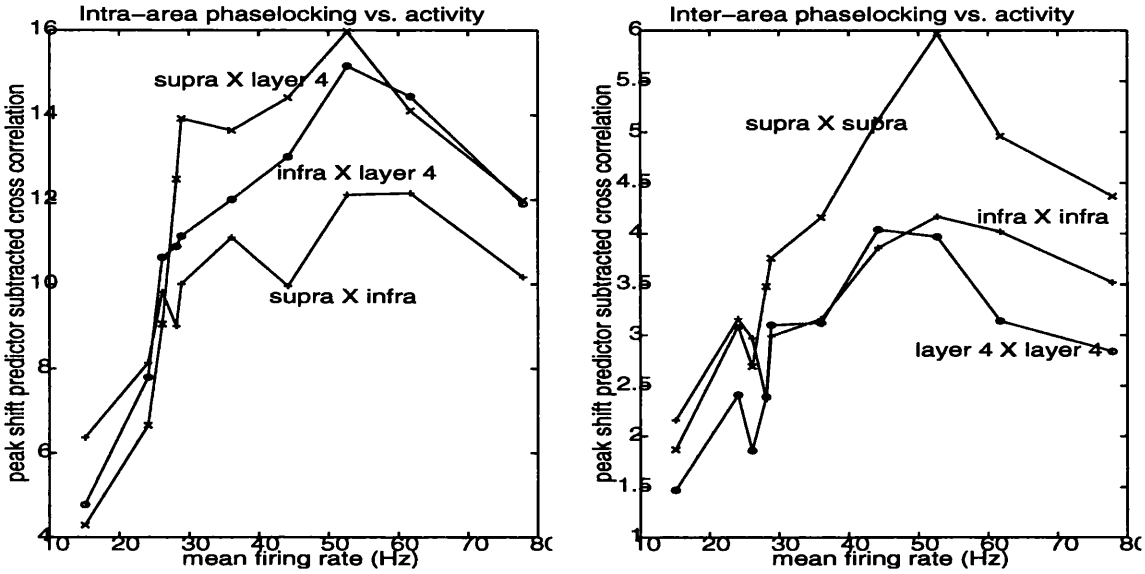

Fig. 2.2 Synchrony vs. mean activity for the first model. (a) This is a plot of the peak shift predictor subtracted cross correlation between mean spike trains of different layers in area one against mean firing rate in population one, as the random input to population one was increased systematically. (b) A plot for the same input levels but here the phase-locking between homologous layers in each area are shown.

The second component of our study represented an exploration of a larger parameter space, using the second model consisting of two areas, each comprising a hundred cells. Figure 2.3 shows the phase-locking between the two populations as a function of mean activity in population one, for 10 different levels of extrinsic connectivity. In these simulations, the input activity level was varied systematically to elicit changes in the dynamics. It can be seen in Figures 2.3a to d that phase-locking increases monotonically between the spike trains or local field potentials, as the activity level increases. Furthermore, the rate of increase of phase-locking with mean activity increases with extrinsic connectivity. This is expressed as an increase in the slope of the regression of phase-locking on mean activity and represents an interaction between mean activity and extrinsic connectivity in producing synchronization. Figures 2.3e and f illustrate the spiking and subthreshold activity in populations one and two at low and high levels of activity, respectively. It is seen that as activity rises, the spiking activity in each population becomes increasingly oscillatory.

Fig. 2.3a

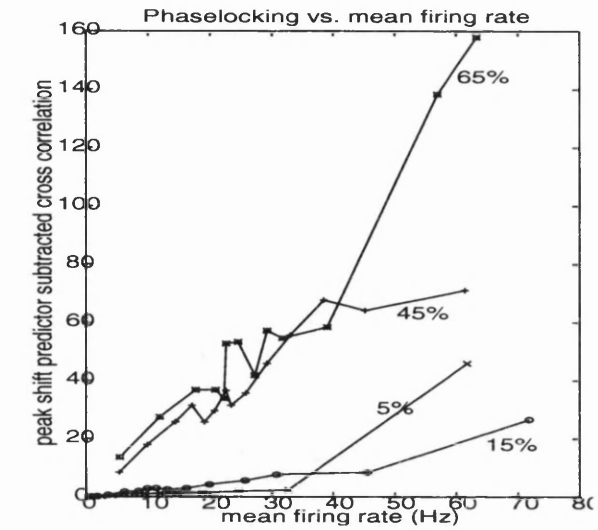

b

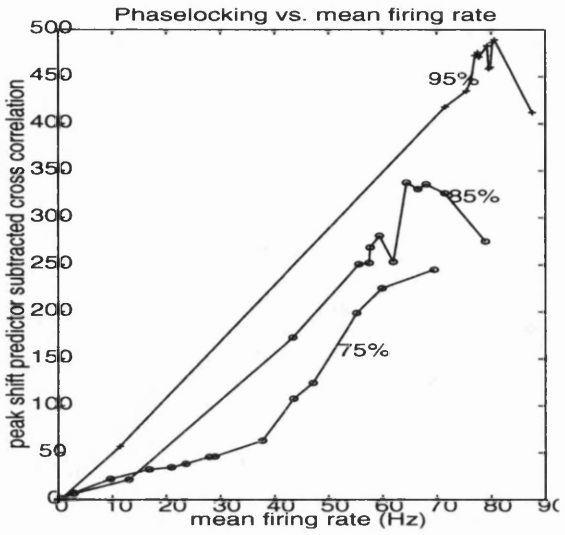

c

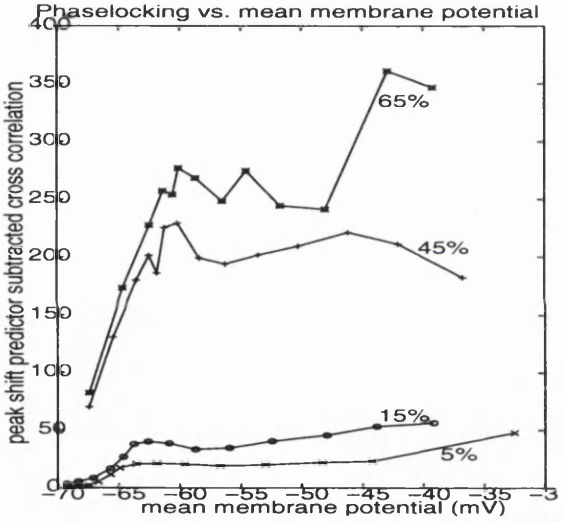

d

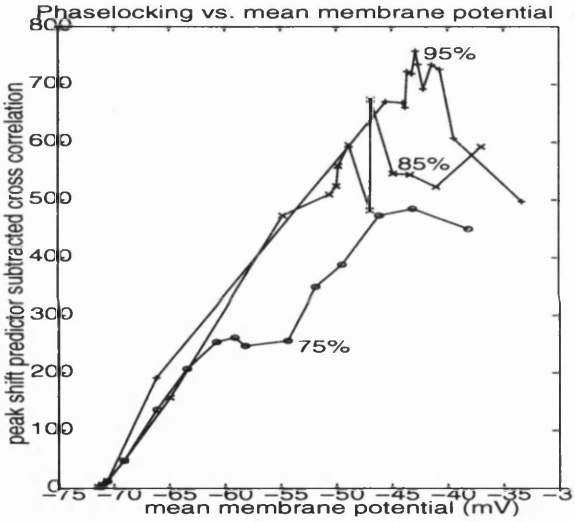

e f

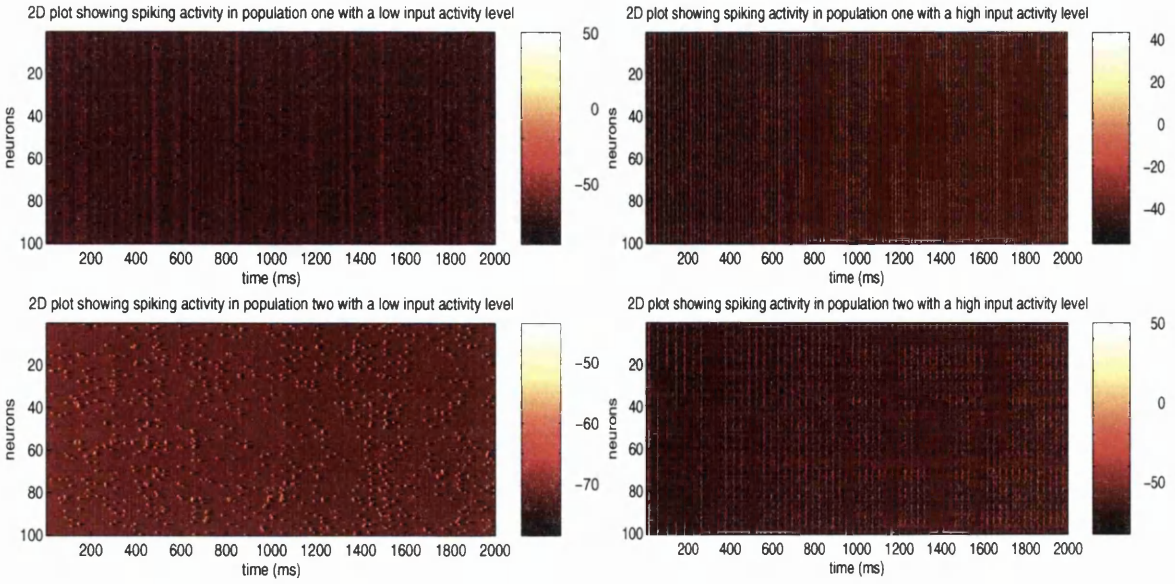

Fig. 2.3 Synchrony vs. mean activity for the second model. (a) and (b) The peak shift predictor subtracted cross-correlation between the time-series of number of cells spiking per ms for each population is plotted against mean number of cells spiking in population one per millisecond for extrinsic reciprocal connectivities of (a) 5%, 15%, 45%, 65% and (b) 75%, 85% and 95%. (b) and (c) The peak cross-correlation between the time-series of mean membrane potential is plotted against mean membrane potential of population one for the same extrinsic connectivities as in (a) and (b). (e) and (f) The spiking activity in populations one and two are plotted over the course of two seconds. Time is plotted horizontally and all one hundred neurons are shown on the vertical axis. The membrane potential is shown in terms of the colour (see the colour scale at the side of the graph). (e) and (f) are for low and high input activity levels respectively.

In the previous simulations, changes in the dynamics were elicited under different levels of extrinsic connectivity by manipulating the input to population one. The results pointed to an interaction between input activity and extrinsic connectivity. To fully characterise these influences, we examined the main effect of connectivity *per se* on synchrony by changing both extrinsic and intrinsic connections. This can be regarded as an analysis of the relationships between synaptic efficacy or anatomical connectivity and functional connectivity. Figure 2.4 shows plots of phase-locking between spike trains for the second model, when the input activity level was kept constant and the inter-area connectivity level, inter-area weights and intra-area weights were manipulated respectively (*i.e.* the density or efficacy of connections were modulated). These simulations were performed with feedback influences mediated either by AMPA or NMDA receptors. As shown in the figure, the phase-locking, within and between populations, increases to a certain level before reaching a plateau and eventually decreasing slightly, as either the extrinsic or intrinsic connectivity level increases (through changing the number of connections or weight values).

Fig 2.4a

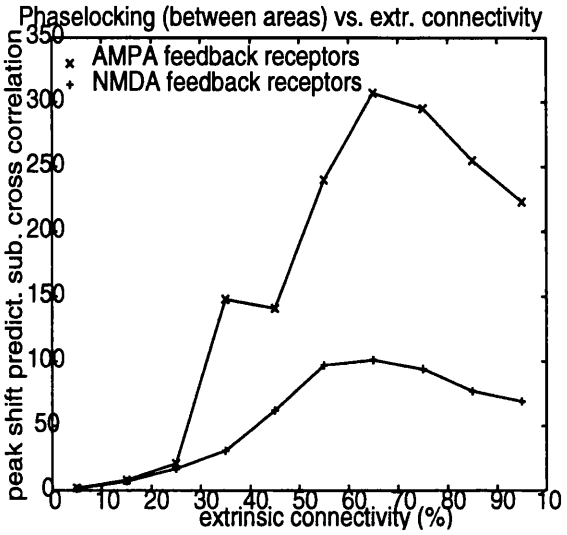
Phaselocking (between areas) vs. extr. connectivity
AMPA feedback receptors
NMDA feedback receptors
peak shift predict. sub. cross correlation
extrinsic connectivity (%)

b

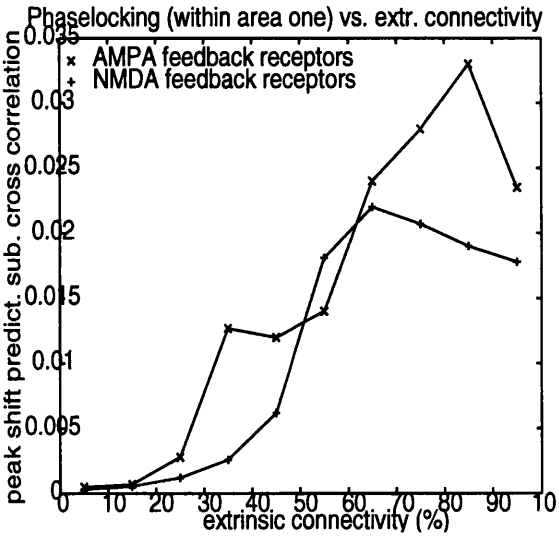
Phaselocking (within area one) vs. extr. connectivity
AMPA feedback receptors
NMDA feedback receptors
peak shift predict. sub. cross correlation
extrinsic connectivity (%)

c

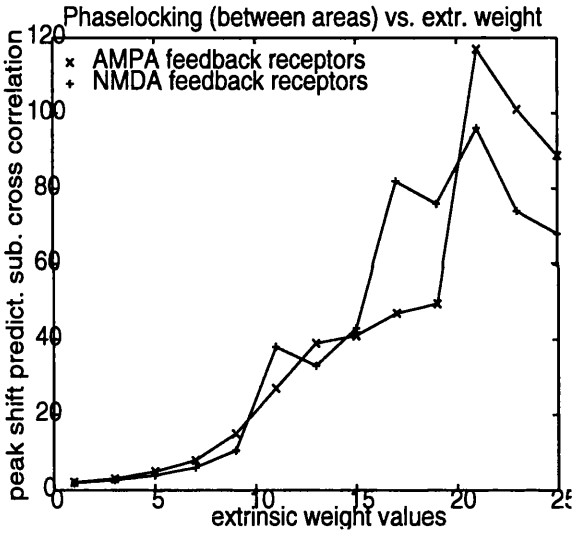
Phaselocking (between areas) vs. extr. weight
AMPA feedback receptors
NMDA feedback receptors
peak shift predict. sub. cross correlation
extrinsic weight values

d

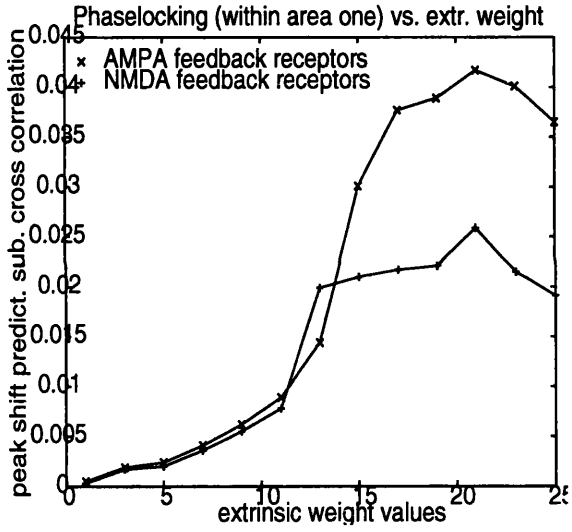
Phaselocking (within area one) vs. extr. weight
AMPA feedback receptors
NMDA feedback receptors
peak shift predict. sub. cross correlation
extrinsic weight values

e

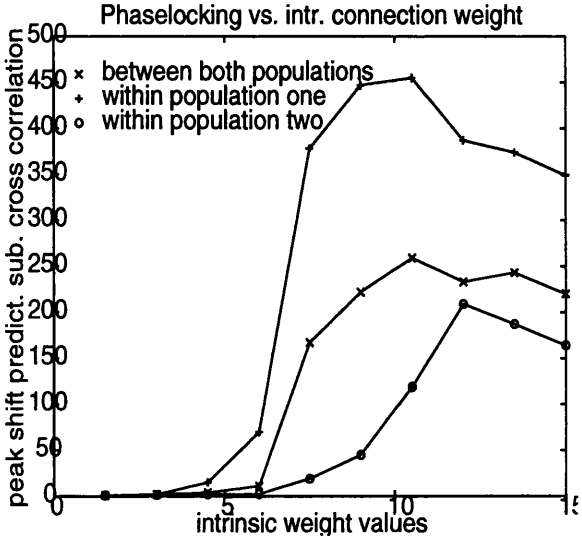
Phaselocking vs. intr. connection weight
between both populations
within population one
within population two
peak shift predict. sub. cross correlation
intrinsic weight values

Fig 2.4 Synchrony as a function of connectivity for the second model. In (a) and (b) the level of intrinsic connectivity was held constant at 90% while the extrinsic connectivity was varied through 5%, 15%, 25%, 35%, 45%, 55%, 65%, 75%, 85% and 95%. Plotted horizontally is the level of extrinsic connectivity. Plotted vertically is the maximum value of the shift predictor subtracted cross-correlation between the two neuronal populations or within population one. (a) The peak cross-correlation between the time-series of number of cells spiking per ms for each population is plotted against extrinsic connectivity. The two cases when the feedback receptors were AMPA and NMDA are shown. (b) The peak cross-correlation between the time-series of spikes per millisecond in one cell and the spikes per millisecond in the rest of population one is plotted against percentage of extrinsic connectivity. Again, this graph shows this plot under both AMPA and NMDA feedback receptors. (c) and (d) are the same as (a) and (b), except that here the number of connections were not changed. Instead, the actual values of the extrinsic weights were varied with the density of extrinsic connections remaining at 5%. Here, extrinsic synaptic weight is plotted horizontally. In (e), intrinsic and extrinsic connectivity levels remained constant (90% and 5% respectively) while intrinsic weights were increased. This plot shows how phase-locking varies between populations and also within each population as the intrinsic weights are increased. These graphs show the results for AMPA feedback receptors but similar findings were obtained with NMDA feedback receptors.

Next, we increased the extrinsic mean transmission delays from five to eight milliseconds. This was done to simulate longer range connections and to assess their effect on the behaviour of phase-locking with activity level. Figure 2.5 shows plots of phase-locking (within and between populations) against activity level varied in four different ways using either AMPA or NMDA feedback connections. As can be seen in Figure 2.5a, the results are almost identical to those of Figure 2.3a, indicating that increasing the transmission delay does not significantly alter the nature of the phase-locking. Figures 2.5c and 5d show the phase-locking between one neuron in population one and the rest of the population. These results suggest that phase-locking varies with activity level in much the same way as between populations. Figures 2.5b and 5d show that changing the receptor types to NMDA does not have a significant effect on how phase-locking varies with activity.

Fig. 2.5a

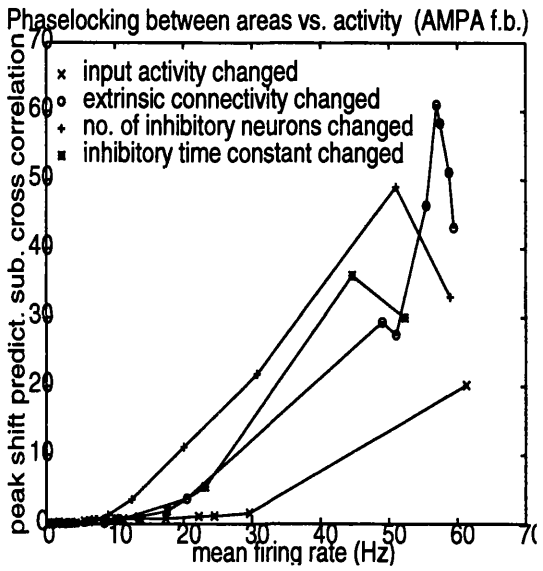

b

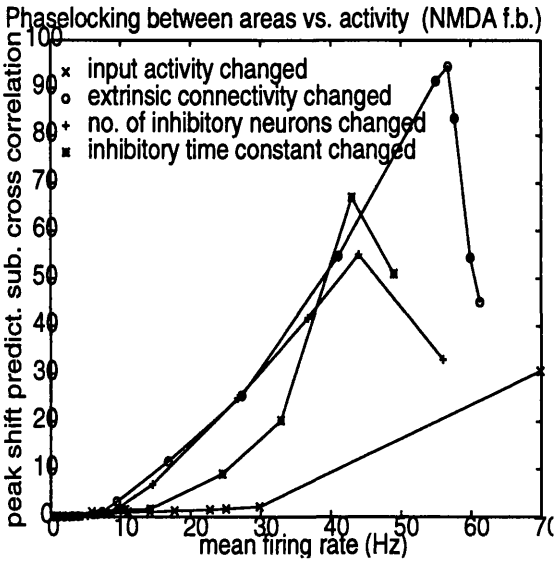

c

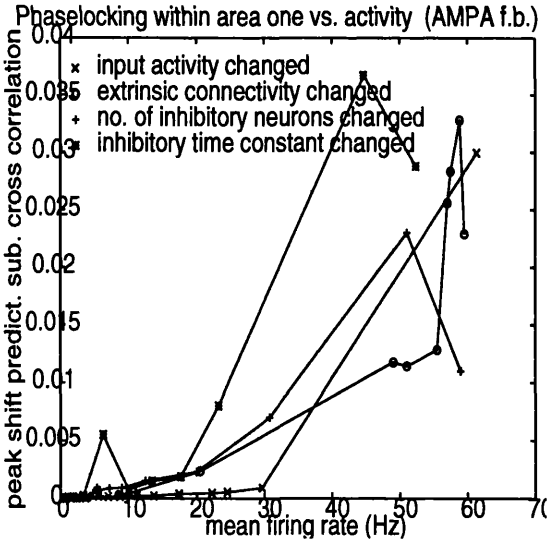

d

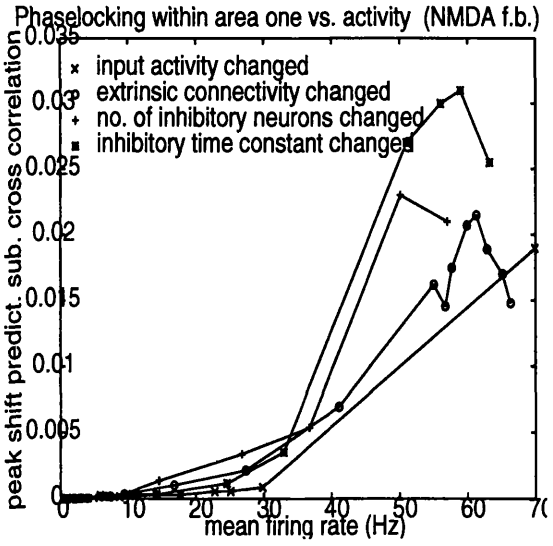

f.b. = feedback

Fig. 2.5 These graphs show how phase-locking varies with neuronal activity when the extrinsic delays were increased to a mean of 8ms. Here, the activity level was varied in four different ways: (i) By changing the input activity levels while all other parameters remained constant. The effect of this manipulation on phase-locking and activity level is denoted by the x's. (ii) By varying the extrinsic connectivity level between 5% and 95% (These data are shown by the 'o's). (iii) By changing the proportion of inhibitory neurons between 60% to 0%. This is denoted by the '+'s. (iv) By changing the values of the inhibitory synaptic time constants from 500 to 0.5 ms ('*'s). In (a) and (c), the feedback receptors were AMPA and in (b) and (d), they were NMDA. (a) and (b) Phase-locking against mean firing rate between populations. (c) and (d) Phase-locking between the firing rates of one cell and the rest of the population.

Figure 2.6 shows the relationship between phase-locking and mean firing rate when the input to area one is changed systematically under different levels of inhibition. The level of inhibition was manipulated either by changing the proportion of inhibitory neurons (Fig. 2.6a) or by changing the value of the inhibitory synaptic time constants (Fig. 2.6b). Under all levels of inhibition within the network, a monotonic relationship between phase-locking and mean activity was evidenced. As inhibition increased, the rate of increase of phase-locking with mean activity decreased. This was evident as a decrease in the slope of the regression of phase-locking on mean activity. These results point to a clear interaction between input activity and inhibition level, where inhibition attenuates the increase in synchrony with mean activity.

Fig. 2.6a b

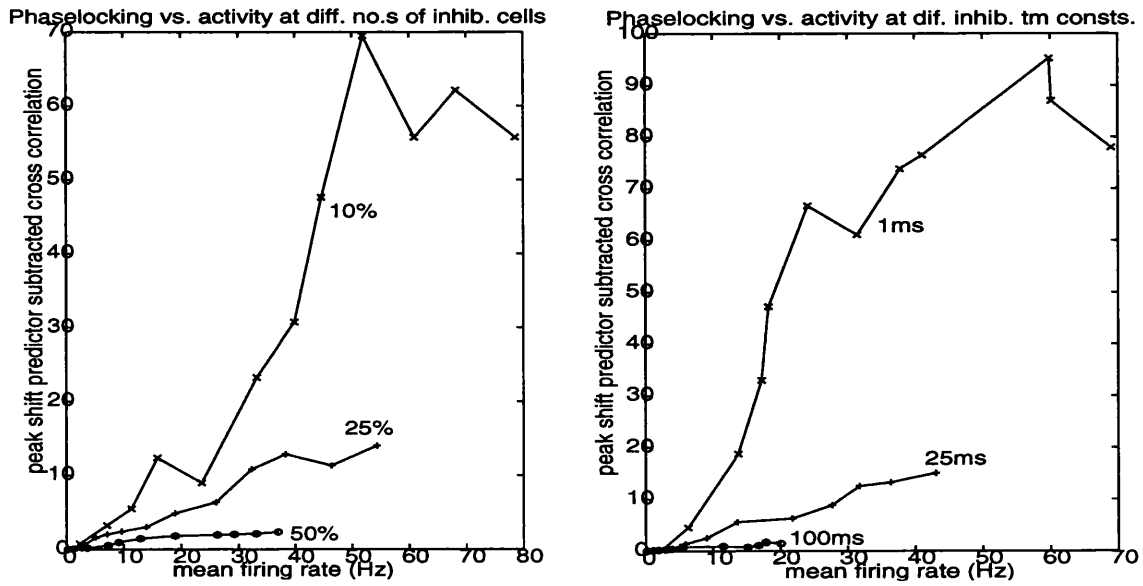

Fig. 2.6 (a) Phase-locking vs. mean firing rate as input to area one is varied systematically with network inhibitory cell proportions of 10, 25 and 50%. (b) This is the same as (a) except inhibition is varied by changing the inhibitory synaptic time constants between 1, 25 and 100ms while keeping the number of inhibitory cells constant. The feedback receptors were AMPA in both cases.

2.4.1 Effective Connectivity and Membrane Time Constants

To address the mechanisms behind the relationship between activity and phase-locking, we assessed how the effective connectivity and mean instantaneous membrane time constants varied with both activity level and phase-locking. The results of this analysis are shown in Figure 2.7. Figures 2.7a and b show how the effective connectivity varies with mean firing rate (Fig. 2.7a) and with phase-locking (Fig. 2.7b), as the input activity level was manipulated. A saturating relationship was observed with a fall off at very high levels. Figures 2.7c and d show the relationship between the mean membrane time constant and mean firing rate (Fig. 2.7c) and between the mean membrane time constant and phase-locking (Fig. 2.7d). As mean firing rate increases, the mean membrane time constant decreases (Fig. 2.7c). The decrease in mean membrane time constant is accompanied by an increase in both synchrony and effective connectivity between the simulated populations. The implications of this finding are discussed below.

Fig. 2.7a b

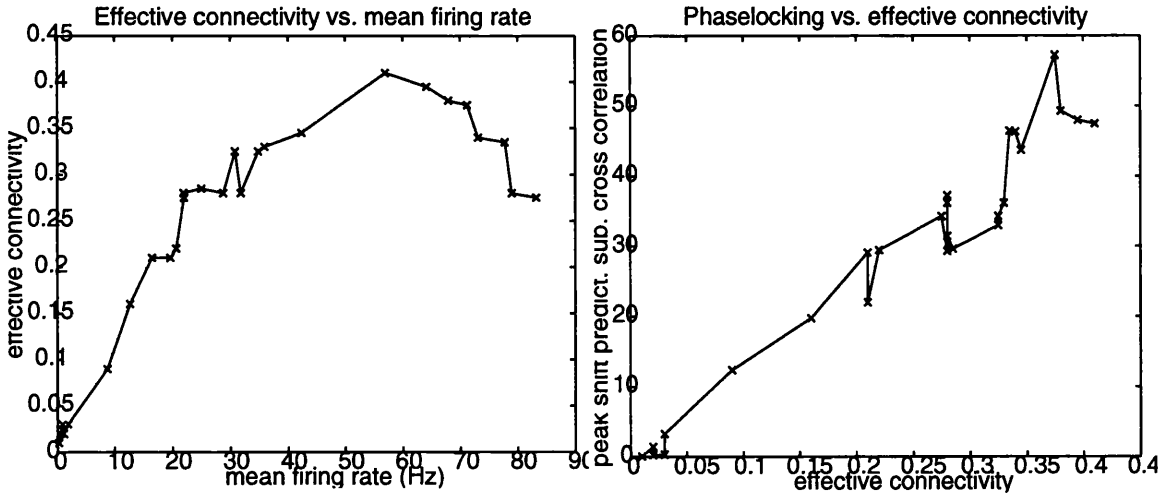

c d

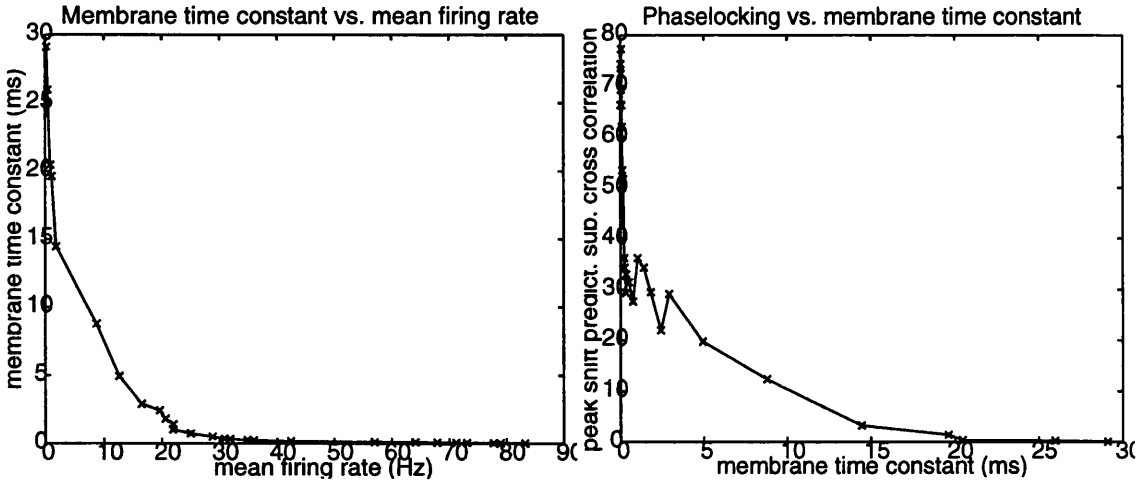

Fig. 2.7 (a) Effective connectivity between the two populations of the second model (as given by the average probability of a cell in population one causing a connected cell in population two to fire) is plotted against average firing rate. The extrinsic connectivity was 25% and the mean firing rate was manipulated by varying the input activity. (b) This is a graph of functional connectivity as given by the peak shift predictor subtracted cross correlation in terms of effective connectivity. (c) This is a plot of the mean membrane time constant, computed for each activity level, against mean firing rate and (d) is a plot of phase-locking as a function of the mean membrane time constant.

2.5 Discussion

Our results suggest that the phenomenon of phase-locking increasing with activity level is a robust effect that is relatively insensitive to the context in which the activity level is varied, to changes in the transmission delays, the type of synapse, the number of cells and also the laminar structure within the populations. They also show that functional connectivity (*i.e.* synchrony) varies with mean activity in much the same way as effective connectivity and that there is an almost monotonic relationship between the two metrics (Fig. 2.7b). These results clearly hold only for the simulations presented, which addressed unstructured, continuous or stationary dynamics. However, it may be reasonable to generalise the inference to real neuronal populations with similar simple architectures if they are expressing relatively stationary dynamics.

2.5.1 Activity Levels and Effective Connectivity

This work indirectly addresses the relationship between rate and synchrony coding and suggests that they may represent two perspectives on the same underlying dynamic. In this view, synchronized, mutually entrained signals enhance overall firing levels and can be thought of as mediating an increase in the effective connectivity between the two areas. Equivalently, high levels of discharge rates increase the effective connectivity between two populations and augment the fast synchronous exchange of signals. In a previous modelling study, Aertsen and Preißl (1990) showed that by increasing the level of network activity, the efficacy of the effective synaptic connections increases: "The efficacy varies strongly with pool activity, even though the synapse itself is kept at a fixed strength throughout all simulations. With increasing pool activity, the efficacy of the connection initially increases strongly to reach a maximum, after which it slowly decays again." This result is consistent with the findings presented in this chapter (Fig. 2.7a) and is intuitive; as the network activity is increased, the individual neuronal connections come into play more. This can be explained in the following way: If network activity is very low, the inputs to a single neuron (say neuron j) will only cause a sub-threshold excitatory post-synaptic potential (EPSP) in neuron j. If some pre-synaptic neuron (say neuron i) fires, so that it provides input to neuron j, this input will be insufficient to cause neuron j to fire. However, if the pool activity is high enough to maintain a slightly sub-threshold EPSP in neuron j, then an input from neuron i is more likely to push the membrane potential of neuron j over the threshold and elicit an action potential. This effect resembles the phenomenon of stochastic resonance (Wiesenfeld and Moss, 1995). As pool activity becomes very large, however, the coincident input to cell j will eventually become enough to make neuron j fire without any input from cell i, thus decreasing the influence that cell i has on cell j and consequently the effective connectivity between the two cells. This may explain the slow decline in effective connectivity as the network activity becomes very large (see Fig. 2.7a). In short, we can say that the pool activity provides a background neuronal tonus, that, depending on its magnitude, will make activity in neuron i more or less viable in eliciting activity in neuron j.

2.5.2 Activity Levels and Synchronization

The above argument pertains to the relationship between mean activity and effective connectivity but does not deal explicitly with the relationship between activity levels and synchronization. The present study examined the mechanistic basis of synchronized and oscillatory dynamics at high levels of activity. The membrane time constants were shown to decrease with mean activity and thus synchrony emerged with shorter membrane time constants. The decrease in time constants is a natural consequence of conjointly increasing membrane conductances through excitatory and inhibitory channels at high levels of activity (see appendix 4). i.e. The overall increase in background synaptic activity causes individual cell membranes to become more leaky, thereby decreasing their effective time constants

(Bernander *et al*, 1991). As activity levels increase, smaller membrane time constants promote the synchronous gain in the network. *i.e.* individual neurons become more sensitive to temporal coincidences in their synaptic inputs, responding with a higher firing rate to synchronous rather than asynchronous inputs. In other words, as the level of activity increases, network interactions tend towards synchronous firing. Put simply, there is a circular causality: Only synchronous interactions can maintain high firing rates when temporal integration is reduced. High firing rates reduce temporal integration. This behaviour underlies the emergence of self-selecting dynamics in which high degrees of synchrony can be both cause and consequence of increased activity levels.

It should be noted that in our model architecture, extrinsic excitatory connections targeted both excitatory and inhibitory neurons within the population. Further simulations are clearly needed to determine if the relative proportion of excitatory targets is an important parameter in relation to the phenomena that we have observed. One conjecture, however, is that it is not the overall excitation or inhibition elicited by afferent input that determines the dynamics, but rather the increase in membrane conductance consequent upon the conjoint increase in balanced excitatory and inhibitory activity. In other words, driving predominantly inhibitory sub-populations will inhibit excitatory cells or driving excitatory cells will excite inhibitory cells. In both cases, the overall level of excitatory and inhibitory presynaptic discharges will reduce the effective membrane time constants and predispose the population to fast dynamic and synchronised dynamics.

2.5.3 Uncoupling of Activity and Synchronization

The overall impression given by our results is that there is an obligatory relationship between mean activity and synchronised interactions. This is mediated by decreases in the effective membrane time constants under high levels of activity. Due to the reduced capacity for temporal integration the only dynamics that can ensue are synchronous ones. It is important, however to qualify this conclusion by noting that, in this study, the inputs driving the coupled neuronal populations were spatiotemporally unstructured and continuous. Clearly, desynchronization between two dynamic cell assemblies is not only a possibility but can be observed in both the real brain and simulations where changes in synchrony have, in some instances, been found to occur without any change in mean firing rate. Such regional decoupling of spike timing and firing rates has been reported in primary sensory cortices (Roelfsema *et al*, 1994, deCharms *et al*, 1996, Fries *et al*, 1997) and may reflect feedback influences from higher cortical areas (Lumer *et al*, 1997). Our input stimulus consisted of unstructured random noise that did not have any spatiotemporal structure. Furthermore, our models did not include any feature selectivity (orientation columns etc.). It is this feature specificity and stimulus structure that may cause a regional decoupling of synchrony and firing rate. This decoupling could specify which neuronal populations are excluded from dynamic cell assemblies coding for the feature in question. It could be that the temporal

patterning of action potentials in primary areas, that show a regional decoupling between synchrony and firing rate, may in turn lead to changes in firing rates in the areas that they target and thus such changes in synchrony will be reflected in changes in global activity levels (*i.e.* summed over all dynamic cell assemblies) if not local activity levels. In other words, a particular population could maintain high levels of desynchronised activity, in relation to its inputs from one cell assembly, if it was part of another dynamic cell assembly that did exhibit a coupling between overall activity and synchrony.

In essence, although the coupling that we have shown between mean activity and synchronization may represent a generic property of cortical dynamics, it should be noted that, desynchronized interactions can arise from non-linear coupling of a stronger sort than that employed in our current model or by specific inputs that selectively engage distinct cohorts of interacting populations. Other mechanisms that may cause synchrony to decouple from firing rates include those that are capable of modulating firing rates as synchrony increases, such as fast synaptic changes. However, in the context of our studies that looked explicitly at stationary dynamics, this is unlikely to be an explanatory factor. These and other parameters have to be explored before any definitive statements can be made about the relationship between mean activity and synchronization in a real world setting. However, our results point to some fundamental aspects of neural interactions, under a minimal set of assumptions. In the next chapter we revisit the relationship between mean activity and synchrony in the context of evoked transients.

2.5.4 Implications

The final point, that can be made on the basis of our findings, relates to macroscopic measures of neural activity such as those used in functional brain imaging. In recent years, functional magnetic resonance imaging and positron emission tomography have been established as tools for localising brain activity in particular tasks using the blood oxygenation level dependent response (BOLD signal in fMRI) and blood flow (PET). The fMRI BOLD signal is attributed to changes in local venous blood deoxygenation. These studies rely on the assumption that such changes are representative of global synaptic activity levels. This is supported by optical imaging studies (Frostig *et al*, 1990) showing that there is a local coupling between neuronal activity integrated over a few seconds, and the micro-circulation (haemodynamics). The lack of temporal sensitivity of fMRI raises the possibility that such measurements will fail to identify areas in which neuronal processes are expressed solely in terms of changes in synchrony. However, the present study demonstrates a clear link between mean firing rates and synchronization, suggesting that metrics based on mean synaptic activity may, in part, be sensitive to changes in synchronization. In the next chapter, we use simulations to address the related issue of evoked transients and dynamic correlations.

Chapter 3: Evoked Neuronal Transients and Dynamic Correlations

3.1 Abstract

In this chapter we used biologically plausible simulations of coupled neuronal populations to address the relationship between phasic and fast coherent neuronal interactions and macroscopic measures of activity that are integrated over time, such as the BOLD response in fMRI. Event related, dynamic correlations were assessed using joint peri-stimulus time histograms and, in particular, the mutual information between stimulus induced transients in two populations. This mutual information can be considered as an index of functional connectivity. Our simulations showed that functional connectivity or dynamic integration between two populations increases with mean background activity and with stimulus-related rate modulation. Furthermore, as the background activity increases, the populations become increasingly sensitive to the intensity of the stimulus in terms of a predisposition to transient phase-locking. This reflects an interaction between background activity and stimulus-intensity in producing dynamic correlations, in that background activity augments stimulus-induced coherence modulation. This is interesting from a computational perspective as background activity establishes a context that may have a profound effect on event-related interactions or functional connectivity between neuronal populations. Finally, total firing rates, that subsume both background activity and stimulus-related rate modulation, were almost linearly related to the expression of dynamic correlations over large ranges of activities. These observations show that under the assumptions implicit in our model, rate specific metrics based upon rate or coherence modulation may be different perspectives on

the same underlying dynamics. This suggests that activity (averaged over all peri-stimulus times), as measured in neuroimaging, may be tightly coupled to the expression of dynamic correlations.

3.2 Introduction

In the previous chapter (and see Chawla *et al*, 1999), we found, using computer simulations of coupled neuronal populations, that mean activity and synchronization were tightly coupled during relatively steady state dynamics. This allowed us to make inferences about the degree of phase-locking or synchronization among, or within, neuronal populations given macroscopic measures of activity such as those provided by neuroimaging. This chapter is about the relationship between fast dynamic interactions among neurons, as characterized by multiunit electrode recordings of separable spike trains, and measures of neural activity that are integrated over time (e.g. functional neuroimaging). In particular we address the question, "can anything be inferred about fast coherent or phasic interactions based on averaged macroscopic observations of cortical activity?". This question is important because a definitive answer would point to ways in which electrophysiological findings (from single and multi-unit recordings in vivo) might inform functional neuroimaging studies that employ a train of stimulus or task events to detect changes in time-integrated activity.

The basic hypothesis of this chapter is that fast dynamic interactions between two neuronal populations are a strong function of their background activity. This hypothesis derives from a series of compelling computational studies (e.g. Boven and Aertsen, 1990, Aertsen and Preiβl, 1991, Aertsen *et al*, 1994). In other words the dynamic coupling between two populations, reflected in changes in their coherent activity over a time-scale of milliseconds, cannot be separated from the context in which these interactions occur. This context is shaped by the population dynamics expressed over extended periods of time and in particular the overall level of activity. This is based on the common sense observation that the responsiveness of one unit, to the presynaptic input of another distant unit, will depend on postsynaptic depolarization extant at the time the presynaptic input arrives. In the previous chapter, using relatively steady state dynamics (ie. in the absence of induced transients), we showed that the mean firing rate and average phase-locking between two populations were tightly coupled in all regions of the model's parameter space. There could therefore be a link between mean activity and the emergence of dynamic correlations over a time scale of milliseconds. Previous modelling work has shown it to be the case that functional and effective connectivity vary strongly with background population activity (Boven and Aertsen, 1990, Aertsen and Preiβl, 1991, Aertsen *et al*, 1994). In this chapter, we pursue this same question but with a more refined analysis of dynamic correlations.

We expected that the emergence of phasic coherent interactions between two populations is both facilitated by, and results in, high mean population activity, suggesting high background

population activity levels may be a necessary condition for the emergence of fast interactions. In order to examine this, we measured the short term correlation structures between two simulated time-series as characterized by the joint peristimulus time histogram (J-PSTH). The advantages of this characterization include a proper assessment of phasic and stochastic interactions over peri-stimulus time, where these interactions are referred to a stimulus or behavioural event. Using simulations, we show that the expression of dynamic correlations is a strong function of the mean activity (averaged over time) extant in the two populations at the time that these interactions are expressed. Furthermore, we show an interaction between background and evoked firing rate changes that is mediated by activity-dependent changes in functional coupling.

Although previous work has established that the effective connectivity among neurons is sensitive to mean levels of population activity, the specific issue we wanted to address in this work was how this activity-dependent change in functional coupling would be expressed in terms of integrated firing rates. This is important from the point of view of neuroimaging where only time integrated measures of activity are available. These averages include a number of components, firstly the background activity and secondly stimulus-related rate modulation. The latter component may be a strong function of the effective connectivity within and among neuronal populations and consequently the background activity itself. The interaction between background and evoked rate modulation mentioned at the end of the previous paragraph is therefore an important phenomenon when trying to interpret responses observed with functional neuroimaging. For example, consider the cortical responses to a train of stimuli measured when the subject was attending and not attending to these stimuli. Increased time integrated responses maybe due to attentional modulation of background activity, increased stimulus related rate modulation or both. Demonstrating an obligatory increase in rate modulation with background activity in neuronal stimulations would greatly simplify the interpretation of imaging results because it would suggest that both mechanisms were being expressed. In order to address the interaction between background activity and stimulus intensity in modulating event-related responses, we varied both while measuring the total integrated activity and dynamic correlations.

This chapter is divided into three sections. The first section describes the synthetic neural model upon which our simulations were based. Section 2 describes a characterization of the model dynamics in terms of short-term interactions using J-PSTHs and mutual information. The final section establishes a relationship between the expression of short-term interactions (dynamic correlations) and macroscopic descriptors of the population dynamics (mean activity), revealed by varying the strength of the simulated stimulus and the background tonic activity levels. On the basis of these simulations we were able to characterise the specific form for the relationship between fast dynamic interactions and mean activity in two neuronal populations and look at the interaction between background activity and stimulus intensity in mediating changes in these measures.

3.3 The Neural Model

Individual neurons, both excitatory and inhibitory were modelled as single-compartment units. Spike generation in these units was implemented according to the Hodgkin-Huxley formalism for the activation of sodium and potassium transmembrane channels (see chapter 1). In addition, synaptic channels provided fast excitation (AMPA) and inhibition (GABAa) as in the previous chapter. Intrinsic (intra-area) connections were twenty percent inhibitory and eighty percent excitatory (Beaulieu *et al*, 1992). Extrinsic (inter-area) connections were all excitatory. Transmission delays for individual connections were sampled from a non central Gaussian distribution. Intra area delays had a mean of 2ms and a standard deviation of 1ms and inter area delays had a mean and standard deviation of 5ms and 1ms respectively. We modelled two areas that were reciprocally connected. Both consisted of a hundred cells that were 90% intrinsically connected and 5% extrinsically connected. Excitatory NMDA synaptic channels were incorporated in the model (see chapter 1, p42), in addition to the excitatory AMPA and inhibitory GABAa synaptic channels. These NMDA channels were only used in the feedback connections.

Transient dynamics were evoked by providing a burst of noise to population one. The simulated spike trains from units in both populations were averaged over the population, binned into four millisecond bins and then smoothed using a Gaussian kernel with a half height full width of 16ms. These spike trains were then analyzed, using the Joint Peri Stimulus Time Histogram (J-PSTH) (Gerstein *et al*, 1969, 1972, 1989, Aertsen *et al*, 1991). The stimulus was provided to population one for a duration of thirty five milliseconds at intervals of five hundred milliseconds. For each analysis, the model was run for a total of 64 seconds of simulated time. This was repeated under different levels of background noise and stimulus intensity, using either AMPA or NMDA feedback receptors.

3.4 Characterizing Dynamic Correlations with the J-PSTH

3.4.1 Peristimulus Time Histograms

The display format (Fig. 3.2) has three components. Plotted along each side of the square matrix (ie. the J-PSTH) are ordinary PST (peri-stimulus time) histograms. PST histograms represent the stimulus time locked average rate modulation. As an index of the total background activity and stimulus-induced rate-modulation, we measured the integral under the PSTH of the first population. This served as our macroscopic measure of neural activity that would be measured by, for example, fMRI or PET and represents the first dependent

variable in our characterization. The second dependent variable was a measure of the dynamic correlations based on the J-PSTH or cross-correlation matrix expressed in terms of mutual information (see below). A detailed explanation of how to read J-PSTHs is given in appendix 5.

3.4.2 Coincidence Time Histogram and Cross Correlogram

The component of the analysis in the right panel (Fig. 3.2) is the PST coincidence histogram or coincidence time histogram (CTH). This represents the stimulus time locked average of near coincident firing (which is simply the leading diagonal of the J-PSTH). This graph thus shows how the level of coherent firing or synchrony (plotted vertically) varies with peri-stimulus time (plotted horizontally). The cross correlogram is the third component. The cross correlogram characterises the degree of coherence averaged over all peristimulus times at some time lag. Because it is not sensitive to dynamic modulation of coherence, it is not used further in this chapter. Similarly, we do not use the CTH because, being a metric of coincident firing at near zero time lags, it is an impoverished metric of dynamic correlations that could be expressed at non-zero time-lags.

3.4.3 A Mutual Information Measure of Dynamic Correlations

For the purposes of this chapter we were interested in how stimulus induced dynamic correlations varied as a function of background noise, stimulus strength and the interaction between these two factors. As a measure of the dynamic correlations, induced between our two simulated populations, we used the mutual information between the stimulus induced transients having corrected for mean rate modulation. The calculation and interpretation of mutual information is described in appendices 6 and 7.

In what follows we examine the way in which the mutual information or functional connectivity changes with integrated firing rate. We did this by manipulating the strength of the stimulus under different levels of background activity. This enabled us to not only assess the effects of changing background activity and stimulus strength on mutual information (and integrated rate) but also to characterise any interaction between these two manipulations. The background noise levels were characterized in terms of the average depolarization produced, namely -65.9, -63.4, -63.2 and -61.2 mV. These values were calculated after applying a given noise level to both populations, running the simulation for 64 seconds and computing the mean membrane potential over units and time. The stimulus intensities used were 10, 25, 50, 75, 125, 150, 175, 200, 225 and 250 Hz. Noise level and stimulus intensity represent our two independent variables that were expected to produce changes in the two dependent variables (integrated rate and mutual information).

3.5 Results

3.5.1 The Relationship between Dynamic Correlations and Integrated Rate

We found that increases in either background noise or the strength of the stimulus were universally associated with increases in both integrated rate and mutual information. Furthermore, both dependent variables (rate and mutual information) were highly coupled in an almost linear fashion. Fig. 3.1b shows plots of mutual information against integrated rate for three different levels of background noise demonstrating the coupling between these measures, irrespective of how different levels of either were elicited. Because of this tight relationship, we focussed on how the independent manipulations (background noise and stimulus intensity) affect mutual information (equivalent effects were observed on integrated rate). Two examples of the mean time course of activity (c.f. local field potential, LFP) in population one under two levels of background activity are illustrated in Fig. 3.1a.

3.5.2 The Effect of Background Activity and Stimulus Intensity on Dynamic Correlations

Fig. 3.1c shows mutual information as a function of stimulus intensity for the three levels of background activity. As background noise increased, the gradient of the mutual information vs. stimulus intensity plot also increased. A formal test for the differences in regression slopes confirmed the significance of this effect (t-statistic = 2.2, residual degrees of freedom = 53, p-value = 0.016 for the average increase from low to high background activities over NMDA and AMPA simulations using multiple regression and the appropriate contrast). This is clear evidence of an interaction between tonic background activity and stimulus-induced rate modulation in the genesis of dynamic correlations. In other words, high background activity increased the sensitivity of evoked dynamic correlations to increased stimulus intensity. This is demonstrated more clearly below. These phenomena were evident irrespective of whether we used NMDA (upper panels) or AMPA-like (lower panels) feedback receptors.

Fig. 3.1a

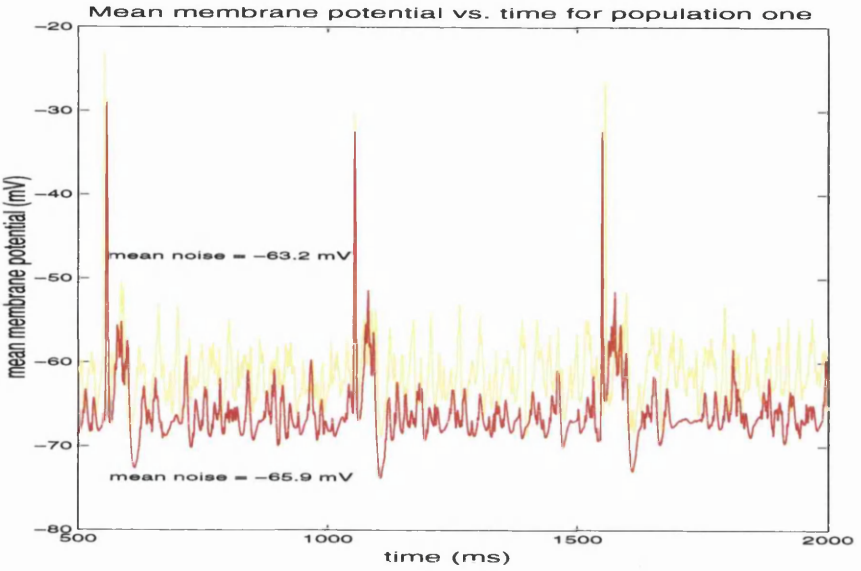
Mean membrane potential vs. time for population one
mean membrane potential (mV)
time (ms)
mean noise = −63.2 mV
mean noise = −65.9 mV

b

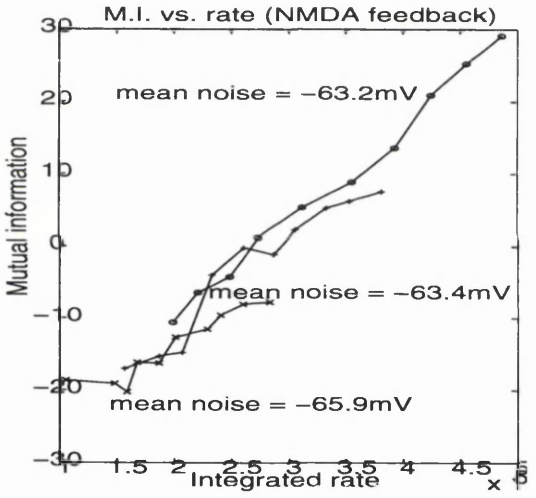
M.I. vs. rate (NMDA feedback)
Mutual information
Integrated rate
mean noise = −63.2mV
mean noise = −63.4mV
mean noise = −65.9mV

c

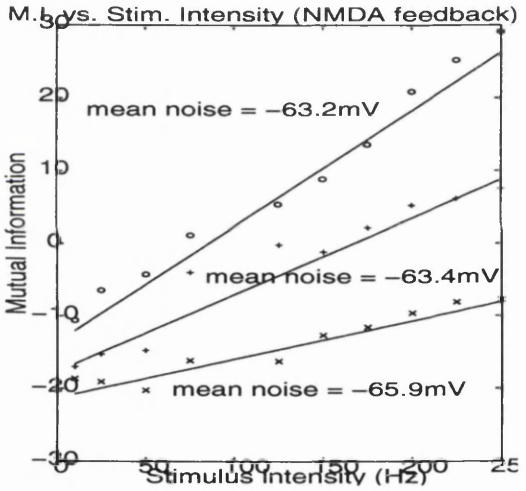
M.I. vs. Stim. Intensity (NMDA feedback)
Mutual Information
Stimulus Intensity (Hz)
mean noise = −63.2mV
mean noise = −63.4mV
mean noise = −65.9mV

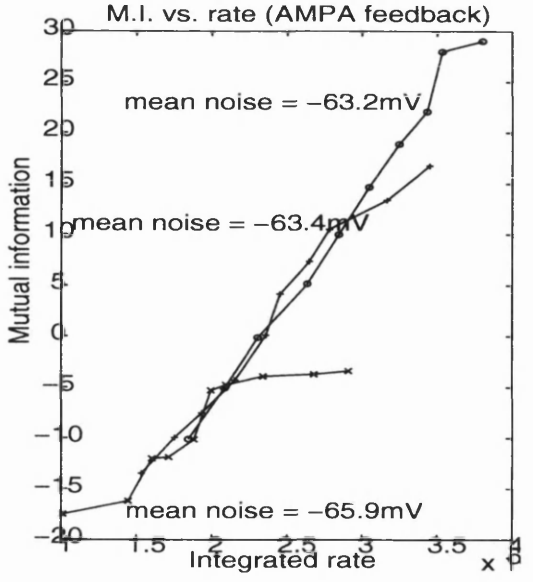
M.I. vs. rate (AMPA feedback)
Mutual information
Integrated rate
mean noise = −63.2mV
mean noise = −63.4mV
mean noise = −65.9mV

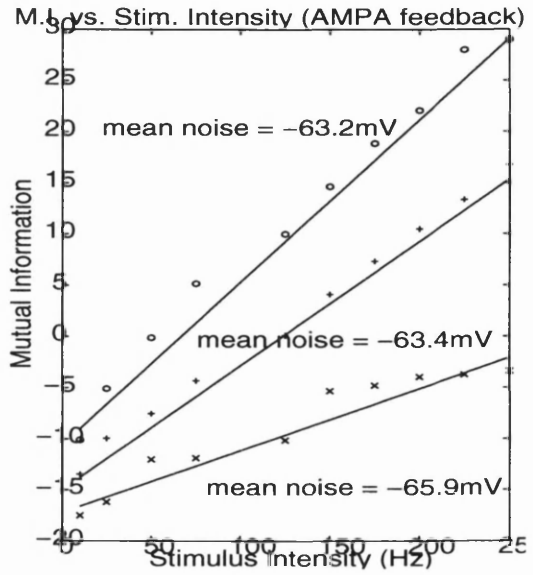
M.I. vs. Stim. Intensity (AMPA feedback)
Mutual Information
Stimulus Intensity (Hz)
mean noise = −63.2mV
mean noise = −63.4mV
mean noise = −65.9mV

Fig. 3.1 (a) illustrates the mean membrane potential for one stimulus strength at two of the background noise levels. This graph shows the mean membrane potential over three inter-stimulus intervals (*i.e.* 1500 ms). (b) Plots of stimulus induced mutual information between the two populations against integrated rate (as indexed by the integral under the PSTH) for three different levels of background activity. The stimulus intensity was varied through 10, 25, 50, 75, 125, 150, 175, 200, 225 and 250 Hz. The upper panel shows the results when the model was implemented with NMDA feedback receptors, and the lower panel with AMPA feedback receptors. (c) shows the same as in (b) but now mutual information is plotted against the stimulus intensities used. In (c), the regression slopes of mutual information on stimulus intensity are plotted.

3.5.4 Examples of these Effects Demonstrated with J-PSTHs

Figure 3.2 presents J-PSTHs between the two populations, at two different levels of background activity and with two different stimulus intensities. It can be seen that, when the stimulus was very weak and the background noise was low, the presence of the stimulus had almost no effect on the synchronous interactions between the populations as it was not strong enough to enable the populations to entrain each other to any extent (see CTH of Fig. 3.2a). However, when the background noise was increased, this same stimulus had a definite effect on the dynamic correlations as can be seen in Fig. 3.2b (the background activity level in Fig. 3.2b is higher than any of the background levels in Fig. 3.1). At the low background activity level as in Fig. 3.2a, when the stimulus was very strong, extremely significant dynamic correlations occurred (Fig. 3.2c), in contrast to when the stimulus was weak and induced minimal dynamic correlations (Fig. 3.2a). At the high background noise level as in Fig. 3.2b, when the stimulus was very strong as in Fig. 3.2c, the synchronization induced never died away and high levels of synchrony were maintained (Fig. 3.2d).

Fig. 3.3 shows mutual information as a function of integrated rate at the very high background activity level as in Fig. 3.2b, d. This shows that at such high background levels, the plot of mutual information vs. integrated rate eventually levels off, at which point, increasing the stimulus intensity will no longer facilitate an increase in the mutual information between the two populations. This demonstrates nicely the "saturation phenomenon" as seen in Fig. 3.2d. Fig. 3.2d showed that with a very high background noise, the stimulus intensity may reach a level at which the synchronization induced never dies away. Increasing the stimulus intensity further then has little or no effect.

Fig. 3.2

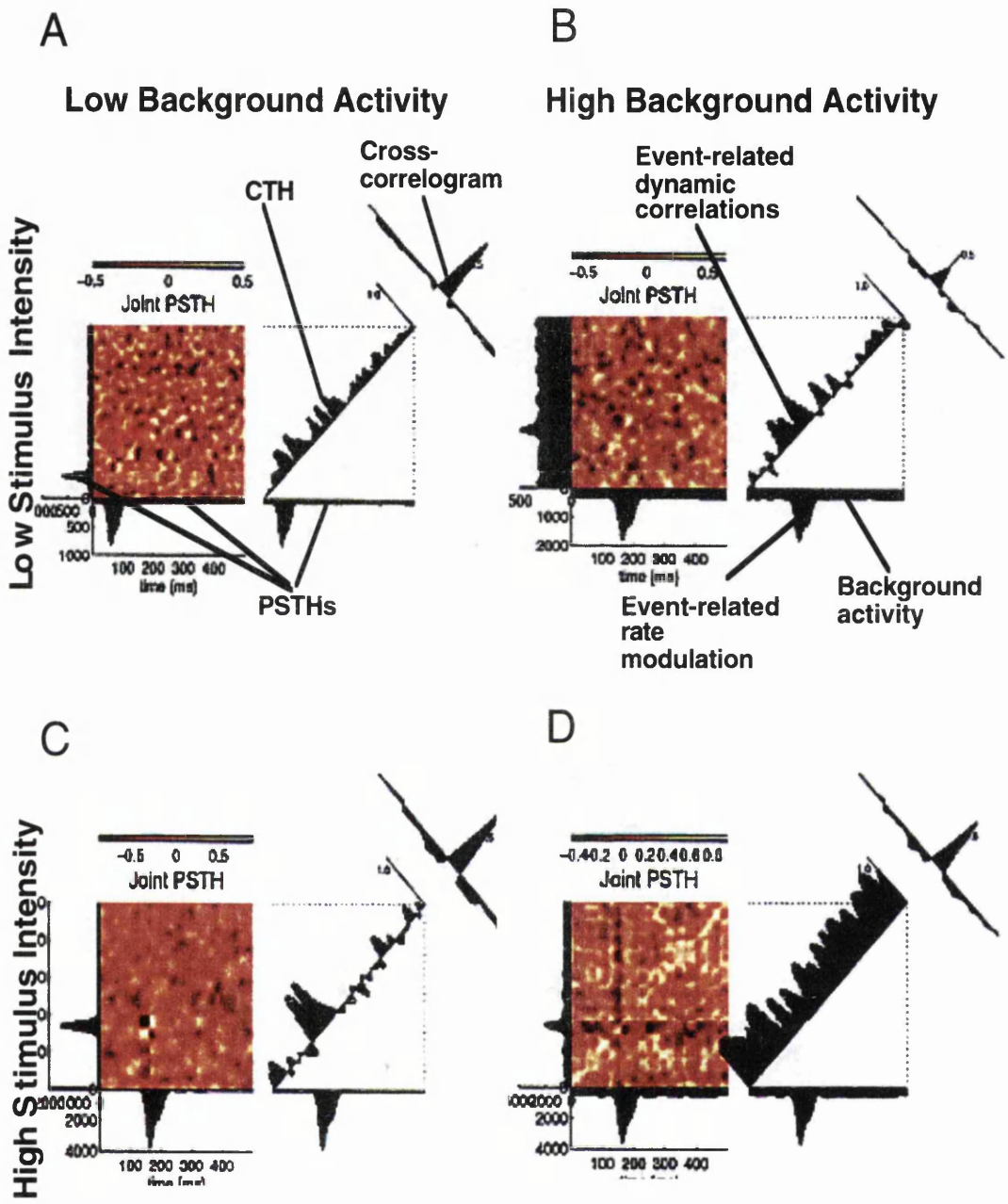

Fig. 3.2 (a) J-PSTH for the simulated populations at the lowest background noise level (see Fig. 3.1) and similarly with a very weak stimulus applied every 500 ms for 35ms. (b) J-PSTH at the highest background noise level (the same as in Fig. 3.3) and with the low intensity stimulus as in Fig. 3.2a. (c) J-PSTH for the neuronal populations at the low background activity as in Fig. 3.2a and with a high intensity stimulus. (d) J-PSTH at a high background activity level as in Fig. 3.2b and with the high intensity stimulus as in Fig. 3.2c.

Fig. 3.3

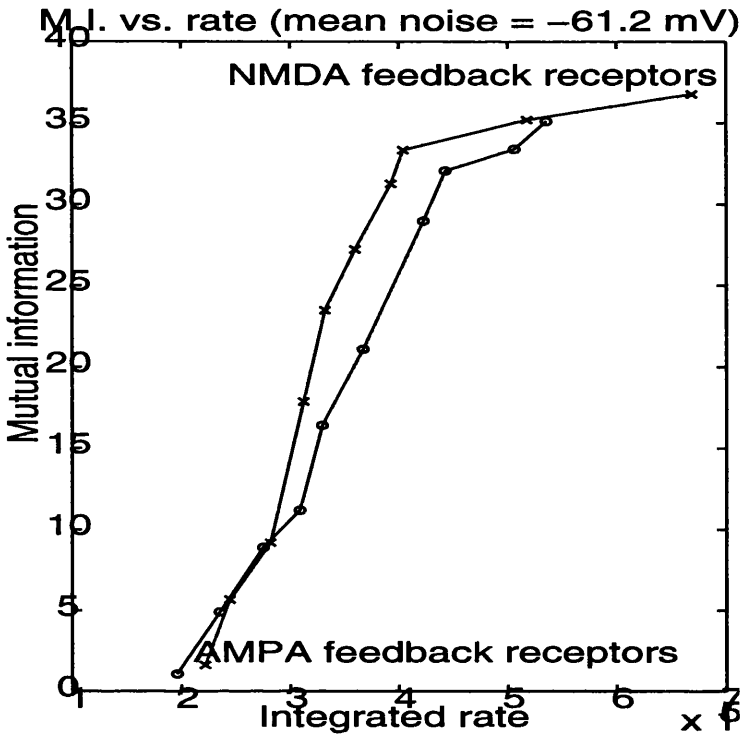

Fig. 3.3 Mutual information is plotted against integrated rate for the highest noise level, as depicted in Fig. 3.2b,d, under both AMPA and NMDA feedback receptors. The stimulus intensity is varied through the same values as in Fig. 3.1.

3.6 Discussion

There are several lines of evidence in support of our findings that a systematic relationship between fast dynamic interactions (measured here in terms of mutual information or functional connectivity) and macroscopic measures exist: Aertsen & Preiβl (1991) investigated the behaviour of artificial networks, analytically and using simulations. They concluded that short term effective connectivity varies strongly with, or is modulated by, pool activity as discussed in the previous chapter (see p66).

In the previous chapter, we demonstrated that sustained synchrony shows a monotonic relationship with mean activity. As mean activity in the network increases, the mean instantaneous membrane time constants decrease, giving rise to a higher level of synchrony. The decrease in time constants is a natural consequence of conjointly increasing membrane conductances through excitatory and inhibitory channels at high levels of activity. Hence, as activity level increases, smaller membrane time constants increase the synchronous gain in the network. *i.e.* individual neurons become more sensitive to temporal coincidences in their synaptic inputs, responding with a higher firing rate to synchronous rather than asynchronous inputs. Therefore, in the present event-related context, as background noise increases, the network becomes more prone to stimulus-induced synchronous transients. This is reflected both in the time that the post-stimulus synchronization endures and a progressive increase in the mutual information vs. stimulus intensity regression slope. The latter effect constitutes an interaction and can be viewed as a stimulus-dependent effect that is context-sensitive. In this instance, the context is set by the tonic background of activity and is mediated through a diminution of the effective membrane time constants.

Our findings provide the basis for two fairly important conclusions. The first is that increasing the tonic or background activity can potentiate the transient or dynamic correlations induced by a salient stimulus or behavioural event. As mentioned above, this simple phenomenon might provide a useful mechanism in the brain for exerting control over functional integration between neuronal populations in a context dependent fashion. For example, attentional modulation of background activity in distinct sensory neuronal populations could be used to selectively enhance neuronal interactions in a topographically constrained way (Frith and Friston, 1997). The fact that a higher mutual information between our simulated neuronal populations was induced under conditions of higher noise is presumably very similar to stochastic resonance (Wiesenfeld and Moss, 1995), wherein small amounts of stochastic noise facilitate non-linear transformations, in this instance effected by interacting neuronal populations. This phenomenon is interesting because of its almost counter-intuitive nature. Indeed, it might be thought that increased background noise may lead to a greater difficulty in distinguishing a transient signal from noise. However, this is not necessarily the case. Mainen and Sejnowski, 1995, have shown that noisier neuronal input can increase the precision of the cell spikes, thus increasing the sensitivity of the cells to their inputs. Their data suggests: "a low intrinsic noise level in spike generation, which could allow cortical neurons to accurately transform synaptic input into spike sequences, supporting a possible role for spike timing in the processing of cortical information by the neocortex." (Mainen and Sejnowski, 1995).

The second conclusion has a more practical importance and pertains to the interpretation of neuroimaging studies in which only macroscopic observations of rate modulation are generally allowed. By simply demonstrating a systematic and consistent relationship between rate modulation (integrated rate over peri-stimulus time) and coherence modulation (the mutual information associated with dynamic correlations), one can be comfortable with the

probability that functional neuroimaging is not totally insensitive to event-related fast coherent interactions of the sort mediated by dynamic correlations. This is important given the possible role that dynamic correlations may play in sensori-motor and cognitive operations (Vaadia *et al.* 1995). This conclusion leads to the more general point that specific metrics based upon rate or coherence modulation may be different perspectives on the same underling dynamics. In this view, synchronized, mutually entrained signals enhance overall firing levels and can be thought of as mediating an increase in the effective connectivity between the two areas. Equivalently, high levels of discharge rates increase the effective connectivity between two populations and augment the fast synchronous exchange of signals. In this sense there is an almost circular causality in the relationship between rate and transient synchronisation. Although we manipulated mean background activity in our simulations, much of the variability in integrated rates over peri-stimulus time, can be accounted for by the dynamic correlations induced by the stimulus. In other words a high mean level of activity facilitates transient coherent interactions, above and beyond those predicted by dynamic rate modulation itself. These dynamic correlations in turn cause a mutual entrainment of the interacting populations and augment activity levels for a period of time. At very high levels of activity any stimulus evoked transient might ignite the system leading to high levels of synchrony and mean activity that are self-maintaining (see Fig.s 3.2 and 3.3).

The statement that the distinction between temporal and rate coding is simply a matter of perspective is a strong one that is made with some expectation of it being refuted. Although it is clearly possible that the information conveyed by the precise timing of spikes is very different from that conveyed by discharge rates, from the point of view of population dynamics it may be the case that changes in spike timing cannot be divorced from changes in firing rate given the neuronal infrastructure employed by the brain. The point being made here is that due to the intimate relationship between the temporal patterning of pre-synaptic events (either in terms of phase-locking as discussed in the previous chapter (and Chawla *et al,* 1999), or in terms of dynamic correlations as considered in the present chapter), and post-synaptic discharge probabilities, an increase in synchronised input will inevitably result in higher population discharge rates. The mechanisms that underlie this relationship may involve increased membrane conductances, decreased effective membrane time constants and an increase in synchronous gain mediated by impoverished temporal integration. Put simply, under the constraints imposed by the emergent non-linear dynamics of neuronal circuits, one cannot change the fine temporal structure of discharge patterns without changing population activity (this is a point being made by the results in Fig. 3.1, showing a monotonic relationship between integrated firing rate and mutual information). If changes in one metric of neuronal dynamics, such as spike timing, are universally associated with changes in another metric, such as population activity, then the two metrics are mutually redundant and reflect different measures of the same underlying dynamics. It should be noted that these observations pertain to, and only to, population codes.

In summary, we have shown that background activity levels in simulated neuronal populations

facilitate and are facilitated by the expression of stimulus induced dynamic correlations. These findings have implications for the context-dependent aspects of stimulus related neuronal interactions and also inform the interpretation of neuroimaging measures of neurophysiology.

Section 2:

Empirical Investigations

Chapter 4: fMRI Methods

4.1 Introduction

In this chapter, we review the pre-processing and analysis of fMRI data and discuss briefly some of the issues that are encountered. The next two chapters describe the application of these methods to empirical studies that were predicated on the theoretical work described in the previous chapters.

4.2 Data acquisition

Our functional imaging experiments were performed using a 2 Tesla magnetom VISION (Siemens, Erlangen) whole body MRI system equipped with a head volume coil. Data were obtained from normal subjects using T2* - weighted fMRI images. In the first functional imaging study in this thesis, (chapter 5, section 1), we acquired 48 axial slices at 100ms/slice giving a repetition time, per volume, of 4.8s. The volume acquired covered the whole brain (48 slices). In the second study, however (chapter 5, section 2), as we had already identified our visual areas in the back of the brain, we acquired only 16 axial slices with a 3mm thickness at 100ms/slice giving a repetition time, per volume, of 1.68s. This allowed us to acquire many more scans in the second study. Contiguous multislice T2* weighted images (TE = 40ms; 64x64 pixels [19.2cm x 19.2cm]) were obtained with echo-planar imaging (EPI). A T2* weighted sequence was chosen to enhance blood oxygenation level dependent (BOLD) contrast.

4.3 Data Analysis

Image processing and statistical analysis were carried out using SPM96 (Friston *et al*. 1996: Friston *et al.* 1995; Worsley and Friston 1995,{http://www.fil.ion.ucl.ac.uk/SPM}). The data were analyzed using multiple regression as implemented in SPM96 using box-car stimulus functions convolved with a haemodynamic response function (see below). As movement-related variance components in fMRI time-series represent one of the most serious confounds of analysis, all volumes were realigned to the first volume (Friston *et al* 1995). This was done by estimating the movement relative to the first scan by using a least squares method and then using the obtained estimates to realign the scans. A mean image was created using the realigned volumes. A structural MRI, acquired using a standard 3-D T1 weighted sequence (1x1x3 mm voxel size), was coregistered to this mean (T2*) image. This ensured that the functional and structural images were in the same space. Finally the structural image was spatially normalised (Friston *et al* 1995) to a standard template (Evans *et al* 1993; Talairach and Tournoux 1988), using a non-linear transformation. This non-linear deformation employs non-linear deformations using spatial basis functions as described in Friston *et al* (1995). The transformation, mapping the structural T1 MRI scan onto the template, was applied to the fMRI data. The data were smoothed using an isotropic Gaussian kernel. Smoothing is useful as this generally increases signal relative to noise. In fMRI, the noise can be regarded as independent for each voxel and has therefore very high spatial frequency components. Secondly, convolving with a Gaussian kernal conditions the data in the sense that the data conform more closely to a Gaussian field model. This is important if one wants to use the theory of Gaussian fields to make statistical inferences about (i.e. assign p-values to) the ensuing regionally specific effects. The requirements that the data be a good lattice representation of a Gaussian field includes (1) that the autocorrelation function be twice differentiable and (2) that the spatial correlations be stationary. Both these requirements are assured (approximately) after smoothing. The final reason for smoothing is that it allows haemodynamic changes from subject to subject to be assessed on a spatial scale that shows meaningful homologies. This is important for intersubject averaging.

Inferences using SPMs can be of two sorts depending on whether one knows where to look in advance: With an anatomically constrained hypothesis, about effects in a particular brain region, the uncorrected p value associated with the height or extent of that region in the SPM can be used to test the hypothesis. With an anatomically open hypothesis (i.e. a null hypothesis that there is no effect anywhere in the brain) a correction for multiple dependent comparisons is necessary. The theory of Gaussian fields provides a way of computing this corrected p-value that takes into account the fact that neighbouring voxels are not independent by virtue of smoothness in the original data. Provided the data are sufficiently smooth the correction based on Gaussian field theory is less severe (i.e. is more sensitive) than a Bonferroni correction for the number of voxels.

4.4 The General Linear Model

The general linear model is an equation $\mathbf{Y} = \mathbf{X}\beta + \varepsilon$ that expresses the observed response variable $\mathbf{Y}$ in terms of a linear combination of explanatory variables $\mathbf{X}$ plus a well behaved error term (see Figure 2). The general linear model is variously known as 'analysis of covariance' or 'multiple regression analysis' and subsumes simpler variants, like the 'T test' for a difference in means, to more elaborate linear convolution models such as finite impulse response (FIR) models. The matrix $\mathbf{X}$ that contains the explanatory variables (e.g. designed effects or confounds) is called the 'design matrix'. Each column of the design matrix corresponds to some effect one has built into the experiment or that may confound the results. These are variously referred to as explanatory variables, covariates, regressors or, in fMRI, stimulus functions.

The general linear model can be used to implement a vast range of statistical analyses. The issue is therefore not so much the mathematics but the formulation of a design matrix $\mathbf{X}$ appropriate to the study design and inferences that are sought. The design matrix can contain both covariates and indicator variables. Each column of $\mathbf{X}$ has an associated unknown parameter. Some of these parameters will be of interest (e.g. the effect of particular sensorimotor or cognitive condition or the regression coefficient of haemodynamic responses on reaction time). The remaining parameters will be of no interest and pertain to confounding effects (e.g the effect of being a particular subject or the regression slope of voxel activity on global activity). Inferences about the parameter estimates are made using their estimated variance. This allows one to test the null hypothesis that all the estimates are zero using the F statistic to give an SPM{F} or that some particular linear combination (e.g. a subtraction) of the estimates is zero using a SPM{t}. The t statistic obtains by dividing a contrast or compound (specified by contrast weights) of the ensuing parameter estimates by the standard error of that compound. The latter is estimated using the variance of the residuals about the least-squares fit. An example of contrast weights would be [-1 1 0 0.....] to compare the differential responses evoked by two conditions, as modelled by the first two condition-specific regressors in the design matrix. If several parameter estimates are potentially interesting (e.g. using polynomial expansions (Buechel et al, 1995) or basis functions of some parameter of interest), then the SPM{F} is usually employed.

Temporal basis functions are important because they provide a graceful transition between conventional multilinear regression models with one stimulus function per condition and FIR models with a parameter for each time point following the onset of a condition or trial type. Temporal basis functions offer useful constraints on the form of the estimated response that retain (i) the flexibility of FIR models and (ii) the efficiency of single regressor models. In practice the implementation of these constrained FIR models involves setting up stimulus functions that model expected neuronal changes [e.g. box cars of epoch-related responses or spikes (delta functions) at the onset of specific events or trials]. These regressors are then

convolved with a set of basis functions that model the HRF, in some linear combination, and are assembled into the design matrix. The basis functions can be as simple as a single canonical HRF, through to a series of delayed delta functions. The latter case corresponds to a FIR model proper and the coefficients are the impulse response function for the event or epoch in question.

The advantage of using temporal basis functions (as opposed to an assumed form for the HRF) is that one can model voxel-specific forms for haemodynamic responses, as in section 1 of the next chapter, and formal differences (e.g. onset latencies) among responses to different sorts of events. The advantages of using basis functions over FIR models are that (i) the parameters are estimated more efficiently and (ii) stimuli can be presented at any point in the inter-stimulus interval. The latter is very important because time-locking stimulus presentation and data acquisition gives a biased sampling over peri-stimulus time and can lead to differential sensitivities, in multi-slice acquisition, over the brain.

4.5 Fixed Effects Analyses

In all three fMRI studies in this thesis, we only report those effects that were conjointly significant in all three subjects. This corresponds to a conjunction analysis using a fixed-effects analysis and allowed us to focus on the most robust and compelling features of our data. A technical point here speaks to the number of subjects analysed and the nature of the inferences we are making. By virtue of the fact that we use subject-specific estimates in our statistical model, these case studies can be regarded as single-subject studies and two replications. The inferences that we are making are quite sufficient at this case-study level and pertain to and only to the subjects studied. The alternative approach would be to make a random effects inference, where the activations would be collapsed within subjects and the degrees of freedom would be approximately the number of subjects studied. In this instance, we would require at least six subjects and probably many more. The motivation for using a random effects analysis is clear when one is trying to compare one group of subjects with another. Our study does not attempt to do this and simply makes observations about three normal subjects. This fixed effects approach is analogous to reporting careful statistical characterizations on two or three non-human primates. We emphasise this point because the distinction between a random and fixed effects analysis is likely to become more important in the future.

4.6 Subjects

All subjects that participated in the studies in this thesis gave informed consent and all of the

studies were approved by the National Hospital for Neurology and Neurosurgery Ethics Committee

4.7 Visual Stimuli

In all the ensuing fMRI experiments, visual stimuli were backprojected onto a screen in the scanner by an LCD video-projector. The active screen area was a square with a diameter of 37°. The screen refresh rate was set to 33.5 per second. The subjects were instructed to maintain visual fixation on the central focus.

4.8 Flicker Photometry

In the next chapter, we scan subjects in conditions where they view purely colour contrast stimuli, In these cases, luminance contrast was minimised using calibration in each individual with flicker photometry, just before the start of the scanning, in the scanner. Flicker photometry is a standard method used to isolate the P and M pathways and then, by targeting the M cells alone, minimise luminance difference between two colours. P cells code for wavelength and have been shown to code for visual stimuli with a tonic response, when the stimuli crosses the receptive field centre. In contrast, M cells code use luminance cues and code for visual stimuli with a fast phasic response (Lee et al, 1979). Therefore, if two colours are flashed quickly enough, the subject only sees one colour as the P cells are not fast enough to change the responses to the two cells and so blend the two responses into one. However, the M cells are still able to change their responses and when the subject sees minimum flicker between the colours, this reflects the minimisation in the M cell responses and consequently the luminance difference between the two stimuli. Obviously, this method is not perfect as it doesn't enable us to completely abolish luminance contrast, as photoreceptors at different eccentricities across the retina differ in their point of equiluminance.

Chapter 5: Speed-Dependent Motion-Sensitive Responses in V5: An fMRI Study

Section 1

5.1 Abstract

In chapter 1, we focused on the behaviour of the single neuron as the basis of the computational studies that comprise this thesis. This chapter serves to introduce the empirical basics of fMRI that underpin the neuroimaging study described in the next chapter. In this chapter we describe a study in which we used fMRI to study brain activity integrated over many neurons (over roughly several mm^3 of cortex). This fMRI study examined motion-sensitive responses in human area V5 as a function of stimulus speed. Consistent with electrophysiological findings, we observed optimal responses at intermediate speeds of around 7 to 30 °/s. The results are consistent with a non-linear (inverted 'U') dependency on speed. The same dependency was also observed in V3a. V1 activation was observed to decrease linearly as speed increased. This is consistent with the fact that speed sensitive cells in V1 have been shown to be tuned to much slower speeds than in V5.

5.2 Introduction

The aim of this experiment was to determine how V5 human visual cortex activation varies as a function of stimulus speed and whether this relationship was the same for motion based on hue or luminance cues. Physiological results (Rodman *et al* 1987, Cheng *et al* 1994) show that most neurons in area V5 have an optimal response at speeds of between 4 and 16 °/s. We were interested in seeing how an fMRI study, assessing brain activation at various speeds, correlated with previous electrophysiological studies. We were also interested in whether colour and luminance elicits a differential motion sensitive response in V5.

A critical feature of our experimental design was that we characterized the speed-dependent responses of V5 under two different stimulus conditions, namely equiluminant and monochromatic. There are clear differences between motion defined by luminant and equiluminant coloured stimuli. Generally, it has been found that conditions of equiluminance deplete motion perception and equiluminant motion has been described as 'incoherent'. Electrophysiological and psychophysical evidence (Livingstone and Hubel, 1987, 1988) suggests that this is due to non-overlapping parallel pathways originating in the retina. Two streams, the magno and parvocellular are thought to analyze colour and luminance autonomously and process these attributes in striate and extrastriate cortex. Wavelength information is relayed by the Pß ganglion cells of the retina to the upper four parvocellular layers of the lateral geniculate nucleus (LGN). The P-cells have comparatively small receptive fields, a slow conduction velocity and are wavelength selective. The parvocellular or colour opponent pathway then continues to the blobs of area V1, the thin stripes and interstripes of area V2 and eventually to area V4. This stream's cells are not as finely tuned to luminance contrast and do not have the temporal resolution of the magnocellular pathway. Magnocellular cells have a high conduction velocity, large receptive fields and are sensitive to luminance contrast. This pathway is fed through the Pα ganglion cells of the retina which project to the lower two layers of the LGN and then to V1 and the thick stripes in V2 to terminate in V5.

If a moving foreground is of the same luminance as the background, the magnocellular pathway would not be able to function on the basis of luminance contrast and so, through the P pathway, foreground would be discriminated from background on the basis of wavelength alone. In this case, the smaller receptive fields and slower conduction velocities of the P cells would be an impediment to the efficient processing of motion. Lee *et al* (1979) used single unit recordings in primates to show that both M and P cells in the LGN respond to a bar moving through the cell's receptive field. They found that M cells code for the movement with a phasic response as a luminance contrast border crosses the receptive field border. In contradistinction, the P cells expressed a more tonic response that endured while the stimulus was in the receptive field. They also demonstrated that P cells have wavelength selectivity but no velocity selectivity, while M cells showed no wavelength selectivity but some were very sharply tuned for velocity. This implies that while M cells code, primarily, for visual motion

and speed, P cells code for the presence of a stimulus and its wavelength properties. Neuronal activity further along the visual processing pathways has also been characterised in terms of its selective responses. It has been found that although both colour and luminance defined stimuli activate neurons in V4 and V5 (Cheng *et al*, 1994), V5 is much more sensitive to luminance contrast than V4. In other words, using isochromatic stimuli, a relatively high luminance contrast will be needed to elicit the same response in V4 that would be elicited in V5 by low luminance contrast. Also, whereas V4 cells show quite a high response for chromatically defined stimuli, in comparison to luminance defined stimuli, and show selectivity for stimulus wavelength, V5 cells elicit only a slight response to isoluminant colour defined stimuli (Gegenfurter *et al*, 1994) and do not show wavelength tuning. Interestingly, Cheng *et al* (1994) showed that many V4 cells are just as tuned for speed as V5 cells but, unlike in V5, they do not show any direction selectivity. V4 and V5 cells evidenced mean optimal tuning at 32 degrees/second. However, they also showed that V5 cells, on the whole, had a slightly wider range of optimal speeds. ie. A few V5 cells had optimal speeds lying outside the range of optimal speeds seen in V4 (0.5 degrees per second at the lower end and 256 degrees per second at the higher end). Taken together, these findings are consistent with what would be expected in V4 and V5 given their affiliation with the P and M pathways respectively. However, some findings, indicate that motion processing may be distributed earlier in the processing pathways and may reflect the reciprocal anatomical connectivity between V4 and V5 (Ungerleider *et al*, 1986). Given this electrophysiological evidence, we were therefore interested in how motion-sensitive responses in V5 varied as a function of speed with stimuli that biased processing towards either the M or P pathways. This was achieved by changing the speed of stimuli under luminance and colour bias conditions respectively.

A further explanation for potential differential speed-sensitive responses, that we wished to explore, was that at slow speeds V5 is thought to receive input primarily from the primary visual cortex (ffytche *et al*, 1996). At faster speeds, visual input to V5 is thought to come directly from the retina through the superior colliculus and then the pulvinar and thus bypass V1. Because extrageniculate pathways bypass areas implicated in colour processing, we wanted to look at the differences between hue and luminance based motion- responses at higher speeds, relative to slower speeds.

Differential responses to stimuli of varying speeds in V5 may therefore reflect (i) speed - dependent responses intrinsic to V5 that are independent of whether processing at earlier stages occurs in the M or P pathways or (ii) differences attributable to the relative amount of P and M processing as stimulus speed increases. To adjudicate between these explanations, we looked at how V5 activation varies as a function of speed under conditions of colour bias, compared with that of luminance bias. Under isoluminant conditions, we assumed that processing in the P pathway was the major determinant of input to V5. Under isochromatic conditions, we assumed that M pathways were implicated. These two pathways have different speed-dependent behaviours. Our prediction was therefore that if (i) V5 responses mirror the

perceptual speed and reflect processing intrinsic to V5 then there should be no difference in the speed-dependency under isochromatic and isoluminant conditions. On the other hand (ii), if V5 responses have a component that is sensitive to the pathways engaged in earlier processing, then we would see different speed dependencies (*i.e.* a speed times cue bias interaction).

5.3 Methods

5.3.1 Stimuli

We used moving dots as our motion stimulus. The dots moved radially at a constant speed from the centre of the screen. We will refer to this stimulus as an "optic flow" stimulus because it is reminiscent of the movement of a visual pattern as one moves towards it. We used a parametric factorial design consisting of colour contrast bias stimuli and luminance contrast bias stimuli, both at five different speeds, plus a stationary dots condition that was used as the control between each moving stimulus presentation. The five speeds used were 3.7, 7.7, 15.4, 30.8 and 61.6 °/s. Optic flow stimuli were employed as this stimuli contains dots moving in many different directions, thus providing stimulation to motion sensitive cells with different direction selectivities. However, the direction of motion of the radially moving dots is constant. V5 stimulation is therefore purely due to motion and not changes of direction. Also, the centre of motion of the stimulus (centre of the optic flow field) is stationary and thus nystagmus is not induced (Tootell *et al*, 1995). In the colour contrast condition, luminance contrast was minimised using calibration in each individual with flicker photometry. It should be emphasised that as it is extremely difficult to attain isoluminance in psychophysical stimuli (we also had the added obstacle of creating isoluminant conditions in the scanner) so luminance contrast was not 'removed' by using flicker photometry but was simply minimised. It might therefore, be more accurate to think of our isoluminant condition as a low luminance heterochromatic condition. The colour contrast condition consisted of a green background upon which red dots (size 0.23°) moved radially from the central focus in random directions towards the border of the screen where they vanished. Background and foreground colours were swapped randomly throughout the runs to prevent bias due to cone dominance. The luminance contrast condition consisted of red dots on a red background. Each condition was followed by a stationary condition (either luminance or colour contrast depending on the prior condition) which consisted of frozen, colour contrast or luminance contrast defined dots in random positions on the screen.

5.3.2 Data Acquisition

We acquired 48 axial slices at 100ms/slice giving a repetition time, per volume, of 4.8s. The volume acquired covered the whole brain (48 slices). Contiguous multislice T2* weighted images (TE = 40ms; 64x64 pixels [19.2cm x 19.2cm]) were obtained with echo-planar imaging (EPI). A T2* weighted sequence was chosen to enhance blood oxygenation level dependent (BOLD) contrast. There were 6 volume scans per condition. We replicated each condition 4 times in 2 sessions, each lasting 20 minutes. 240 image volumes were acquired in each session. Each condition lasted for 29.28 seconds. Three normal right-handed volunteers (aged between 20 and 45, 2 female, 1 male) participated in the study.

5.3.3 Data Analysis

The data were smoothed using a 6mm isotropic Gaussian kernel full width at half maximum. The data were analyzed from two perspectives. First we assessed the effects of motion, relative to stationary conditions and the interaction between motion and contrast-bias using conventional 'box-car' stimulus functions (convolved with a haemodynamic response function) that modelled the effects of each condition separately. The significance of condition-specific effects was assessed using the ensuing SPM{F}s. By using appropriate contrasts of condition-specific effects, SPMs of the t-statistic (SPM{t}) were created to identify regionally specific interactions. In the second analysis, we focussed specifically on parametric variation in haemodynamic responses as a function of speed. These responses were activations relative to stationary stimuli. This analysis implicitly discounts the stationary condition by using it as a reference and characterises speed-response relationships within the motion conditions only. To allow for non-linear relationships, we used an orthogonal polynomial expansion of (contrast bias specific) stimulus-functions reflecting stimulus speed. This expansion comprised first and second order terms, treating the motion vs. stationary effect as a confound. The significance of the ensuing polynomial regressions were assessed with SPM{t}s in the usual way and interactions with contrast-bias were assessed in terms of first and second order components using the appropriate contrasts and SPM{t}. Statistical inferences were made using Gaussian random field theory to correct for multiple dependent comparisons. To illustrate motion selective tuning of the responses, we selected voxels that constituted a maxima in the SPM{t} testing for inverted "U" relationships (*i.e.* negative second order component). The mean activities per epoch of motion stimuli were computed and plotted as a function of speed.

5.4 Results

The posterior region of the inferior temporal gyrus and sulcus were activated bilaterally by

motion in both the colour and luminance context in all three subjects. These areas correspond to bilateral V5 (Watson *et al* 1993, Zeki *et al* 1991). Bilateral activation was also seen in the calcarine sulcus and in the area of the superior part of the middle occipital gyrus that extended to the border of the angular gyrus. We refer to these areas as V1 and as V3a (Tootell *et al* (1997)) respectively (Fig. 5.1.1, Table 5.1.1). In short, under conditions of both colour and luminance contrast, activation was seen in V1, V5 and V3a under all motion conditions relative to stationary dots. Differential speed responses were seen, within the motion conditions, in certain areas: Under colour bias, activation in bilateral V1 was observed to decrease linearly with speed in all subjects (Fig. 5.1.2). With luminance bias stimuli, a non-linear, 'inverted U' response to speed was seen in V5 in subjects one and two (Fig. 5.1.3) with optimal responses between 7.7 and 30.8 degrees per second. In subject three, a linear decreasing response to speed was seen in left V5 (Fig. 5.1.3c) of the sort observed in V1 (Fig. 5.1.2). Using colour bias stimuli, a non-linear type response was also seen in right V5 in subjects one and two (Fig. 5.1.3e, g), with optimal responses observed at 7.7 and 15.4 degrees per second. Also, under colour bias, a non-linear response was seen in right V3a in subjects two and three with optimal speeds of 7.7 degrees per second in each case (Fig. 5.1.4). Testing for an interaction between stimulus speed and cue contrast (colour vs luminance bias) using appropriate contrasts, showed no evidence for differential speed-dependent responses.

	x co-ord	y co-ord	z co-ord	F-ratio
right V1	6	-87	-3	5.32
left V1	-6	-87	-9	6.55
right V5	45	-78	-6	24.69
left V5	-42	-72	6	20.95
right V3a	24	-87	21	20.99
left V3a	-21	-87	21	15.52

Table 5.1.1 Co-ordinates of the maxima in left and right V1, V5 and V3a in the analysis employing condition-specific stimulus waveforms (SPM(F) in Figure 5.1.1) testing for an overall response to the 12 different conditions. The table gives the F-values ($p < 0.05$ corrected) of the maxima in left and right V5 and V3a of each subject.

Fig. 5.1.1a b

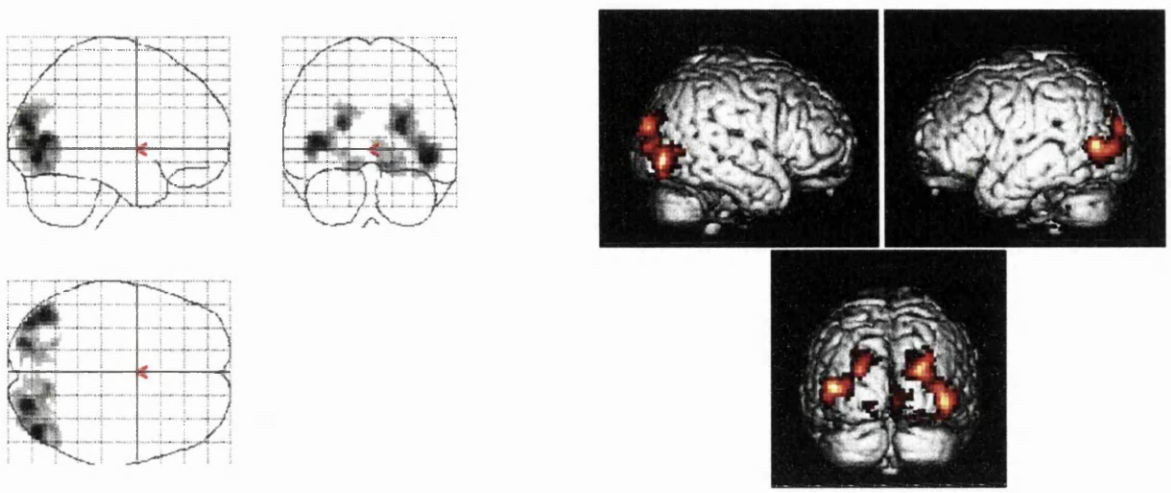

Fig. 5.1.1 a) Maximum Intensity projections of the SPM{F} (threshold p = 0.05 corrected) from the analysis using condition-specific box car stimulus waveforms. b) Bilateral regional effects in V1, V5 and V3a rendered on a structural MRI scan. Each region shown was significant at $p < 0.05$ (corrected).

Fig. 5.1.2a d

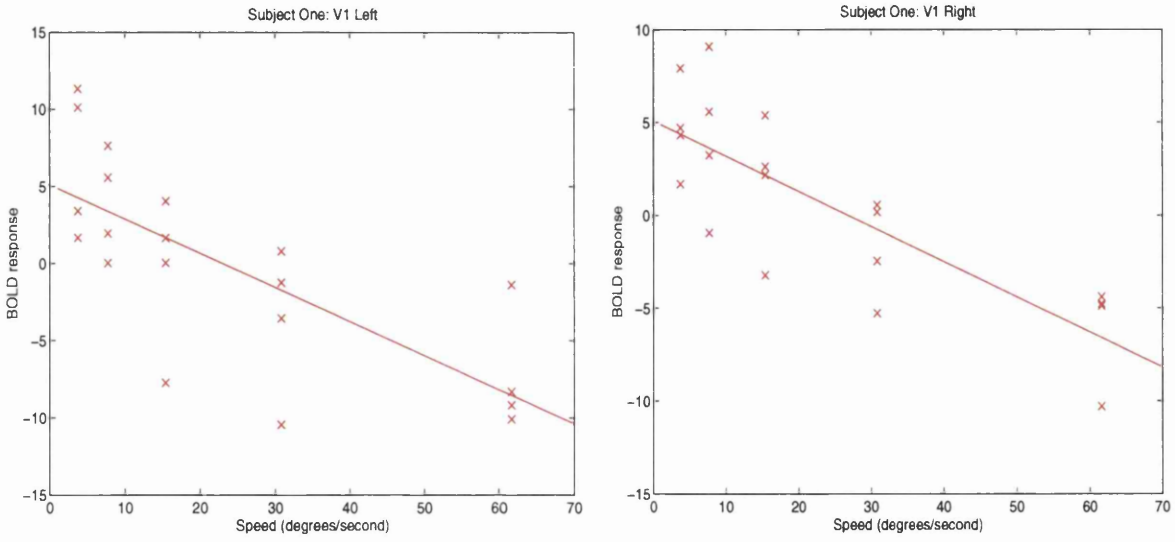

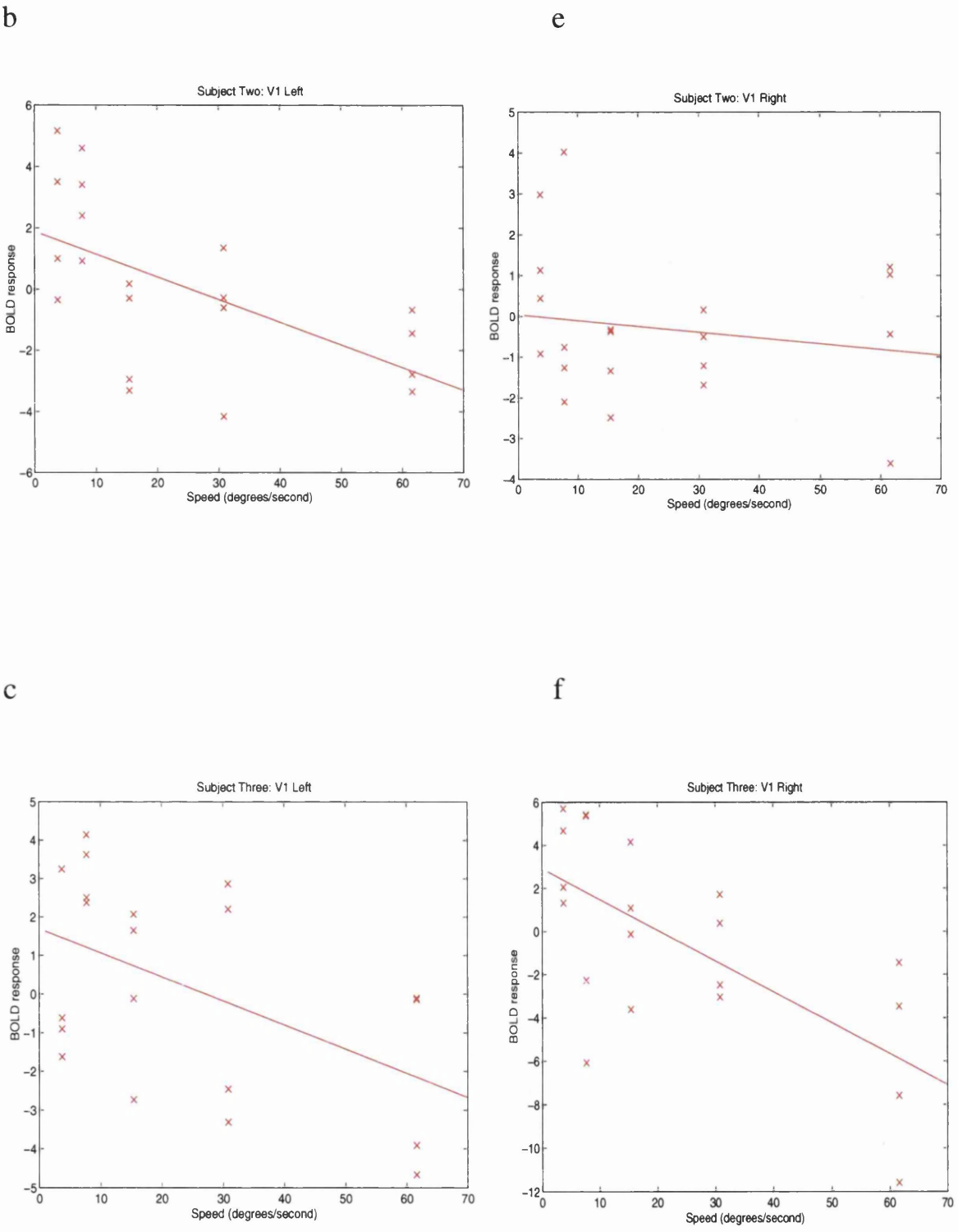

Fig. 5.1.2 Graph showing how V1 activation varies with stimulus speed under colour bias conditions in each subject. (a), (b), (c) show left V1 with Talairach co-ordinates of (9, -87, -3), (-12, -90, -12), (-9,-81,-15) mm respectively. (d), (e), (f) show right V1 with Talairach co-ordinates of (12, -84, -3), (2,-87,3), (6,-87, -3) mm. These regressions were significant at $p < 0.05$ (corrected).

Fig. 5.1.3a

b

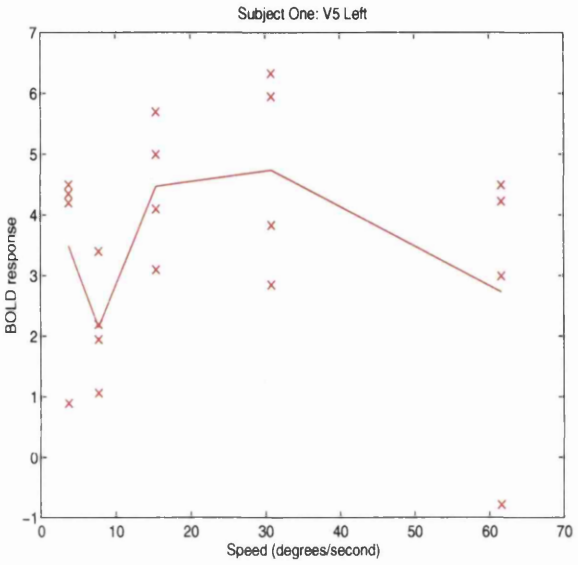
Subject One: V5 Left
BOLD response
Speed (degrees/second)

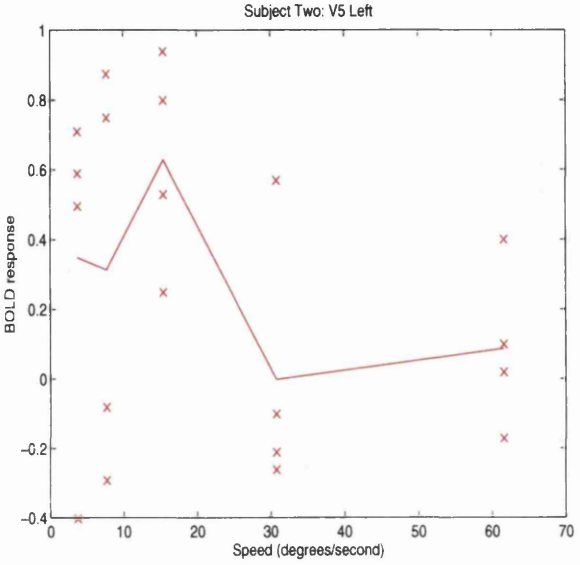
Subject Two: V5 Left
BOLD response
Speed (degrees/second)

c

d

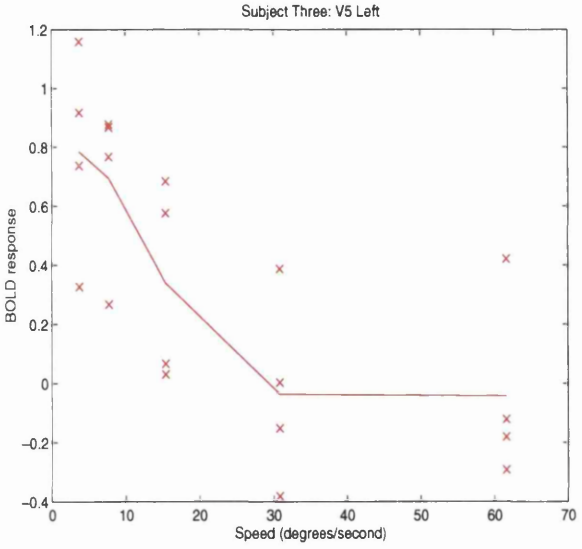
Subject Three: V5 Left
BOLD response
Speed (degrees/second)

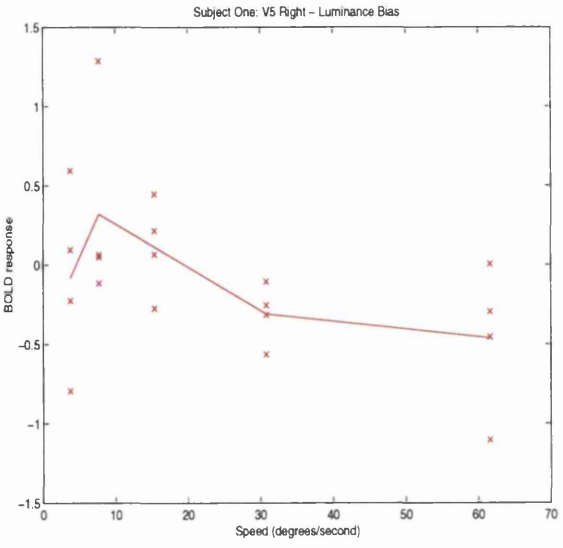
Subject One: V5 Right – Luminance Bias
BOLD response
Speed (degrees/second)

e

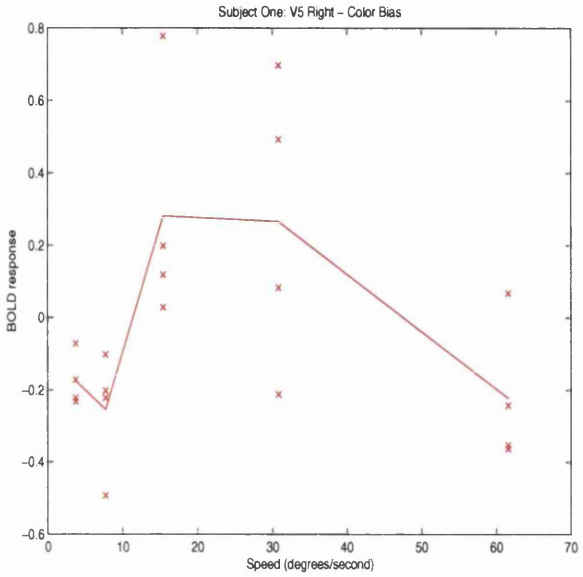

f

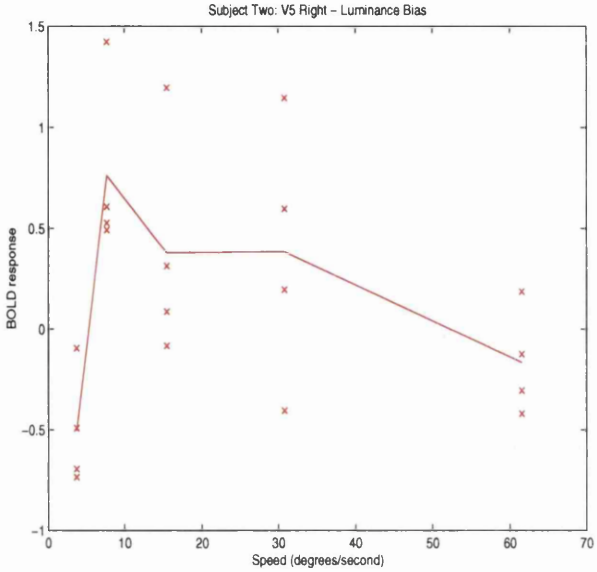

g

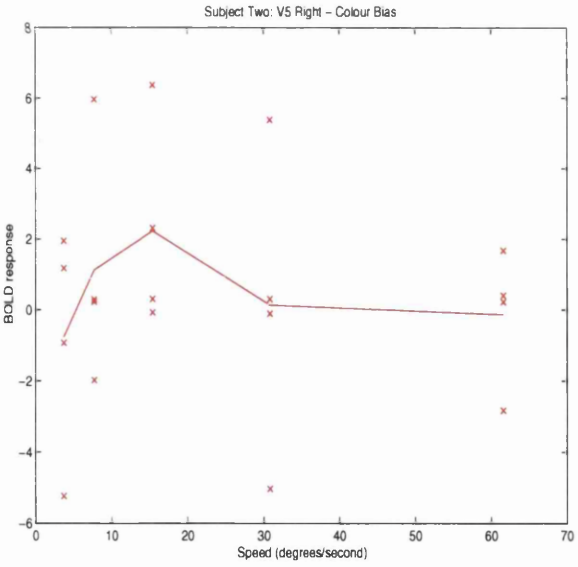

Fig. 5.1.3 Graph showing how V5 activation varies with stimulus speed in all subjects. (a), (b), (c) show left V5 in all subjects under luminance bias conditions with Talairach co-ordinates of (-48, -69, 9), (-42, -72, -9), (-36, -84, 3) mm respectively. (d, (e) show right V5 for subject one under luminance and colour bias respectively, (48, -60, -3), (42, -69, 6). (f), (g) show right V5 for subject two under luminance and colour bias respectively, (45, -60, 3), (45, -69, 6). These regressions were significant at $p < 0.01$ (uncorrected).

Fig. 5.1.4 a b

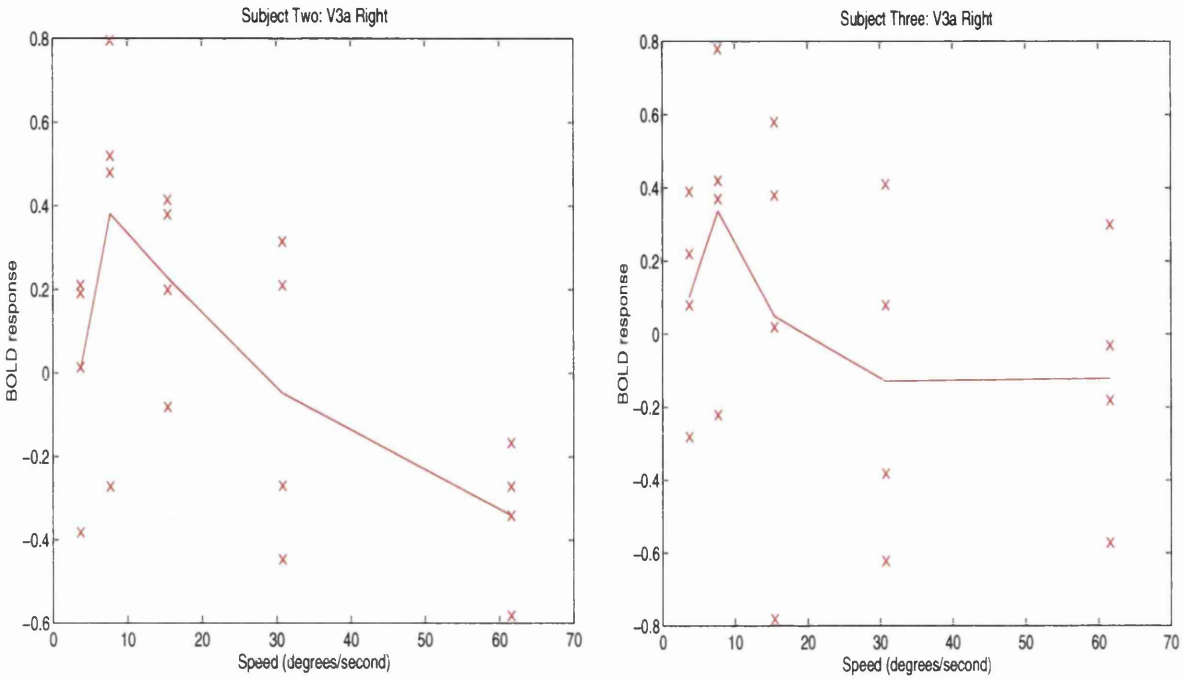

Fig. 5.1.4 Graph showing how right V3a activation varies with stimulus speed under colour bias conditions [in (a) subject one, (b) subject two] with Talarairach co-ordinates of (24, -87, 12), (33, -84, 18) mm. These regressions were significant at $p < 0.01$ (uncorrected).

Testing for an interaction between cue contrast (colour/luminance) and motion (pooled over all speeds and relative to stationary) showed an interaction in bilateral V1 and V5 (colour > luminance) and in right V3a (luminance > colour) (Fig. 5.1.5).

	Interaction one				Interaction two			
	x	y	z	Z-score	x	y	z	Z-score
R V5	42	-75	6	4.0				
L V5	-42	-60	6	3.4				
R V1	15	-96	6	4.8				
L V1	-9	-84	3	4.1				
R V3a					33	-81	9	4.0

Table 5.1.2 Location of the maxima in V1, V5 and V3a in the analysis using the SPM(t) to test for an interaction between cue contrast and visual motion. Interaction 1 corresponds to colour > luminance and interaction 2 to luminance > colour. The table also shows the Z-score ($p < 0.05$ (uncorrected)) of the maxima.

Fig. 5.1.5a b

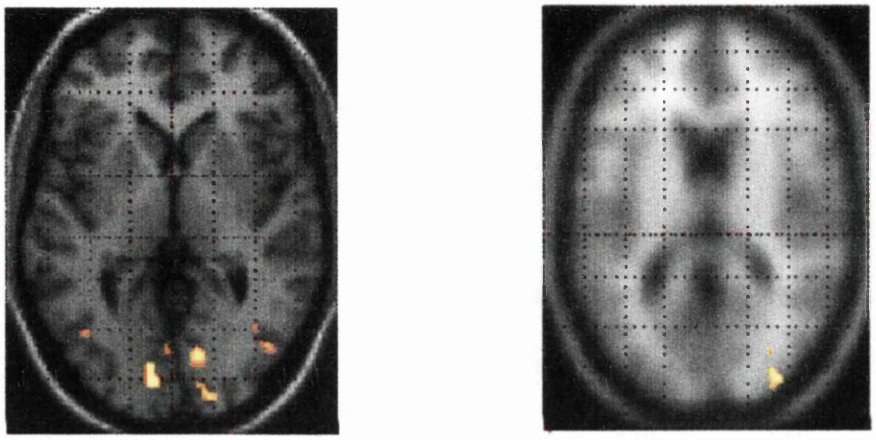

Fig. 5.1.5 SPM(t)s (shown on structural MRI scans) showing areas that evidenced an interaction between cue contrast and motion. a) corresponds to colour > luminance and b) to luminance > colour. The voxels shown were significant at $p < 0.05$ (uncorrected).

5.5 Discussion

A non-linear inverted 'U' dependency of V5 activation with speed is consistent with electrophysiological results (Rodman *et al*, 1987, Cheng *et al*, 1994) and could result from differential adaptation intrinsic to V5. Rodman *et al* (1987) found that V5 cells fall within four speed classes: "S1: cells with similar speed tuning for excitatory responses in both preferred and anti-preferred directions. S2: cells with similar speed tuning for excitatory

responses to anti-preferred motion. NT: cells whose responses to anti-preferred motion were not speed sensitive. 'Unclassified' cells had ambiguous speed tuning or no response for anti-preferred motion." Of these, the highest proportion of cells in area V5 are S1 followed by S2 followed by NT followed by unclassified. Apart from the unclassified cells (which make up only a very small proportion of V5 cells), all cells showed a non-linear response to speed with optimal activation at around 16°/s (S1), 14°/s (S2) and 5°/s (NT). Lagae *et al* (1993) classified V5 cells as tuned (33%), low pass (22%), broad band (19%) and mixed (22%), leaving 4% unclassified. They also found that these cells showed a non-linear response to speed, with optimal activations at around 1.7°/s (low pass), 7.3°/s (broadband), 9.1°/s (tuned), 5.8°/s (mixed) and 5.3°/s (unclassified).

A significant response was also seen in area V3a that was roughly of the same form as that seen in V5. It has been shown that almost all V3 complex cells are selective for the speed of the stimulus and about half [42% (Felleman *et al*, 1987)] are selective for its direction of motion. Also V3 cells show a similar non-linear response to speed with the optimal speeds of most cells being around 16 °/s and the distribution of optimal speeds ranging from 4 to 32 °/s.

In light of these findings, it is therefore not surprising that we found such a non-linear response to speed in certain parts of V5 and V3a. The non-linear effect that we have shown is not as comprehensive as has been shown electro-physiologically. This is most likely due to the facts that: (i) optimal speeds in V5 and V3a have been found to be very varied with many cells tuned to speeds that are quite slow and (ii) fMRI cannot resolve responses in individual cells. This means that the ability to detect highly tuned responses is reduced as one is forced to look at population responses that will have a range of optimal speeds. As optimal speeds among V5 and V3a neurons have been shown to vary a great deal amongst different cells, it is pleasing that at least some regions in V5 and V3a show this 'inverted U' behaviour using neuroimaging techniques.

The linear decreasing response to speed observed bilaterally in V1 is also interesting. It has been shown that the motion sensitive cells in V1 are directionally selective for much slower speeds than in V5 (Mikami *et al*, 1986). Also, it is known that at slow speeds, V5 gets its information via V1 while at higher speeds, motion processing bypasses V1 and reaches V5 from the retina via extrageniculate pathways involving the superior colliculus and pulvinar (ffytche *et al*, 1996). It could be that the response observed in V1 would also have been non-linear, had we started with much slower speeds.

Interestingly, the non-linear responses found in V5 and V3a were not demonstrated bilaterally in all subjects. The reason for this is somewhat unclear, although it should be remembered that failing to demonstrate that an effect is significant does not mean it is not there. For subject three, a linear decreasing response to speed was seen in left V5. This may be due to the optimal speeds being at or below the slowest speed of 3.7 degrees per second employed in this study.

An explanation for potential differential speed-sensitive responses is that, at slow speeds, V5 is thought to receive input primarily from the primary visual cortex (ffytche *et al*, 1996). At faster speeds, visual input to V5 is thought to bypass V1 through extra-geniculate pathways involving the pulvinar. Therefore at faster speeds, V5 responses may be mediated by different afferents. Because extrageniculate pathways bypass areas implicated in colour processing, we predicted a greater difference between hue and luminance based motion-responses at higher speeds, relative to slower speeds. Despite testing explicitly for an interaction between stimulus speed and cue contrast (colour vs luminance bias), we could find no evidence for differential speed-dependent responses. This would suggest that V5 responses, in terms of speed, are not sensitive to earlier processing differences that implicate M or P pathways or geniculate vs. extrageniculate pathways to a different extent. However, finding no evidence for differential speed-dependent responses does not mean that they do not exist (see below).

When we tested for an interaction between stimulus motion (pooled over all speeds) and contrast, differential activation was seen bilaterally in the calcarine sulcus (V1) and also bilateral V5. In these regions, colour cues produced a greater activation than luminance cues. For luminance > colour, an interaction was seen in right V3a. It could be said therefore, that contrast cues do have an effect on motion processing, in that colour defined motion activates V1 and V5 more and luminance defined motion activates V3a more. Colour enhanced motion-responses in V1 and V5 are consistent with the psychophysical findings of Morgan and Ingle (1994) that colour, added to luminance defined motion stimuli, enhances the motion percept by increasing the maximum spatial displacement at which apparent motion is perceived. A possible explanation for our finding is that V5 is extremely sensitive to luminance contrast (Cheng *et al*, 1994) and in our colour contrast condition, there may have been enough residual or artefactual luminance contrast to effectively saturate the luminance response of cells in V5. These responses may then have been augmented by colour-derived motion processing.

It should be emphasised that it is extremely difficult to attain isoluminance in psychophysical stimuli and that we had to contend with the added difficulty of creating isoluminant conditions in the scanner. We performed heterochromatic flicker photometry while subjects lay in the scanner. However, after taking into account other possible sources of artifact, it might be more accurate to suggest that our isoluminant condition was a 'low luminance heterochromatic condition'.

Some of the shortcomings of this study were addressed in a subsequent study described below. Although it may be important to minimise artifacts in psychophysical experiments for the quantification of perceptual deficit, our study addresses differential cortical activation under colour and luminance bias cues. The stimuli that we used were certainly sufficient to introduce this bias.

In conclusion, optimal responses in human V5 were observed at intermediate speeds of around 7 to 30 °/s. This finding is consistent with electrophysiological data. A non-linear (inverted 'U') dependency on speed was also observed in V3a. We also found that V1 activation decreased linearly as speed increased. This is consistent with the fact that speed sensitive cells in V1 have been shown to be tuned to slower speeds than in V5.

Section 2: A Replication Study

5.6 Abstract

In the previous section, we used fMRI to examine motion-sensitive responses in human area V5 as a function of stimulus speed. As predicted by electrophysiological findings, we observed optimal responses at intermediate speeds of around 7 to 30 °/s. These results revealed a non-linear (inverted 'U') dependency on speed that was also evident in V3a. In this section we repeated the experiment using an improved stimulus and a larger range of speeds. We replicated our previous findings and extended our characterization of speed-dependent responses: Optimal responses were seen in V5 at speeds of 4 and 8 °/s and in V3a at speeds of 4 to 16 °/s. We were also able to show an interaction between speed (fast vs. slow) and contrast (colour > luminance) in V5. This interaction was anticipated on the basis of the different properties of the geniculate and extrageniculate inputs to V5. Finally, we were also able to demonstrate an interaction between motion (moving vs. stationary) and contrast (colour > luminance) in V4. This suggests that for V4, colour specific responses are augmented in the context of motion; or equivalently, that colour contrast enhances any motion sensitive responses in V4.

5.7 Introduction

In the previous section, we tried to determine how V5 human visual cortex activation varies as a function of stimulus speed and whether this relationship was the same for motion based on hue or luminance cues. At slow speeds V5 is thought to receive input primarily from the primary visual cortex (ffytche *et al*, 1995, 1996, Beckers *et al*, 1995) while, at faster speeds, visual input to V5 may bypass V1 through extra-geniculate pathways involving the pulvinar. We therefore predicted that there should be a greater difference between hue and luminance

based motion-responses at high speeds, relative to slow speeds, as extrageniculate pathways circumnavigate areas associated with colour thereby processing precluding any interaction between colour and motion processing. Despite testing for an interaction between stimulus speed and cue contrast (colour vs luminance bias) in our previous study, we found no evidence for differential speed-dependent responses (Chawla *et al*, 1998). However, failing to find evidence for differential speed-dependent responses does not mean that they do not exist. One of the aims of the current experiment was to test for this interaction again, having addressed some of the potential shortcomings of the stimuli employed in the previous study.

In our previous study, when we tested for an interaction between stimulus motion (pooled over all speeds) and contrast, differential activation was seen in the calcarine sulcus (V1) and V5. This interaction addresses the integration of colour and motion processing while discounting differential speed-dependency *per se*. In these areas, colour cues elicited a greater motion-sensitive response than luminance cues. For luminance > colour, an interaction was seen in V3a. As V5 is extremely sensitive to luminance contrast (Cheng *et al*, 1994), it could have been that there was enough luminance contrast in our colour stimuli to saturate the luminance response of cells in V5. The present study revisits this issue by substantially reducing the luminance artifact in the stimulus. In the current experiment, two improvements were made. (i) Firstly, the dots were enlarged by a factor of ten. This minimises luminance and hue contrast due to chromatic abberation at the dot borders. (ii) The range of speeds were extended to incorporate slower speeds. This enabled a better characterization of speed-dependent responses.

In short this second study had two aims: (i) To replicate the finding of an inverted 'U' speed-dependent response in V5 and V3a and (ii) to revisit the issue of interactions between hue vs. luminance and speed with an improved stimulus.

5.8 Methods

5.8.1 Stimuli

We used radially moving dots to provide a motion stimulus, as in the first section of this chapter. We used a parametric factorial design consisting of colour contrast stimuli and luminance contrast stimuli, both at six different speeds plus stationary. A blank screen was used as the control between each stimulus condition. The six speeds used were 1, 2, 4, 8, 16 and 32 °/s. The size of the dots in our stimulus was 2.3°.

5.8.2 Data Acquisition

We acquired 16 axial slices with 3mm thickness at 100ms/slice giving a repetition time, per volume, of 1.68s. Contiguous multislice T_2* weighted images (TE = 43ms; 64x64 pixels [19.2cm x 19.2cm]) were obtained with echo-planar imaging (EPI). There were 18 volume scans per condition (i. e. stimuli presented continuously at a given speed using hue or luminance contrast). Each condition lasted for 30.24 seconds. We replicated each condition twice in a session lasting for 28.22 minutes. 1008 image volumes (56 replicated conditions) were acquired in a session. Three normal right-handed volunteers (aged between 19 and 22, 2 female, 1 male) participated in this study.

5.8.3 Data Analysis

The data were smoothed using a 6mm isotropic Gaussian kernel full width at half maximum. In our statistical model, the data from all three subjects were included in the same fixed effects model. This model comprised subject-specific condition effects and confounds (low frequency components and global activity). This constitutes a case-study of three subjects, allowing contrasts to be specified for (i) each subject separately and (ii) testing for average effects over subjects (see Fig. 5.2.1).

We assessed the effects of motion, relative to the stationary condition, the interaction between speed (highest vs. lowest) and contrast (colour vs. luminance) and the interaction between motion (motion vs. stationary) and contrast. In assessing the speed by contrast interaction, we used the highest and lowest speeds to bias as far as possible towards extra-geniculate (and magnocellular) and geniculate (and parvocellular) processing respectively. These analyses used conventional 'box-car' stimulus functions (convolved with a haemodynamic response function) that modelled the effects of each condition separately. By using appropriate contrasts of condition-specific effects, SPMs of the t-statistic (SPM{t}) were created to identify regionally specific main effects and interactions. The SPM(t)s were transformed to SPM(Z) for display and tabulation. Statistical inferences were made using Gaussian random field theory to correct for multiple dependent comparisons. However, because we restricted our hypothesis to V1, V5, V3a and V4 we report all maxima at $p < 0.05$ (uncorrected), only if the areas survived this threshold in all three subjects. The SPMs shown in Figure 5.2.1 represent a conjunction analysis over all subjects. In other words, the SPMs show the effect tested for, assessed over subjects, but only in voxels where this effect was significant conjointly in every subject-specific analysis. Because of the separable nature of the design matrix, this corresponds to an uncorrected significance of $p < 0.05^3$.

5.8.4 Characterising Speed-Dependent Responses

To characterise speed dependent responses within motion sensitive areas, we focussed on the maxima from the analyses testing for a main effect of motion in V5 and V3a using the parameter estimates of the response at each speed, in each stimulus context, in each subject. In these and only these analyses, we smoothed the data with a 12mm kernel to get a more representative estimate of the regional responses in these areas.

5.9 Results

5.9.1 Main Effect of Motion

As in our previous study, the posterior region of the inferior temporal gyrus and sulcus were activated bilaterally by motion in both the colour and luminance context in all three subjects. These areas correspond to bilateral V5 (Watson *et al* 1993, Zeki *et al* 1991). Bilateral activation was also seen in the calcarine sulcus and in the superior part of the middle occipital gyrus that extended to the border of the angular gyrus. We refer to these regions as V1 and V3a (Tootell *et al* (1997)) respectively (Fig. 5.2.1a and b, Table 5.2.1). In short, under conditions of both colour and luminance contrast, activation was seen in V1, V5 and V3a under all motion conditions relative to stationary dots.

5.9.2 Speed × Contrast interaction

Testing for an interaction between stimulus speed (fast relative to slow) and cue contrast (colour > luminance bias) using appropriate contrasts showed an interaction in a bilateral V5 satellite in all subjects (see Fig. 5.2.1c). The direction of this interaction suggests that at faster speeds, relative to slower speeds, colour cues elicit a greater response. This is consistent with the interaction in V4 reported next but is somewhat counterintuitive given that optimal speeds using hue contrast are higher than those using luminance contrast.

Subject	Area name	x co-ord	y co-ord	z co-ord	Z-score
One	right V1	16	-90	-2	5.74 *
	left V1	-8	-98	4	4.55 *
	right V5	58	-56	-2	7.94 *
	left V5	-46	-66	2	7.11 *
	right V3a	30	-90	22	7.12 *
	left V3a	-24	-86	14	8.03 *
Two	right V1	24	-100	-2	2.13
	left V1	-8	-96	-6	2.46
	right V5	46	-78	-4	2.99
	left V5	-44	-82	-2	3.20
	right V3a	26	-94	16	3.11
	left V3a	-12	-96	30	2.86
Three	right V1	16	-92	-8	4.68
	left V1	-12	-90	-4	3.88
	right V5	48	-68	2	3.05
	left V5	-38	-74	2	4.25
	right V3a	18	-80	24	2.95
	left V3a	-20	-80	28	2.86

Table 5.2.1 Co-ordinates of the maxima in left and right V1, V5 and V3a testing for the main effect of motion against stationary in each individual subject. The table gives the Z-scores of the maxima in left and right V1, V5 and V3a of each subject that survived a statistical significance of $p < 0.001$ uncorrected. Voxels surviving a $p < 0.05$ correction are denoted by an asterix (*).

Fig. 5.2.1a

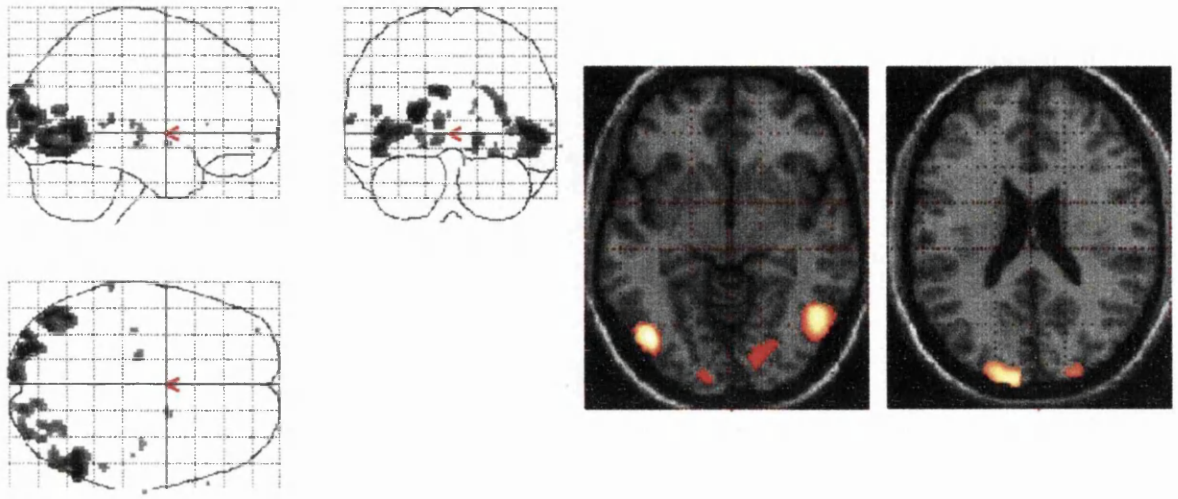

b

c

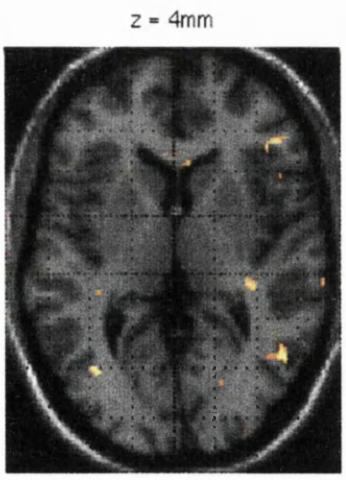

d

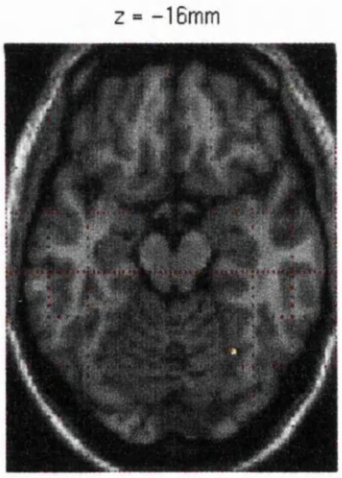

Fig. 5.2.1 a) SPM{Z} (threshold $p < 0.01$ uncorrected) showing the main effect of motion vs. stationary over subjects. b) SPM{Z} (threshold $p < 0.05$ uncorrected) showing the main effect of motion vs. stationary over subjects and rendered on a structural MRI scan. The left panel shows bilateral regional effects in V1 and V5 and the right panel shows bilateral V3a. (c) shows V5 from the SPM{Z} (threshold $p < 0.05$ uncorrected) of the interaction between speed (highest vs. lowest) and cue contrast (colour > luminance) over subjects. (d) shows V4 from the SPM{Z} (threshold $p < 0.05$ uncorrected) of the interaction between motion (pooled over all speeds) vs. stationary and cue contrast (colour > luminance) over subjects. The voxels in these SPMs were significant in all subjects when assessed separately and therefore represent a conjunction analysis.

Subject	Area	x	y	z	Z-score
One	left V5	-42	-66	2	1.88
	right V5	52	-60	2	2.31
Two	left V5	-38	-74	4	2.29
	right V5	44	-74	2	1.77
Three	left V5	-44	-78	6	3.97
	right V5	48	-72	8	1.82

Table 5.2.2 Location of the maxima in V5 in the analysis testing for an interaction between cue contrast and speed (fast relative to slow). The table also shows the Z-scores ($p < 0.05$ uncorrected) of the maxima.

5.9.3 Motion × Contrast Interaction

Testing for an interaction between cue contrast (colour > luminance) and motion (pooled over all speeds relative to stationary) showed an interaction in right V4 in all subjects (Fig. 5.2.1d). This represents a positive interaction between colour and motion in augmenting V4 responses and replicates an earlier study (Phillips *et al*, in preparation).

Subject	Area	x	y	z	Z-score
One	right V4	26	-70	-12	2.95
Two	right V4	18	-66	-14	1.78
Three	right V4	22	-82	-10	2.84

Table 5.2.3 Location of the maxima in V4 in the analysis using the SPM(Z) to test for an interaction between cue contrast and visual motion. The table also shows the Z-scores ($p < 0.05$ uncorrected) of the maxima.

5.9.4 Non-Linear Speed Dependent Responses

Differential speed responses were seen, within the motion conditions, in the maxima of V5 and V3a from the main effect of motion in all three subjects. Figure 5.2.2 shows the speed-dependent responses in V5 in all three subjects. A non-linear "inverted U" response was evident in each case with optimal speeds at 4 or 8 °/s.

Figure 5.2.3 shows the speed-dependent responses in V3a in all three subjects. A non-linear "inverted U" response to speed was observed, this time with optimal speeds between 4 and 16 °/s. It is remarkable that the same optimal speeds were seen universally in both hemispheres of the same subject under both colour and luminance contexts in both V5 and V3a. The probability of this happening by chance is incredibly small, speaking to the biological plausibility of these results (particularly given that these voxels were identified by a contrast that was orthogonal to the inverted "U" behaviour observed).

Fig. 5.2.2a **Right** **Left**

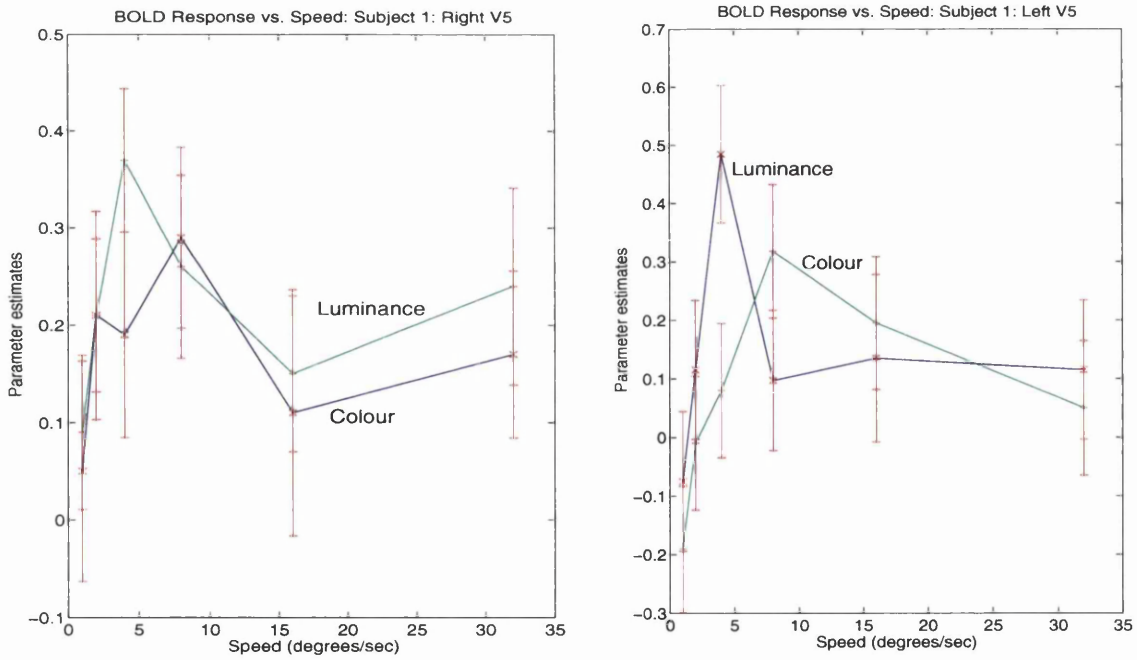

b

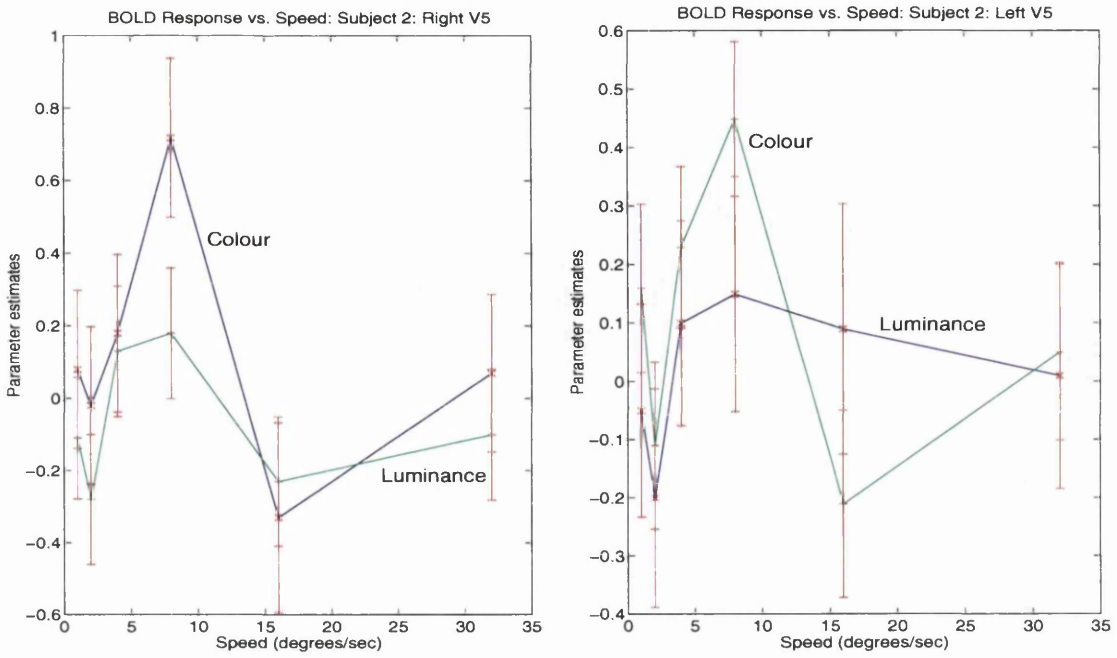

c

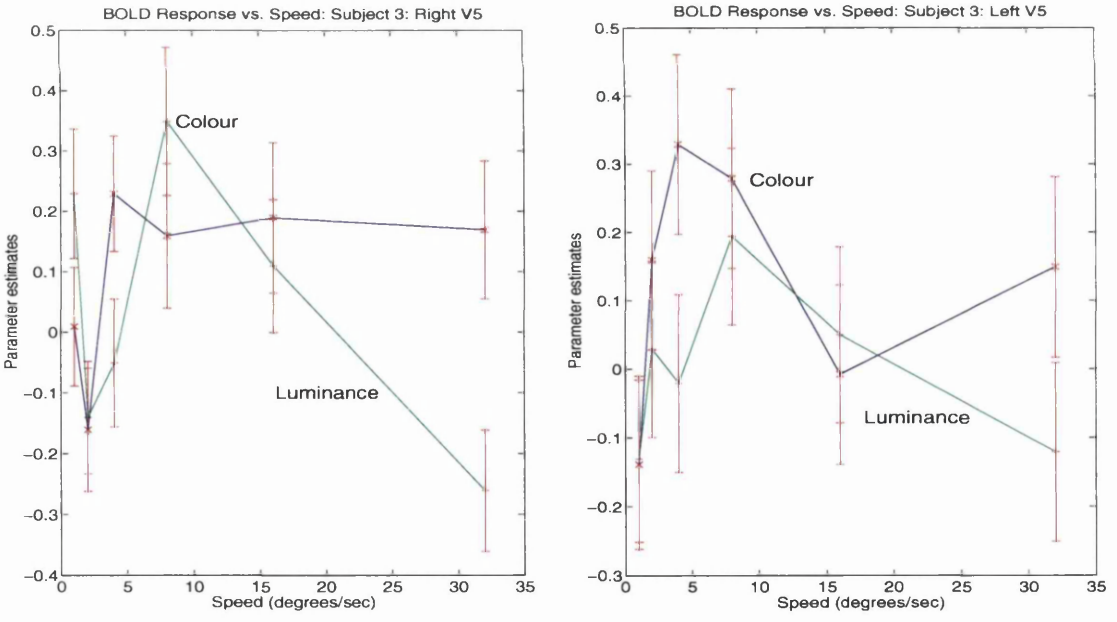

Fig. 5.2.2 Graph showing how activation in the V5 maxima from the main effect of motion compared to stationary varies with stimulus speed in all subjects. (a) shows right and left V5 in subject one under both colour and luminance bias conditions. (b) shows right and left V5 for subject two. (c) shows right and left V5 for subject three.

Figure 5.2.3a **Right** **Left**

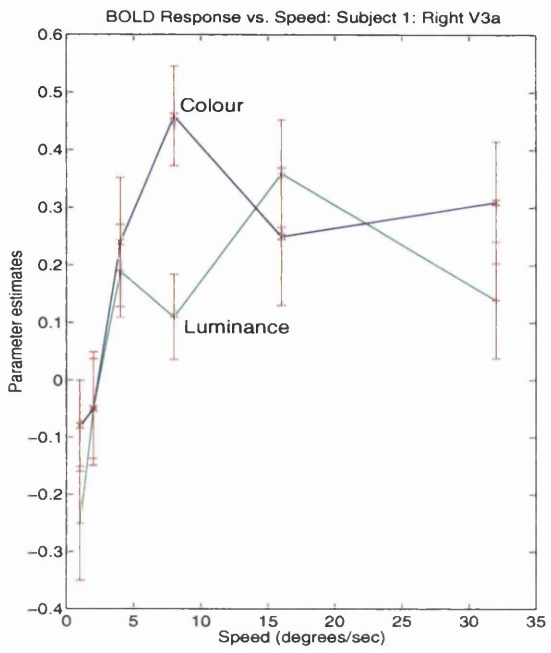

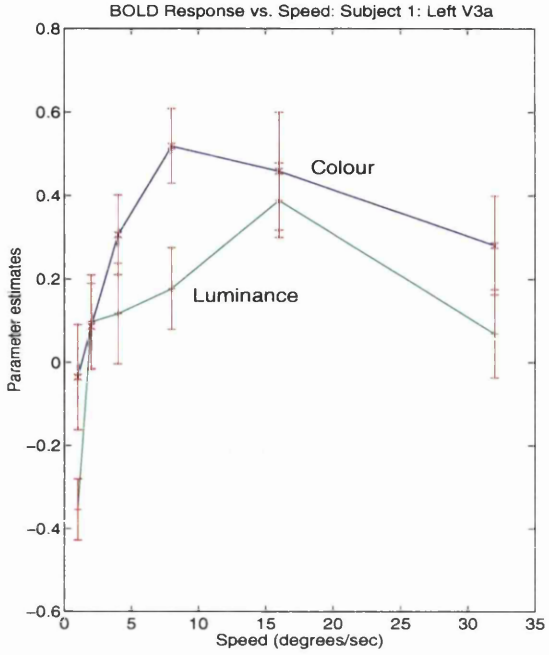

b

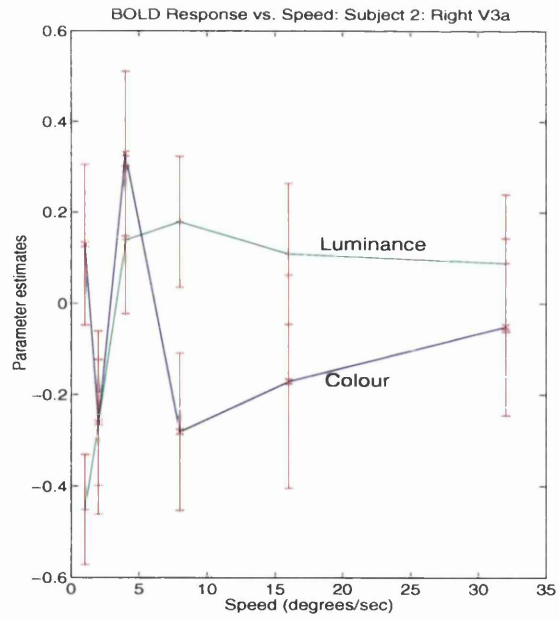

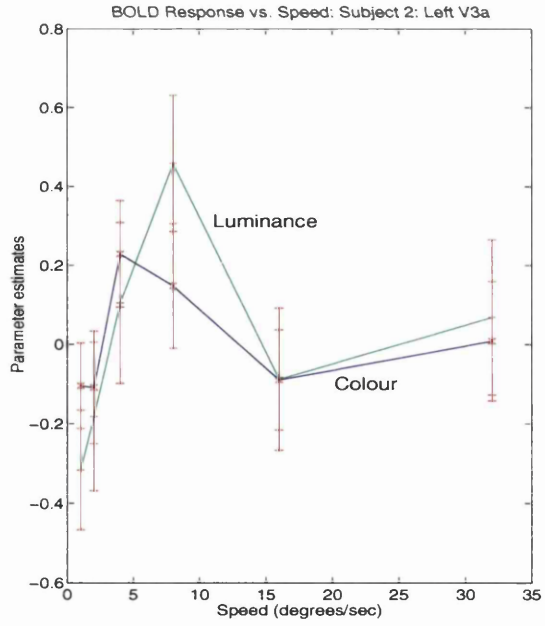

c

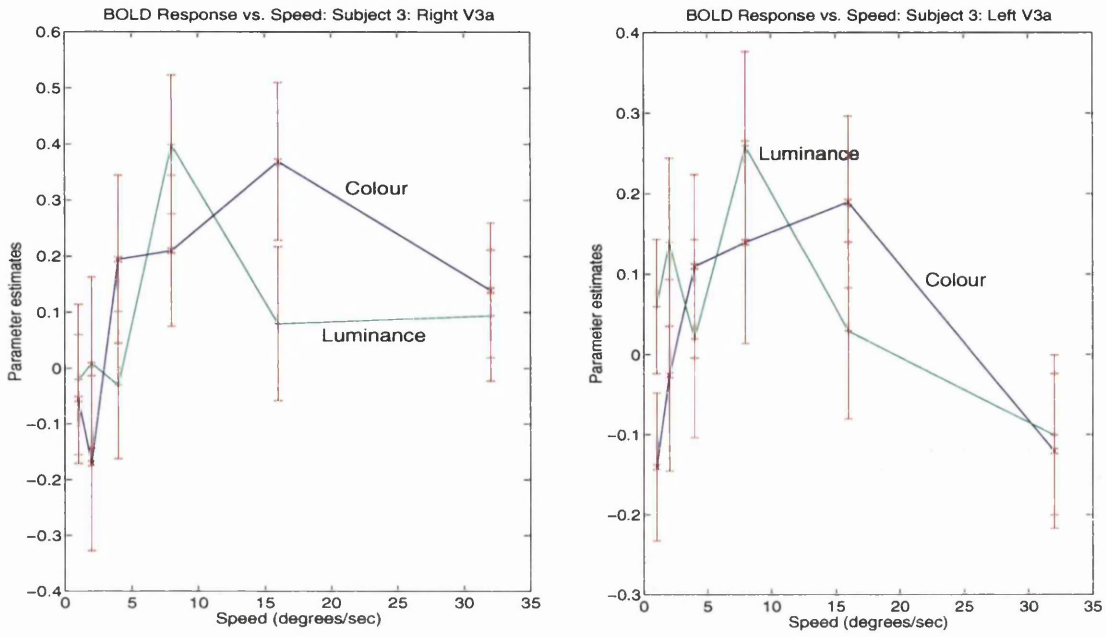

Fig. 5.2.3 Graph showing how activation in the V3a maxima from the main effect of motion compared to stationary varies with stimulus speed in all subjects. (a) shows right and left V3a in subject one under both colour and luminance bias conditions. (b) shows right and left V3a for subject two. (c) shows right and left V3a for subject three under colour and luminance bias.

5.10 Discussion

A non-linear inverted 'U' dependency of V5 activation with speed is consistent with electro-physiological results (Rodman *et al*, 1987, Cheng *et al*, 1994) and could result from differential speed-selective responses intrinsic to V5. A significant motion response was also seen in area V3a that had roughly the same form as that seen in V5. It has been shown that almost all V3 complex cells are selective for the speed of the stimulus and about half (42%, Felleman *et al*, 1987) are selective for its direction of motion. Furthermore, V3 cells show a similar non-linear response to speed with the optimal speeds of most cells being around 16 °/s ranging from 4 to 32 °/s.

In this section, the non-linear effect in V5 and V3a is more compelling than that reported in

the first study of this chapter (Chawla *et al*, 1998). In the present study, the non-linear responses came from the maxima from the main effect of motion whereas before we looked for them explicitly. However, as before, these non-linear effects (*i.e.* selectivities) are not as "tight" as when characterised electro-physiologically. This is most likely due to the fact that fMRI cannot resolve response profiles of individual cells. This means that the ability to detect highly tuned responses is reduced as one is forced to look at population responses that have a range of optimal speeds.

A potential explanation (that motivated our experimental design) for differential motion- and speed-sensitive responses under different contrasts (luminance vs. colour) is that, at slow speeds, V5 is thought to receive input primarily from the primary visual cortex (ffytche *et al*, 1996). At faster speeds, visual input to V5 is thought to bypass V1 through extra-geniculate pathways involving the pulvinar. Therefore at faster speeds, V5 responses may be mediated by different afferents. Because extrageniculate pathways completely bypass areas implicated in colour processing (and because of the differential demands put upon magnocellular and parvocellular pathways), we predicted a difference between hue and luminance based motion-responses in V5 at higher speeds, relative to slower speeds. Consistent with this prediction, an interaction between speed (fast relative to slow) and cue contrast was seen in V5. Because of the non-linear speed-dependent responses, one should be careful not to overinterpret the exact form of these interactions.

When we tested for an interaction between stimulus motion (pooled over all speeds) and contrast, differential activation was seen in V4. This result replicates the finding of an independent study that looked explicitly for motion vs. colour interactions using just one speed (8 °/s) (Phillips *et al*, in preparation). In this region, colour cues produced a greater activation than luminance cues. Colour enhanced motion-responses at a neurophysiological level are consistent with the psychophysical findings of Morgan and Ingle (1994). This suggests that for V4, colour specific responses are augmented in the context of motion; or equivalently, that colour contrast enhances any motion sensitive responses in V4. The latter interpretation could imply motion responses intrinsic to V4, or an integration between distinct visual processing pathways via reciprocal connections with V5 (Felleman and Van Essen, 1991).

In conclusion, optimal responses in human V5 and V3a are observed at intermediate speeds of around 4 to 16 °/s. This finding is consistent with electrophysiological data in single neurons and replicates our previous findings. We were also able to show for the first time an interaction between speed *per se* and contrast (colour vs. luminance) in V5. This interaction was anticipated on the basis of the various ways in which visual input can reach V5. Finally, we replicated the findings of Phillips *et al* (in preparation), in finding an interaction between motion and contrast in V4. This suggests a modulatory interaction of colour on motion processing pathways via reciprocal connections, or intrinsic responses to dynamic stimuli in V4.

Chapter 6: The Physiological Basis of Attentional Modulation in Extrastriate Visual Areas

6.1 Abstract

Selective attention to colour or motion enhances cortical activity in functionally specialised areas of extrastriate cortex, but the underlying mechanisms of this attentional modulation remain unclear. Functional neuroimaging in humans was used to investigate the physiological basis of such effects, by dissociating the modulation of transient activity evoked by a visual stimulus from the baseline activity established by a particular attentional set. Significantly, baseline activity in motion and colour sensitive areas of extrastriate cortex was enhanced by selective attention to these attributes even in the absence of a moving or coloured stimulus. Further, when baseline activity increased, there was a concomitant increase in visually evoked responses. These results are consistent with the hypothesis, motivated by computational modelling studies described in chapters 3 and 4, that attention modulates the sensitivity of neuronal populations to inputs by simply changing background activity. Our modelling studies indicate that increases in background activity augment fast synchronous stimulus-induced interactions. This mechanism provides for a baseline "gain control" that emerges spontaneously from the population dynamics.

6.2 Introduction

A substantial amount of experimental evidence, from humans and non-human primates, implicates the extrastriate visual area, V5 (located in the posterior region of the inferior temporal gyrus and sulcus) in motion processing and area V4 (located in the fusiform gyrus) in colour processing (Chawla *et al*, 1999, 1998, Tootell *et al*, 1995, Watson *et al* 1993, Zeki *et al*, 1991, Lueck *et al*, 1989, Livingstone and Hubel, 1988, Dubner and Zeki, 1971). Over the past decade, evidence has emerged to suggest that attention to colour or motion enhances activity in V4 or V5 respectively. In non-human primates, the effect of attention on neuronal activity is to enhance both baseline activity (Luck *et al*, 1997, Ferrera *et al*, 1994), before a visual stimulus is presented, and the activity evoked by a stimulus with the attended attribute. Treue and Maunsell (1996) showed, in studies of macaque visual cortex, that the responses of most V5 cells are reduced when attention is directed to moving stimuli that are outside the cells receptive field; however responses were enhanced when attention is directed to stimuli within the receptive field. In humans, neuroimaging techniques (positron emission tomography (PET) (Corbetta *et al*, 1991) and functional magnetic resonance imaging (fMRI) (Buechel *et al*, 1998, O'Craven *et al*, 1997)) show that V5 activity is enhanced when subjects are paying attention to moving stimuli relative to passively viewing the stimuli or indeed, paying attention to a different attribute such as colour. Enhanced V4 responses to stimuli have also been demonstrated as a result of attending to their colour (Corbetta *et al*, 1991, Haenny and Schiller, 1988, Spitzer *et al*, 1988). Haenny and Schiller found, in 72% of the cells in V4 that they tested electrophysiologically, an enhanced response of around 20% and increased selectivity, under conditions of attention. Spitzer and colleagues used electrophysiological techniques to show that cell responses in V4 increased as a colour discrimination task became more difficult, requiring a higher level of attention. The responses also became more selective as difficulty increased: In an easy task, cells responded to both target and unattended stimuli (in the receptive field). However, as the task became more difficult, responses to target stimuli were enhanced and responses to unattended stimuli were attenuated. More recently, McAdams *et al* (1999), examined how attention affected the orientation tuning of 262 isolated neurons in monkey V4. They trained the monkeys to "perform a delayed match to sample task in which oriented stimuli were presented in the receptive field of the neuron being recorded. On some trials the animals were instructed to pay attention to those stimuli, and on other trials they were instructed to pay attention to other stimuli outside the receptive field." They found that, "attention enhanced the responses of V4 neurons (median 26% increase)", although "selectivity, as measured by the width of its orientation-tuning curve, was not systematically altered by attention. The effects of attention were consistent with a multiplication scaling of the driven response to all orientations." These results suggest that extrastriate responses to visual stimuli are modulated according to task demands. In other words, responses to individual attributes can be selectively enhanced by attention.

The above studies show attentional modulation of stimulus evoked responses. Fewer studies

have explicitly investigated attentional modulation of baseline activity. Ferrera *et al* (1994) explored baseline shifts in neuronal responses, in the context of working memory. They found in macaque that both baseline activity and activity evoked by a moving stimulus appear to change with expectation. Even when subjects viewed a blank screen, activity in 32% of V5 cells showed a doubling of baseline activity. This study employed a delayed match to sample task, using direction of motion as the matching criterion. Modulation of delay period or baseline activity was not related to information in the cue (*i.e.* the specific direction that was relevant on that trial), suggesting that this effect may be modulated, in part, by attention. When interpreting our results, in relation to these findings, we assume that baseline attentional modulation is mediated by the same sort of tonic discharge associated with delay period activity that is evoked by such working memory tasks. Luck *et al* (1997) also showed in V4, using monkey electrophysiology, that attention can modulate both baseline and stimulus evoked activity, depending on the relative locations of visual stimuli within the cells receptive fields (see below for a fuller discussion of this work in relation to our study).

Enhanced baseline activity is taken to reflect attentional 'set' or expectation, whereas changes in stimulus evoked activity reflect changes in sensory processing (Corbetta *et al*, 1991). However the functional significance and relationship between changes in 'set' and changes in evoked activity is not known. In functional neuroimaging studies on humans, it has been difficult to unambiguously dissociate activity due to attentional set and that due to stimulus evoked responses (Rees *et al*, 1997) because of the relatively long periods of time over which haemodynamic signals are integrated. Here, by using a novel event-related paradigm and fMRI, we show just such a dissociation in V5 and V4, revealing a relationship between attentional set and evoked activity that is in accord with hypotheses based on computational studies.

Our specific hypothesis, motivated by computational studies of simulated neuronal populations (Chawla *et al*, 1999, also see chapters 2 and 3), provides a model for attentional modulation and speaks to some important conclusions based on monkey electrophysiology: Unit electro-recording studies (Luck *et al*, 1997) have suggested that when multiple stimuli fall within a cells receptive field, they compete for the cells response in a manner that can be biased in favour of the attended stimuli. Earlier in this thesis, we have shown that stimulus-evoked rate modulation increases with tonic, background population activity suggesting that attentional modulation, of evoked responses, may be mediated by simply increasing background activity in the appropriate functionally specialised populations. This leads to the intuitively remarkable hypothesis that tonic cortical activation should be seen when attending to a specific attribute of the sensory field in the appropriate functionally specialised cortical area. Importantly this effect *should be seen in the absence of any stimuli*. Furthermore, the computational results predict a specific form for the relationship between changes in background activity and evoked transient activity: In areas that show attention-specific increases in baseline activity, one would expect to see positive modulation of transient responses evoked by stimuli when they are presented.

Here, for the first time in humans, we test and confirm these theoretical predictions by dissociating activity associated with attentional set and that evoked by presentation of a visual stimulus. We conducted an event-related fMRI (Josephs *et al*, 1997, Buckner *et al*, 1996) experiment in which we examined transient V5 (V4) responses to motion (colour) stimuli under different levels of attention. The technique of event related fMRI resembles that used to record event-related potentials in electrophysiology, where different stimuli are presented repeatedly over time. Subjects viewed a stationary monochromatic random dot display where the dots intermittently changed colour and moved radially. By asking subjects to detect and discriminate among these and sporadic target events, using either colour or motion cues, attentional modulation of activity evoked by the transient stimuli could be measured. However, our design also allowed measurement of the modulation of baseline activity, *between* successive stimuli, due to attentional set or expectation. During these times, the stimulus was stationary and did not change colour. We characterised these two different measures of attentional modulation in two functionally specialised extrastriate visual areas (V4 and V5), replicating our findings independently in three subjects, in both hemispheres.

6.3 Methods

6.3.1 Stimulus Presentation

The stimulus was identical in all conditions and consisted of stationary random green dots (with a size of 0.1°) on a green background of differing luminance. Transient visual events occurred intermittently and consisted of random red dots on a green background that moved radially. There were 500 dots on the screen at any time. In a previous fMRI study (Chawla *et al*, 1999, 1998, also see chapter 2), we characterised V5 activity as a function of speed. We found optimal responses at speeds of around 10°/s and therefore used this as the speed of our motion stimuli. In 25% of the events, the speed was reduced to 7°/s or the colour of the dots was a slightly lighter shade of red.

Subjects viewed the visual display for periods of 98 seconds, interleaved with periods when the screen was blank (as a low level control). Before each presentation of the visual display, a visual cue was used to instruct subjects to attend to either motion or colour attributes of the stimulus. In the motion attention condition, the subjects were told to discriminate the slower moving dots from the faster moving dots and respond with a key press. In the colour attention condition, the subjects were told to detect the slightly pinker dots. As these events were only subtly different from the normal events, and the subjects were not aware of their 25% sparsity, attention was maintained at high levels. The compound colour-motion stimulus events lasted for one second and were presented sporadically where the inter-stimulus intervals (ISIs) were selected from a random 'uniform' distribution that ranged from one to 36 seconds. One special design problem we faced was to ensure the effects of attention on

baseline activity and the modulation of evoked responses were as unconfounded or orthogonal as possible. This was achieved by deleting occasional events such that each attention condition had at least one "long" ISI of 33 secs (+/- 3secs). These intervals were needed to disambiguate attentional effects on the transient haemodynamic response to stimulus events from background activity associated with a particular attentional set (Friston *et al*, 1998) (see below).

6.3.2 Data Acquisition

Each volume comprised 32 axial slices with 3mm thickness (in plane resolution 3mm x 3mm) giving a repetition time, per volume, of 2.8s. Each experimental condition lasted for 98 seconds (35 volume scans) and was followed by a blank screen lasting for 19.6s (7 volume scans). We replicated each condition 10 times in a session, lasting for 39 minutes and 12 seconds. 840 image volumes (20 replicated conditions) were acquired in a session. Three normal right-handed volunteers (aged between 19 and 26, all female) participated in the study.

6.3.3 Data Analysis and Statistical Model

The data were smoothed using a 6mm isotropic Gaussian kernel full width at half maximum. Our fixed-effects statistical model comprised subject-specific effects (baseline attention effects, responses to stimulus events and the interaction between these two) and confounds (a constant term for each subject, low frequency components, global activity and stimulus events that were responded to). This analysis constituted a case-study of three subjects, allowing contrasts to be specified for (i) each subject separately and (ii) testing for average effects over subjects (see Fig. 6.1).

Our conclusions depend heavily on being able to separate measures of set-related baseline activity from measures of stimulus-evoked activity in the same brain region. To do this we used multi-linear regression, implemented in the context of statistical parametric mapping at each and every voxel using SPM97. The ensuing regression model is simply a linear combination of regressors or time-varying explanatory variables that best explain the observed time-series. In this instance, there were effectively three regressors of interest. These regressors modelled an effect of attentional set, event-related haemodynamic responses and the interaction between these two factors. The first regressor was 1 under attention to motion and -1 for scans acquired under attention to colour. Evoked responses were modelled by a delta function (*i.e.* spike) at the occurrence of every event. The interaction is simply the product of these two and accounts for differential evoked responses under both levels of attention. Haemodynamic responses to these effects were modelled by convolving the regressors with a synthetic haemodynamic response function and its temporal derivative.

Variations in cortical activity, about the mean of each voxel time-series, are expressed in terms of the relative contribution of these three effects, or more precisely the corresponding parameter estimates obtained with least squares. Statistical inferences are based on t-statistics (the parameter estimates divided by their standard error) that are assembled into a SPM{t}. The t-values were used only to infer that the effects described were significant (see below). The effects themselves are presented in terms of the parameter estimates, namely the difference in baseline activity associated with attentional set, the degree of evoked haemodynamic response and the attention-dependent component of these evoked responses (*i.e.* the interaction). In order to ensure that parameters are estimated efficiently, it is important to avoid correlations between the explanatory variables. This was a critical aspect of our experimental design and involved at least one long ISI during each attentional condition. The resulting small correlation co-efficients (< 0.3), between the attentional set regressors and those modelling attention specific events, do not ensure independence but make our estimates of any effects that are separable more efficient. However, it is important to appreciate that the parameter estimates are identical to those that would have been obtained if we had orthogonalized each effect with respect to the remaining effects in the design matrix. Put simply, this means that the results reported in the figures are the estimated responses to any particular effect, having removed any component that could be explained by the others. This renders our estimated responses conservative and, by virtue of the fact that they were still significant, robust. Had we not minimised the co-linearity between the regressors, by experimental design, it is possible that we would have seen no effect of attention (because it could be modeled by the interaction) and no effect of evoked response modulation (because it could be modeled by changes in attention). The actual estimates of activity in Figures 6.2 and 6.3 correspond to the parameter estimates where the constant term has been added back to the attentional baseline estimates. Fig.s 6.2a,c,e,6.3a,c,e show the average baseline activity, over and above which the stimulus event effects are seen. In Fig.s 6.2b,d,f,6.3b,d,f the dots around the estimated haemodynamic responses correspond to the original fMRI data adjusted for confounds and baseline attentional effects.

By using appropriate contrasts of condition-specific effects, SPM{t}s were created to test for regionally specific main effects and interactions. The SPM(t)s were transformed to SPM(Z) for display and tabulation. Statistical inferences were made using Gaussian random field theory to correct for multiple dependent comparisons. However, because we restricted our hypothesis to V1, V5, V3a and V4 we report all maxima at $p < 0.05$ (uncorrected), only if the areas survived this threshold in all three subjects. The SPMs shown in Figure 6.1 represent a conjunction analysis over all subjects. In other words, the SPMs show the effect tested for, averaged over subjects, but only in voxels where this effect was significant conjointly in every subject-specific analysis. Because of the separable nature of the design matrix, this corresponds to an uncorrected significance of $p < 0.05^3$.

6.4 Results

6.4.1 Behavioural

All subjects reported the task to be demanding and that they had to maintain attention to the attribute (colour or motion) in question. All subjects responded correctly on between 80 and 92% of target events (see methods) and incorrectly on between 20 and 24% of non-target events (Table 6.1). These results show that the subjects were able to discriminate the target events from the normal events, although the difference was sufficiently subtle that the subjects sometimes mistook non-target events for target events.

	SPEED		COLOUR		OVERALL	
Subject	%correct	%incorre	%correct	%incorre	%	%incorre
One	83	19	92	22	88	20
Two	75	11	94	31	80	21
Three	88	22	94	25	92	24

Table 6.1 Performance of each subject in the colour and motion target detection tasks. %correct denotes the number of events that the subject responded to correctly. %incorrect denotes the number of false positive responses.

6.4.2 Neurophysiological

The experimental design allowed us to model the effects of attention in terms of baseline changes and stimulus responses separately. Here we present findings that reflect the activity evoked by transient visual events *per se*, the effect of attentional set, and the interaction between the transient event and attentional set. The latter reflects the modulation of evoked responses by attention to colour or motion.

Fig. 1a

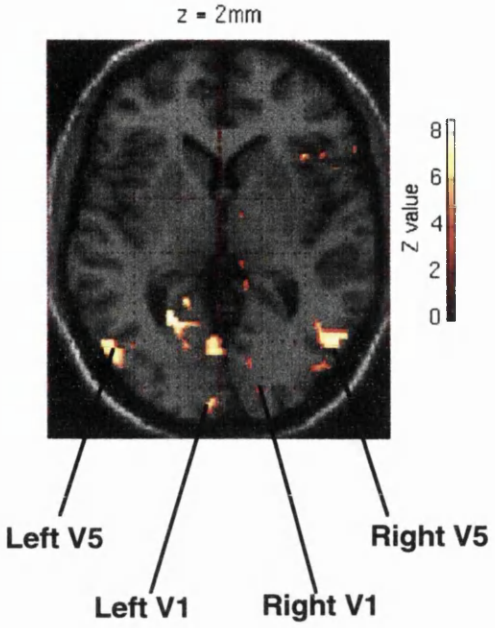

b

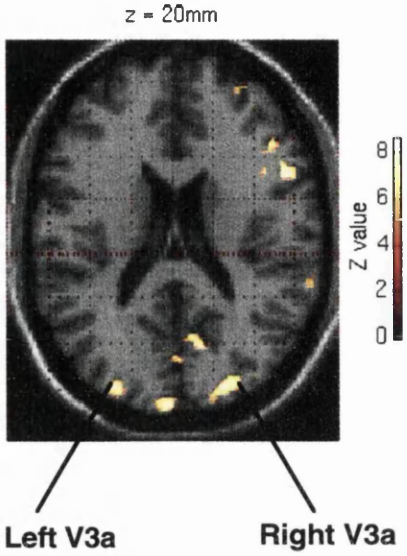

c

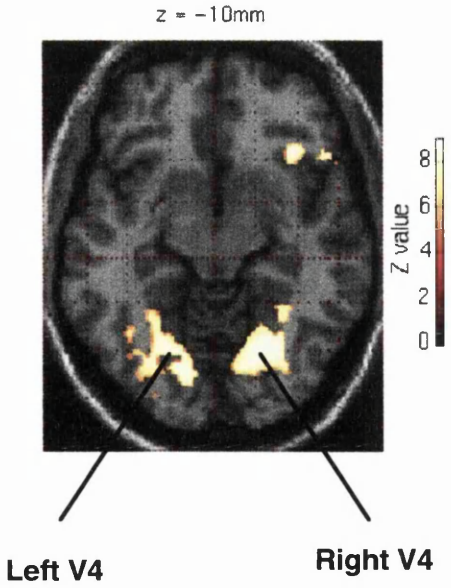

Fig. 6.1 SPM{Z} (threshold $p < 0.01$ uncorrected) showing the main effect of the stimulus vs. baseline over subjects, masked with the main effect from each individual subject (*i.e.* a conjunction of significant effects over all three subjects) and rendered on a structural MRI scan. (a) bilateral regional effects in V1 and V5. (b) bilateral V3a. (c) bilateral V4.

6.4.3 Activity Evoked by Transient Visual Events

Figure 6.1a shows the haemodynamic response due to the main effect of stimulus events (pooled over colour and motion). In each of the subjects, responses were seen bilaterally in the calcarine sulcus (primary visual cortex or V1), in the posterior region of the inferior temporal gyrus and sulcus known as area V5 (Watson *et al*, 1993, Zeki *et al*, 1991) (Fig. 6.1a), in the area of the superior part of the middle occipital gyrus that extended to the border of the angular gyrus, referred to as V3a (Tootell *et al*, 1997) (Fig. 6.1b) and in the fusiform gyrus or V4 (Lueck *et al,* 1989, Livingstone and Hubel, 1988) (Fig. 6.1c, Table 6.2).

6.4.4 Activity due to Attentional Set

A main effect of motion attentional set, obtained by subtracting the colour from the motion attention baseline was evident in areas V5 and V3a in all subjects (Table 6.2). A main effect of colour attention was observed in V4 in all subjects (Table 6.2). Table 6.2 shows the Z-scores of the main effect of attentional set as they appear in the maxima from the main effect of the stimulus events. In addition to the areas shown in Table 6.2, there were a small number of voxels that evidenced a main effect of motion attention in V4, bilaterally in all subjects at $p < 0.05$ (uncorrected). This finding is not considered further here, because it was not expressed at the V4 maximum for the main effect of events.

Subject	Area	Z - Score (M. E.	x	y	z	Z - Score (motion baseline -	Z - Score Interaction (motion >
One	Left V5	7.71**			6	2.78*	1.95*
	Right V5	6.89**	52		6	2.42*	1.86*
	Left V3a	3.92*			28	2.27*	-1.79*
	Right V3a	7.77**	24		26	3.02*	0.72
	Left V1	8.52**	- 8		0	1.11	0.84
	Right V1	7.39**	16		6	0.58	-0.80
	Left V4	7.72**				-2.82*	-1.90*
	Right V4	8.37**	30			-2.43*	-1.96*
Two	Left V5	7.43**			0	2.66*	2.22*
	Right V5	7.46**	56		0	2.99*	2.37*
	Left V3a	7.22**			26	2.80*	-0.63
	Right V3a	7.47**	22		22	2.89*	1.47
	Left V1	6.39**	- 2		- 2	-1.50	0.87
	Right V1	3.84*	10		- 2	-2.29*	0.66
	Left V4	7.55**				-2.64*	-1.91*
	Right V4	7.00**	18		- 6	-2.70*	-1.89*
Three	Left V5	7.45**			6	2.12*	2.53*
	Right V5	7.03**	44		12	2.07*	2.75*
	Left V3a	7.94**			30	3.05*	-0.78
	Right V3a	6.39**	20		34	2.66*	-0.33
	Left V1	6.92**	14		6	0.43	0.19
	Right V1	3.46*	- 8		2	-0.78	1.79*
	Left V4	7.82**				-2.83*	-2.06*
	Right V4	8.25**	38			-2.56*	-2.12*

Table 6.2 Talairach co-ordinates of the maxima in V1, V5, V3a and V4 testing for the main effect of the stimulus event in each subject. The table gives the Z-scores of the maxima from the stimulus main effect ($p < 0.001$ uncorrected). The table also contains the Z-scores of the main effect (M. E.) of motion/colour baseline and the interactions (motion > colour and *vice versa*) in that order. These Z-scores are from the same voxels as in the main effect of the stimulus and are significant at $p < 0.05$. Note that the Z-scores for the group were much larger, but we elected to show subject-specific Z-scores to demonstrate the reproducibility of these results.

Fig. 6.2a

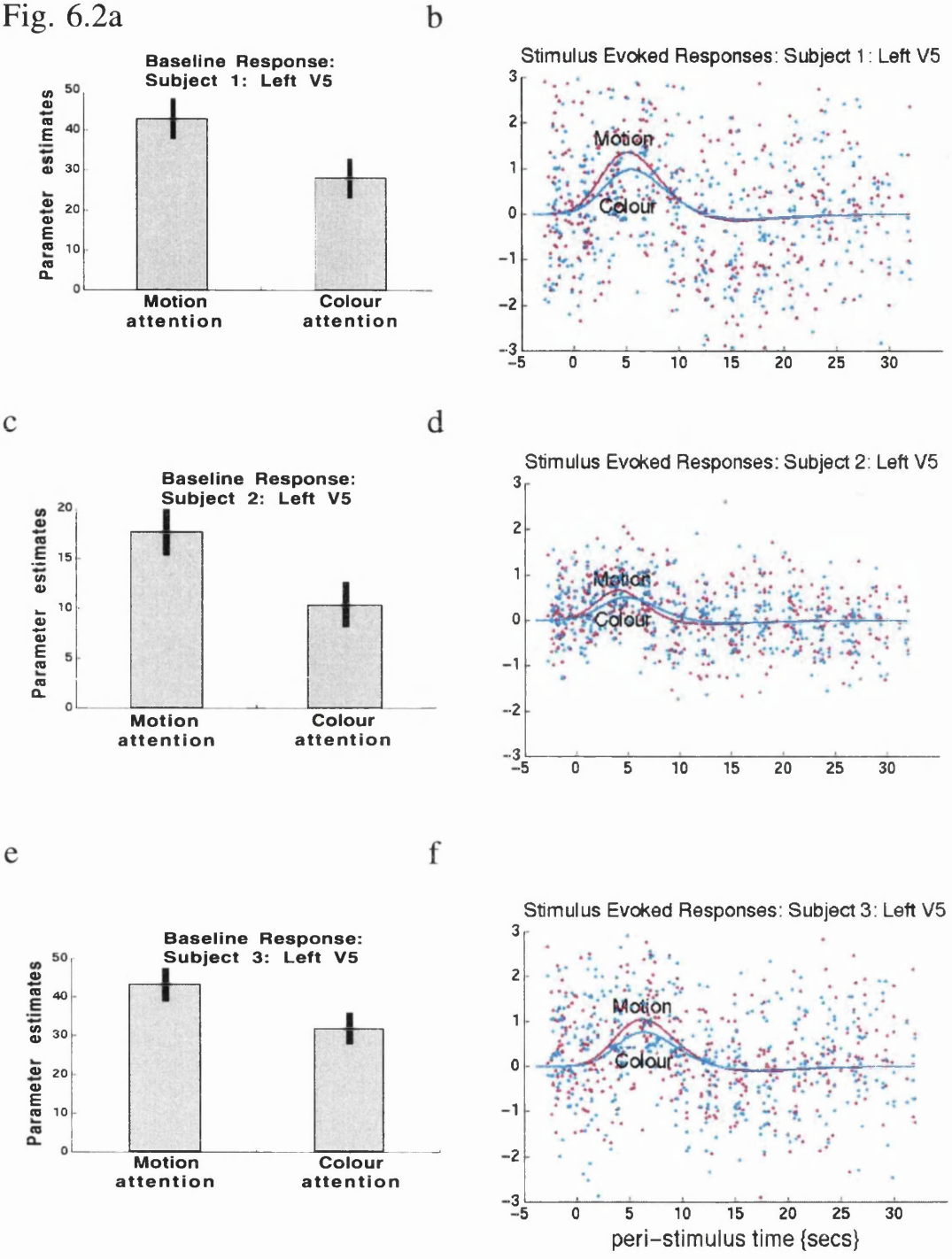

Fig. 6.2 Activity and responses in V5 as a function of attention in all subjects. (a) Parameter estimates with standard errors for baseline effects under both levels of attention in left V5 in subject one. (b) Adjusted data and fitted haemodynamic responses following the stimulus events under each attentional context (having adjusted for baseline effects) in left V5 for subject one. (c) and (d) show the same as (a) and (b) but in left V5 for subject two and (e) and (f) are for left V5 in subject three. The units are dimensionless and represent % whole brain mean signal. The magenta and cyan lines in b, d and f represent evoked responses under motion and colour attention respectively.

Fig. 6.3a

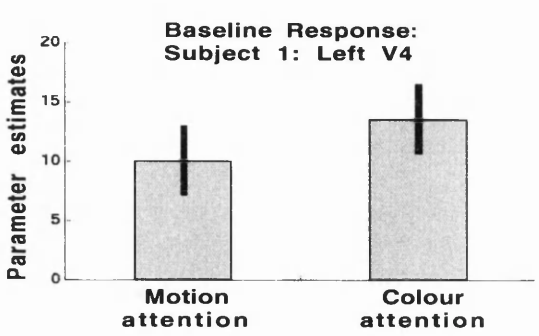

b

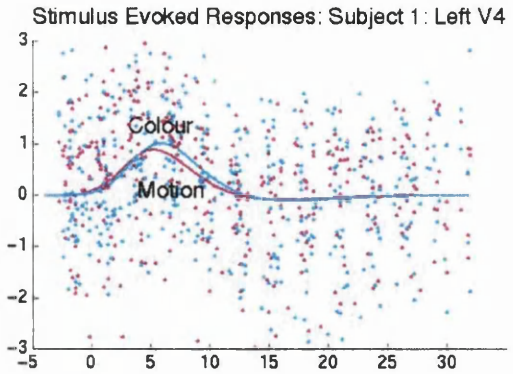

c

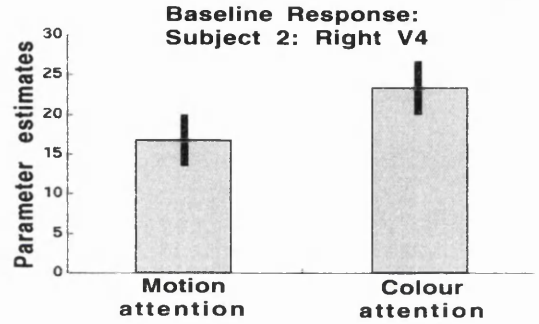

d

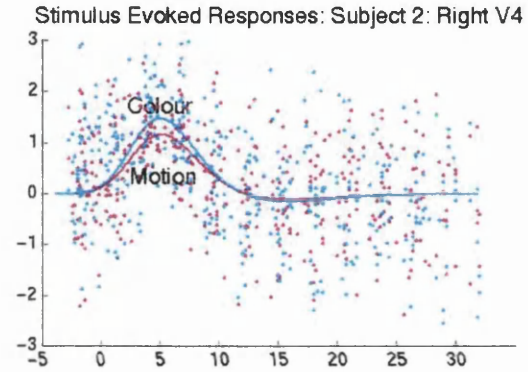

e

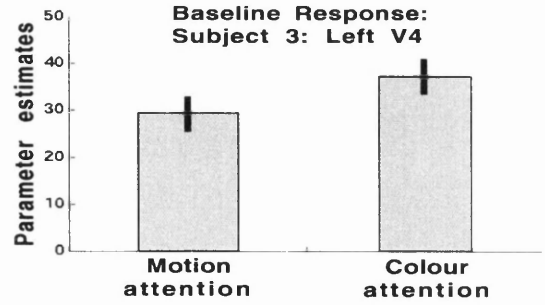

f

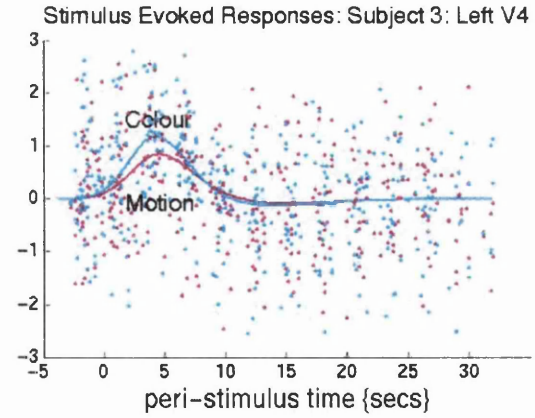

Fig 6.3 Activity and responses in V4 as a function of attention in all subjects. (a) Parameter estimates with standard errors for baseline effects in left V4 in subject one. (b) Adjusted data and fitted haemodynamic response curves following the stimulus events under each attentional context (having adjusted for baseline effects) in left V4 for subject one. (c) and (d) show the same as (a) and (b) but in right V4 for subject two and (e) and (f) are for left V4 in subject three. The magenta and cyan lines in b, d and f represent evoked responses under motion and colour attention respectively.

6.4.5 Interactions Between Attentional Set and Evoked Responses

To examine attentional modulation of evoked responses, we tested for interactions in the maxima of regions showing a main-effect of events in V5 and V4. In V5 (see Fig. 6.1a) in all subjects, greater haemodynamic responses were elicited by events under motion attention relative to colour attention (Fig. 6.2b,d,f). This modulation was expressed over and above the increased differential motion attention baseline described above (Fig. 6.2a,c,e). Furthermore, in the maxima of V4 (see Fig. 6.1c), an increased response was seen to events under colour attention as opposed to motion attention (Fig. 6.3b,d,f), this time in the context of an increased colour attention baseline (Fig. 6.3a,c,e). These results suggest that attention modulates both baseline activity and evoked responses in a way that is congruent with the functional specialisation of V4 and V5 and in accord with our predictions. These effects were seen bilaterally in V4 and V5 in all subjects. Examples from one hemisphere in each subject are shown in Figures 6.2 and 6.3.

6.5 Discussion

This event-related fMRI study revealed regionally specific effects of attention at two levels: Firstly, a baseline response to attentional set (motion), was observed in bilateral V5, in all subjects and a baseline response to colour attention was observed in V4. Secondly, greater evoked haemodynamic responses to stimuli under motion attention (after discounting baseline effects) were seen in V5 and greater stimulus responses under attention to colour were observed in V4.

The phenomena reported above are interesting in that there is enhanced activity in V5 when the subject attended to motion, *even when there was no motion in the visual field* (*i.e.* viewing stationary monochromatic dots) (Fig. 6.2a,c,e). In the same way, there was enhanced activity in V4, when the subject viewed monochromatic dots, but attended to colour (Fig. 6.3a,c,e).

The relationship between changes in set-related activity with attention and changes in visually evoked responses suggests that attention increases baseline activity within V5/V4, and in so doing increases the sensitivity to motion/colour stimuli. This observation may seem counterintuitive as increasing background activity might be thought to lead to a greater difficulty in distinguishing a transient signal from noise. However this result was fully anticipated by our computational work and the results of single-unit recording studies (Luck et al, 1997, Ferrera et al , 1994). In previous computational studies (see chapter 3), we used biologically plausible simulations of coupled neuronal populations to address the relationship between phasic and fast coherent neuronal interactions and macroscopic measures of activity that are integrated over time such as the BOLD (blood oxygenation level dependent) response in fMRI. Our simulations indicated that an attentional 'biasing signal' may mediate its effects

in a relatively simple way: Increased baseline activity leads to decreased effective post-synaptic membrane time constants (by increasing membrane conductance, see Chawla et al, 1999 and chapter 2) and a selective amplification of stimulus-related synchronous interactions (*i.e.* a predisposition to phase-locking). This reflects an interaction between background activity and stimulus-intensity in producing dynamic correlations. In other words, background activity augments stimulus-induced dynamics. This is interesting from a computational perspective as background activity establishes a context that may have a profound effect on event-related responses. This background-dependent increase in response sensitivity may constitute one of the physiological mechanisms underlying attention modulation and this was the motivation for the current experiment.

The issue of whether attention modulates baseline activity has also been examined electrophysiologically by Luck *et al* (1997). This study examined the role of attention in areas V1, V2 and V4 in monkey, using a paradigm where attention was directed to one of two stimulus locations. In V4, when the attended stimulus fell within the cell's receptive field (RF) and the ignored stimulus outside the RF, a 30-40% increase in baseline firing rate was seen, but no modulation of stimulus-evoked responses. Conversely, when both attended and ignored stimulus locations fell within the cell's RF, attentional modulation of evoked responses, but not baseline, were seen. These results suggest that attentional modulation is due to top down control mechanisms that affect either background *or* sensory-related activity, depending on the neuron recorded. However, our hypothesis posits that attentional modulation of baseline population activity is sufficient to mediate an increase in the gain of the population to sensory inputs. The electrode recording results above would be consistent with this mechanism if enhanced sensory-related responses in one set of cells were caused by increased input from another set of cells that expressed a baseline shift. The relationship between background activity and stimulus-evoked responses found empirically in this fMRI study and in previous computational simulations need not necessarily exist at the level of single cells and may be mediated by interactions among cells. Our empirical findings and mechanistic explanation in terms of population dynamics concurs with the suggestion from Luck et al (1997), that modulation of baseline activity "may reflect a top down signal that gives a competitive advantage to a stimulus" with an attended attribute, that is mediated by "a biasing signal that favours one population of cells over another (reflected by the baseline shift)". It remains a possibility that our results can be explained by presynaptic activity in modulatory afferents that sensitize cells to sensory inputs through voltage-dependent and other non-linear post-synaptic effects. This would preclude a mechanistic role for population dynamics. However, the existence of cells that show a postsynaptic baseline shift argues against modulatory effects, at a purely synaptic level, as a sufficient explanation.

Event-related potential recordings in human subjects have also demonstrated an interaction between target processing and antecedent attentional shifts. The early component (P1 and N1) of the visual evoked potential are known to be modulated by previous attentional allocation (Mangun *et al*, 1994). These authors found that these attention related negativities,

in the cue-target interval are associated with increased stimulus-locked P1 and N1 components.

It is interesting and unpredicted, that certain voxels in V4 showed a main effect of motion attention. Ferrera *et al* (1994) also found increased "delay period" or background activity in V4 cells during a motion discrimination task, "even though this pathway is not generally viewed as playing a major role in motion processing", although it was "significantly lower than in MT (V5)". However, only a few voxels in V4 showed this behaviour. Another interesting result from this study was the increase in motion attentional baseline activity in V3a. However, we were unable to demonstrate an interaction between attentional set and evoked responses in this region.

In conclusion, both a main effect of attention (where V5 (V4) activity is increased by motion (colour) attention even when there is no motion (colour) stimulus present) and an interaction between attention and the stimulus was found. This suggests that the main effect of attention (increase in background activity) might engender the interaction (increased sensitivity). It is possible, given our simulation results, that attention modulates responses purely by increasing the background activity within a population. In other words, a sufficient explanation for attentional modulation is a simple tonic background effect that is translated by non-linear neuronal interactions into a modulation of evoked transients. Likely candidates for areas that feed afferents to the visual areas, to increase background activity, have been inferred on the basis of labelling (Morecraft *et al*, 1993) and lesion studies (Mesulam *et al*, 1981). Areas implicated in attentional modulation are the frontal eye fields, cingulate, premotor, lateral prefrontal, orbitofrontal, opercular, posterior parietal, lateral and inferior temporal, parahippocampal and insular regions as well as subcortical regions such as the pulvinar. Specifically, areas implicated in mediating visual attention include the frontal cortex, occipital cortex, parietal cortex, medial thalamus and the superior colliculus (Buechel *et al*, 1998). These afferents could increase the gain of the neurons through the emergent dynamics at a population level and render them more sensitive to the attended stimulus.

General Discussion

From the work covered in this thesis, a compelling picture of neuronal processing or how neurons encode information emerges; namely that neuronal correlations or interactions are strongly linked to overall levels of neuronal activity. In other words, the extent to which different neurons engage in fast dynamic exchanges among each other is largely dependent on the neuronal population firing rates and *vice versa. i.e.* as one metric is varied (either neuronal activity or the extent of synchronization), so is the other. This informs the interpretation of functional neuroimaging results, in that it allows one to make inferences about the fast dynamic neuronal interactions that are taking place given macroscopic measures of activity, that are integrated over space and time, such as the BOLD response. Additionally, as a result of the strong coupling between overall activity and neuronal synchrony, there is also a strong relationship between background activity and stimulus evoked activity: Increased background activity renders the populations more prone to fast synchronous dynamics and in so doing increases the sensitivity of the neurons to an incoming stimulus and enhances stimulus evoked activity. This phenomenon may explain the mechanisms underlying certain cognitive functions. Indeed, in the final chapter of this thesis, we tested and confirmed that this theory may account for attentional modulation, *i.e.* the change in neuronal processing that occurs when the subject is attending to a stimulus attribute rather than being incidently exposed to it.

C1 Rate and Synchrony Coding

In chapter 2, we establish, using our neuronal population simulations, that there is a relatively robust monotonic relationship between neuronal phase-locking and activity levels. This indirectly addresses the relationship between rate and synchrony coding and suggests that they may simply represent two perspectives on the same underlying dynamic. In this view, synchronized, mutually entrained signals enhance overall firing levels and can be thought of as mediating an increase in the effective connectivity between and within neuronal populations. Equivalently, high levels of discharge rates increase the effective connectivity in the populations and augment the fast synchronous exchange of signals. Although it is clearly possible that the information conveyed by the precise timing of spikes is very different from that conveyed by discharge rates, from the point of view of population dynamics it may be that changes in spike timing cannot be divorced from changes in firing rate given the neuronal infrastructure employed by the brain. Further, due to the relationship between the temporal patterning of pre-synaptic events (either in terms of phase-locking as discussed in chapter 2, or in terms of dynamic correlations as considered in chapter 3), and post-synaptic discharge probabilities, an increase in synchronised input will inevitably result in higher population discharge rates. The demonstration of such a clear link between mean firing rates and synchronization suggests that metrics based on mean synaptic activity, such as fMRI and PET, may, in part, be sensitive to changes in synchronization.

To explore possible mechanisms that may underlie this link between neuronal synchrony and activity, an investigation of how the membrane time constants vary with activity was undertaken in chapter 3. These time constants were found to decrease with mean activity implying that synchrony emerges with shorter time constants (see Fig. 2.7 from chapter 2). The decrease in time constants is a natural consequence of conjointly increasing membrane conductances through excitatory and inhibitory channels at high levels of activity. As activity levels increase, smaller membrane time constants promote the synchronous gain in the network. *i.e.* individual neurons become more sensitive to temporal coincidences in their synaptic inputs, responding with a higher firing rate to synchronous rather than asynchronous inputs. Therefore, in the event-related context considered in chapter 3, as background noise increases, the network becomes more prone to stimulus-induced synchronous transients. This is reflected both in the time that the post-stimulus synchronization endured (see Fig. 3.2 from chapter 3) and a progressive increase in the mutual information vs. stimulus intensity regression slope (see Fig. 3.1 from chapter 3). The latter effect constitutes an interaction and can be viewed as a stimulus-dependent effect that is context-sensitive. The context is set by the tonic background of activity and is mediated through a progressive diminution of the effective membrane time constants.

C2 Functional Imaging

The interaction between background and evoked rate modulation mentioned at the end of the previous paragraph is an important phenomenon when trying to interpret responses observed with functional neuroimaging. For example, in chapter 5, we used fMRI to show that the BOLD response in human visual "motion area" V5, varies with visual speed, in the same way as macaque V5 neuronal responses. It is relatively well established, through optical imaging studies as mentioned in the introduction, that cortical haemodynamics co-vary with local neuronal activity levels, However, as we have shown in this thesis, if integrated population activity increases, so does synchrony. In chapter 6, we tested a specific prediction of our modelling work in the human brain using fMRI: We showed in chapter 3, that increased mean population activity also increases the gain of the neurons to afferent input, due to the concomitant increase in neuronal synchrony and neuronal interactions. In chapter 6, we tested the hypothesis that this phenomenon may account for attentional modulation. For example, consider the cortical responses to a train of stimuli measured when the subject is attending and not attending to some attribute of these stimuli. Increased responses maybe due to (i) attentional modulation of background activity, (ii) attentional modulation of stimulus-dependent responses or (iii) both, that renders the neuronal populations more sensitive to the stimuli. Using fMRI, we were able to dissociate activity due to attentional set, or expectation, (this represents background activity) and that due to stimulus evoked responses, to investigate the interaction between attentional set and stimulus responses. We showed the same type of interaction between set-related responses and stimulus responses that we observed between background activity and stimulus induced rate-modulation in our simulated neuronal populations. In this attentional study, we focused on the visual cortex and, in particular, on the "colour" and "motion areas", V4 and V5. Our experiment tested whether attentional modulation, of evoked responses, may be mediated by simply increasing background activity in the appropriate functionally specialised populations. Using event-related fMRI, we showed regionally specific effects of attention at two levels: (i) A baseline response to attentional set (motion), was observed in V5 and a baseline response to colour attention was observed in V4. (ii) Greater evoked haemodynamic responses to stimuli under motion attention (after removing baseline effects) were seen in V5 and greater stimulus responses under attention to colour were observed in V4.

The form of the relationship between changes in set-related activity with attention and changes in evoked responses to transient visual events suggests that attention increases the background activity within V5/V4, and in so doing increases the sensitivity to motion/colour stimuli. Although we showed that our theory may account for attentional modulation in visual cortex, we clearly imply that this mechanism may be responsible for attention in a more general sense. For example attentional modulation of this sort may occur in auditory cortex when the subject is attending to the particular tones, amplitudes or frequencies of sounds. Alternatively, it may occur in olfactory cortex when the subject attends to particular odours. In short, the link between neuronal activity and dynamic correlations and the context it

establishes, in which there is a profound interaction between background activity and stimulus evoked responses, may mediate the neuronal correlates of the processes that allow us to attend to and "perceive" our environment rather than passively "sense" it.

C3 Conclusion

In conclusion this thesis has addressed the relationship between overall levels of neuronal activity at a population level and the incidence of fast dynamic, synchronous interactions among neurons that constitute the populations. The motivation for this work was to develop a better understanding of what measures, like the BOLD signal in fMRI can tell one about the underlying neuronal dynamics. Computational studies pointed to a robust and monotonic relationship between the degree of synchronous interactions and population activity both in terms of continuous dynamics and those evoked by transient inputs to neuronal populations. The coupling between synchronous gain and mean activity, at a population level may be mediated by the obligatory decease in effective membrane time constants associated with high levels of population activity. This is a central contribution of the work presented in this thesis. From this work we developed the hypothesis that modulation of the population responses to any afferent input could be effected simply by changes in baseline or background mean population activity. By using attention modulation as a specific example of this effect we were able to predict, and confirm, changes in baseline and evoked activity observed with functional magnetic resonance imaging.

In summary, the selection of synchronous dynamics depends upon small effective membrane time constants. A reduction in effective membrane time constants occurs with increases in population activity. The conclusion is therefore that high levels of mean population activity will facilitate the expression of average synchronous interactions. It is important to realise that this coupling is at a population or average level. It does not preclude independent rate and temporal coding at the level of single units but does suggest that at the population level, synchrony and rate codes are linked in an obligatory way simply because of the nature of the neuronal infrastructure that engenders the dynamics. From the point of view of neuroimaging, the identification of two regional increases in mean activity suggests that somewhere there will be an average increase in synchronous interactions. Neuroimaging *per se* does not allow any inferences about where these interactions are taking place. For example, the synchrony could exist within two unconnected populations or reflect synchronous interactions between the two cortical areas implicated by neuroimaging. A further qualification is that effective membrane time constants can be decreased by other mechanisms such as the opening of specific channels by modulatory afferents to a population. However, because of the circular causality outlined earlier in this thesis, the results of this modulatory input will be an increase in synchronous gain and concomitant increases in mean activity. In short, whenever we see increases in mean synaptic activity with functional neuroimaging we can infer an increase in synchronous interactions.

The hypothesis that synchrony and mean activity are tightly coupled at a population level but not necessarily at the level of a single unit speaks to the interactions between different scales. From this perspective it is important to note that only neuroimaging is in a position to measure the synaptic activity at a population level whereas electrophysiology is required to make inferences about synchrony at the level of single or small numbers of neurons. It follows that a complete characterisation of the relationship between synchrony and mean activity at both the single unit and population level will require a combination of functional neuroimaging and electrophysiological techniques. Future work could use techniques that measure electrical activity at a millisecond time scale in the human brain such as electroencephalography (EEG) (this technique uses electrodes on the scalp to measure brain activity), to address further the interpretation of integrated measures of activity, such as those obtained by neuroimaging. In this way the link between BOLD signal, overall activity and correlations may be investigated empirically, using combined fMRI and EEG, in humans, or combined fMRI and electrode recordings, in non-human primates. With the advent of non-human primate fMRI and the increasing spatial resolution of distributed dipole source estimation in human EEG and MEG these multi-scale studies may be possible in the next few years. Indeed, such combinations of empirical techniques will prove vital, as fMRI is becoming more and more widely used within the neuroscience community to characterize the neurological correlates of perception and cognition.

References

Abeles M, 1982, Role of the cortical neuron: integrator or coincidence detector? *Isr J Med Sci* **18**: 83-92

Aertsen A & Preissl H, 1991, Dynamics of activity and connectivity in physiological neuronal Networks. In Non Linear Dynamics and Neuronal Networks Ed Schuster HG VCH publishers Inc., New York NY USA: 281-302

Aertsen A, Erb M, Palm G, 1994, Dynamics of functional coupling in the cerebral cortex: an attempt at a model-based interpretation, *Physica D* **75**: 103 - 128

Ahmed B, Anderson J, Douglas R, Martin K, Nelson J, 1994, Polyneuronal innervation of spiny stellate neurons in cat visual cortex. *J Comp Neurol* **341**: 39 - 40

Bashir *et al*, 1993, Induction of LTP in the hippocampus needs synaptic activation of glutamate metabotropic receptors. *Nature* **363**: 347 - 350

Beaulieu C & Colonnier M, 1983, The number of neurons in the different laminae of the binocular and monocular regions of area 17 in the cat. J. Comp. Neurology **217**: 337-344

Beaulieu C & Colonnier M, 1985, A laminar analysis of the number of round-asymetrical and flat-symmetrical synapses on spines, dendritic trunks and cell bodies in area 17 of the cat. *J. Comp. Neurology* **231**: 180-189

Beaulieu C, Kisvarday Z, Somogyi P, Cynader M, 1992, Quantitative distribution of GABA-immunopositive and -immunonegative neurons and and synapses in the monkey striate cortex (area 17), *Cerebral Cortex* **2**: 295 - 309

Beckers G & Zeki S, 1995, The consequences of inactivating areas V1 and V5 on visual

motion perception. *Brain* **118**: 49-60

Bernander O, Douglas R J, Martin K A C, Koch C, 1991, Synaptic background activity influences spatiotemporal integration in single pyramidal cells, *Proc. Natl. Acad. Sci. USA*, **88**: 11569 - 11573

Bliss & Lomo, 1973, Long lasting potentiation of synaptic transmission in the dentate area of the anaesthetised rabbit following stimulation of the perforant path. *J. Physiol.* **232**: 331 - 356

Boven KH, Aertsen AMHJ, 1990, Dynamics of activity in neuronal networks give rise to fast modulations of functional connectivity. In: Parallel processing and neural systems and computers. Elsevier Science Publishers, North Holland: **53** - 56

Bower & Beeman, 1994, The book of genesis, Springer Verlag New York, Inc.

Bruce CJ, Desimone R, Gross CG, 1981, Visual properties of neurons in a polysensory area in superior temporal sulcus of the macaque. *J. Neurophysiol.* **46**: 369 - 384

Brugge JF, Merzenich MM, 1973, Responses of neurons in auditory cortex of the macaque monkey to monaural and binaural stimulation. *J. Neurophysiol.* **36**: 1138 - 59

Buckner Rl, Bandettini PA, O'Craven KM, Savoy RL, Petersen SE, Raichle ME, Rosen BR, 1996, Detection of cortical activation during averaged single trials of a cognitive task using functional magnetic resonance imaging. *Proc. Natl. Acad. Sci. USA* **93**: 14878 - 14883

Buechel C, Josephs O, Rees G, Turner R, Frith CD, Friston KJ, 1998, The functional anatomy of attention to visual motion: A functional MRI study. *Brain* **121**: 1281 - 1294

Calabresi P, Mercuri NB, Stefani A, Bernardi G, 1990, Synaptic and intrinsic control of membrane excitability of neostriatal neurons. I. An in vivo analysis. *J. Neurophysiol.* **63(2)**: 651-662

Chatfield C & Collins AJ, 1980, Introduction to Multivariate Analysis. Chapman and Hall

Chawla D, Phillips J, Buechel C, Edwards R, Friston KJ, 1998, Speed-Dependent Motion Sensitive Responses in V5: An fMRI study. *NeuroImage* **7**: *86-96*

Chawla D, Buechel C, Edwards R, Ashburner J, 1999, Josephs O, Howseman A, Friston KJ, Speed-Dependent Responses in V5: A Replication Study. *NeuroImage* **9**: *508 - 515*

Chawla D, E. Lumer ED, Friston KJ, 1999, The Relationship between Synchronization among

Neuronal Populations and their Mean Activity Levels. *Neural Computation* **11**: *1389 - 1411*

Chawla D, E. Lumer ED, Friston KJ, Relating Macroscopic Measures of Brain Activity to Fast Dynamic Neuronal Interactions. *Neural Computation. In press*

Chawla D, Rees G, Friston KJ, 1999, The Physiological Basis of Attentional Modulation in Extrastriate Visual Areas. *Nature Neuroscience* **2(7)**: *1 - 6*

Chelazzi L, 1995, Neural mechanisms for stimulus selection in cortical areas of the macaque subserving object vision. *Behav. Brain. Res.* **71**: 125 - 34

Cheng K, Hasewage T, Saleem K, Tanaka K, 1994, Comparison of neuronal selectivity for stimulus speed, length, and contrast in prestriate visual cortical areas V4 and MT of the macaque monkey. *J. Neurophysiol.* **71(6)**: 2269 - 80

Crick F and Koch C, 1998, Constraints on cortical and thalamic projections: the no-strong loops hypothesis. *Nature* **391**: 245-250

Conde F, Lund J, Jacobwitz D, Baimbridge KG, Lewis D, 1994, Local circuitneurons immunoreactive for calretinin, calbindin D-28k or parvalbumin in monkey prefrontal cortex: distribution and morphology. *J Neurosci* **341**: 95 - 116

Corbetta M, Miezin FM, Dobmeyer S, Shulman GL, Petersen SE, 1991, Selective and divided attention during visual discriminations of shape, colour and speed: functional anatomy by positron emission tomography. *J. Neurosci* . **11**: 2383 - 402

Cowey A & Heywood CA, 1995, Theres more to colour than meets the eye. *Behav. Brain. Res.* **71**: 89 - 100

Cronin J, 1987, Mathematical aspects of Hodgkin-Huxley neural theory (Cambridge University Press)

Daw NW, 1972, Color coded cells in goldfish, cat, and rhesus monkey. *Invest. Ophthalmol.* **11**: 411 - 17

deCharms RC, Merzenich MM, 1996, Primary cortical representation of sounds by the coordination of action potential timing. *Nature* **381**: 610-613

Desimone R & Ungerleider LG, 1989, Neural mechanisms of visual processing in monkeys. In: *Handbook of neurophysiology*, edited by F. Boller & J. Graffman. New York: Elsevier **2**: 267 - 299

Desimone R, Albright TD, Gross CG, Bruce C, 1984, Stimulus selective properties of inferior temporal neurons in the macaque. *J. Neurosci.* **4**: 2051 - 2062

Desimone R & Ungerleider L, 1989, Neural mechanisms of visual processing visual procesing in monkeys. In: Handbook of of neuropsychology, F. Boller & J. Graman, eds. Amsterdam Elsevier, p267 - 299

De Yoe EA & Van Essen DC, 1985, Segregation of efferent connections and receptive field properties in visual area V2 of the macaque. *Nature* **317**:58-61

Domenici L, Harding GW, Burkhalter A, 1996, Patterns of synaptic activity in forward and feedback pathways within rat visual cortex. *J. Neurophysiol.* **74**: 2649 - 64

Dubner R & Zeki SM, 1971, Response properties and receptive fields of cells in an anatomically defined region of the superior temporal sulcus in the monkey. *Brain Res.* **35(2)**: 528 - 32

Engel AK, Konig P, Kreiter AK, Gray CM, Singer W, 1990, Temporal Coding by coherent oscillations as a potential solution to the binding problem, in Nonlinear Dynamics and Neural Networks, VCH: 3: 26

Engel AK, Konig P, Kreiter AK, Singer W, 1991, Interhemispheric synchronization of oscillatory neuronal responses in cat visual cortex. *Science* **252**: 1177 - 9

Felleman DJ and Van Essen DC, 1987, Receptive field properties in area V3 of macaque monkey extrastriate cortex, *J. Neurophysiol.*, **57(4)**: 889-920

Felleman DJ and VanEssen DC, 1991, Distributed Hierarchical Processing in the Primate Cerebral Cortex. *Cerebral Cortex* **1**: 1-47

Ferrera VP, Rudolph KK, Mausell JHR, 1994, Responses of neurons in the parietal and temporal visual pathways during a motion task. *J. Neurosci.* **14**: 6171 - 86

ffytche DH, Guy CN and Zeki S, 1995, The parallel visual motion inputs into areas V1 and V5 of human cerebral cortex. *Brain* **118**: 1375-94

ffytche, D. H., C . N. Guy and S. Zeki, 1996, Motion specific responses from a blind Hemifield *Brain* **119**: 1971 - 1982

Freguelli *et al*, 1993, Metabotropic glutamate receptors and calcium signalling in dendrites of CA1 neurons. *Neuropharm.* **32**: 1229 - 1237

Freiwald WA, Kreiter AK, Singer W, 1995, Stimulus dependent intercolumnar synchronization of single unit responses in cat area 17. *Neuroreport.* **6**: 2348 - 52

Frien A, Eckhorn R, Bauer R, Woelbern T, Kehr H, 1994, Stimulus-specific fast oscillations at zero phase between visual areas V1 and V2 of awake monkey. *NeuroReport* **5**: 2273-77

Fries P, Roelfsema PR, Engel A, Konig P and Singer W, 1997, Synchronization of oscillatory responses in visual cortex correlates with perception in interocular rivalry. *Proc Natl Acad Sci USA* **94**: 12699-12704

Friston KJ, 1994, Functional and Effective Connectivity in Neuroimaging: A Synthesis. *Human Brain Mapping* **2**: 56 - 78

Friston KJ, Ungerleider LG, Jezzard P, Turner R, 1995, Characterizing Modulatory Interactions Between Areas V1 and V2 in Human Cortex: A New Treatment of Functional MRI Data. *Human Brain Mapping* **2**: 211-224

Friston KJ, Ashburner J, Frith CD, Poline JB, Heather JD, Frackowiak RSJ, 1995, Spatial registration and normalisation of brain images. *Human Brain Mapping* **2**:165-189

Friston KJ, Holmes AP, Worsley KJ, Poline JB, Frith CD, and Frackowiak RSJ, 1995, Stastistical parametric maps in functional imaging: A general linear approach. *Human Brain Mapping* **2**: 189-210

Friston KJ, Williams S, Howard R, Frackowiak RSJ, Turner R, 1996, Movement related effects in fMRI time series. *Magnetic Resonance in Medicine* 346-355

Friston KJ, 1997, Transients, Metastability and Neuronal Dynamics. *NeuroImage* **5**: 164-171

Friston KJ, Josephs O, Rees G, Turner R, 1998, Nonlinear Event-Related Responses in fMRI. *Magnetic Reson. Med.* **39**: 41 - 52

Frith CD & Friston KJ, 1996, The role of the thalamus in "top down" modulation off attention to sound. *NeuroImage* **4**: 210 - 215.

Frostig RD, Lieke EE, Ts 'o DY, Grinvald A, 1990, Cortical functional architecture and local coupling between neuronal activity and the microcirculation revealed by in vivo high-resolution optical imaging of intrinsic signals. *Proc. Natl. Acad. Sci. USA*, **87**, 6082-86

Gegenfurtner KR, Kiper DC, Beusmans JMH, Carandini M, Zaidi Q, Movshon JM, 1994, Chromatic properties of neurons in MT. *Vis. Neurosci.* **11**:455-66

Gerstein GL & Perkel DH, 1969 Simultaneously recorded trains of action potentials: Analysis and functional interpretation *Science* **164**:828-830

Gerstein G L & Perkel H, 1972, Mutual temporal relationships among meuronal spike trains, *Biophysical Journal* **12**: 453 - 473

Gerstein GL, Bedenbaugh P & Aertsen AMHJ, 1989 Neuronal assemblies *IEEE Trans. on Biomed. Engineering* **36**:4-14

Girard P & Bullier J, 1989, Visual activity in area V2 during reversible inactivation of area 17 in the macaque monkey. *J. Neurophysiol.* **62**: 1287-1301

Gray CM & Singer W, 1989, Stimulus specific neuronal oscillations in orientation columns of cat visual cortex *Proc. Natl. Acad. Sci USA* **86**:1698-1702

Gray CM *et al*, 1992, Synchronization of oscillatory neuronal responses in cat striate cortex: temporal properties. *Vis Neurosci.* **8**: 337 - 47

Gray CM, Konig P, Engel AK, Singer W, 1989, Oscillatory responses in cat visual cortex exhibit inter-columnar synchronization which reflects global stimulus properties, *Nature* **338**: 334 - 337

Gray CM, Engel AK, Konig P, Singer W, 1990, Temporal properties of synchronous oscillatory neuronal interactions in cat striate cortex, in Nonlinear Dynamics and Neural Networks, VCH: 27:56

Grinvald A, Anglister L, Freeman JA, Hildesheim R, Manker A, 1984, Real-time optical imaging of naturally evoked electrical activity in intact frog brain. *Nature* **5962**: 848 - 50

Grinvald A, Lieke E, Frostig RD, Gilbert CD, Wielsel TN, 1986, Functional architecture of cortex revealed by optical imaging of intrinsic signals. *Nature* **6095**: 361 - 4

Gross CG, Rocha-Miranda CE, Bender DB, 1972, Visual properties of neurons in inferiortemporal cortex of the monkey. *J. Neurophysiol.* **35**: 96 - 111

Haenny PE & Schiller PH, 1988, State dependent activity in monkey visual cortex. I. Single cell activity in V1 and V4 on visual tasks. *Exp. Brain Res.* **69(2)**: 225 - 44

Heywood CA, Gaffan D, Cowey A, 1995, Cerebral achromatopsia in monkeys. *Eur. J. Neurosci.* **7**: 1064 - 73

Hikosaka K, Iwai E, Saito HA, Tanaka K, Polysensory properties of neurons in the anterior

bank of the caudal superior temporal sulcus of the macaque monkey. *J. Neurophysiol.* **60**: 1615 - 1637

Hubel DH, 1988, Eye, Brain and Vision, *Scientific American Library*

Hubel DH & Livingstone MS, 1987, Segregation of form color and stereopsis in primate area 18. J. *Neurosci.* **7**:3378-3415

Hubel DH & Wiesel TN, 1962, Receptive fields, binocular interaction and functional architecture in the cats visual cortex. *J. Physiol. (Lond.)* **160**: 106 - 54

Hubel DH & Wiesel TN, 1965, Receptive fields and functional architecture in two non striate visual areas (18 and 19) of the cat. *J. Neurophysiol.* **28**: 289 - 99

Hubel DH & Wiesel TN, 1968, Receptive fields and functional architecture of monkey striate cortex. *J. Physiol. (Lond)* **195**: 215 - 43

Hubel DH & Wiesel TN, 1977, The Ferrier Lecture: Functional architecture of macaque monkey visual cortex. *Proc. R. Soc. Lond. B.* **198**: 1 - 59

Johnson RR, Burkhalter A, 1996, Microcircuitry of forward and feedback connections within rat visual cortex. *J. Physiol.* **160**: 106 - 154

Josephs O, Turner R, Friston KJ, 1997, Event-related fMRI. *Hum. Brain Map.* **5**: 243 - 248

Kaas JH and Hackett AT, 1998, Subdivisions of Auditory Cortex and Levels of Processing in Primates. *Audiol. Neurootol.* **3**: 73 - 85

Kawaguchi Y, 1995, Physiological subgroups of nonpyramidal cells with specific morphological characteristics in layer ii/iii of rat frontal cortex. *J Neurosci* **15**: 2638 - 2655

Konig P, Engel AK, Singer W, 1995, Relation between oscillatory activity and long-range synchronization in cat visual cortex, *Proc. Natl. Acad. Sci. USA* **92**: 290 - 294

Lagae L, Raigual S, Orban GA, 1993, Speed and direction selectivity of macaque middle temporal neurons. *J. Neurophysiol.* **69**: 19 - 39

Lee BB, Creutzfeldt OD, Elefandt A, 1979, The responses of magno- and parvocellular cells of the monkeys lateral geniculate body to moving stimuli. *Exp. Brain Res.*, **35(3)**: 547 - 57

Livingstone MS, and Hubel DH, 1987, Psychophysical evidence for separate channels for the perception of form colour movement and depth. *J.Neurosci.* **7(11)** 3416-3468

Livingstone MS and Hubel DH, 1988, Segregation of form, colour, movement and depth: anatomy physiology and perception. *Science* **240**: 740 - 749

Lorenzon NM, Foehring RC, 1992, Relationship between repetitive firing and afterhyperpolarizations in human neocortical neurons. *J. Neurophysiol.* **67(2)**: 350 -363

Luck SJ, Chelazzi L, Hillyard SA, Desimone R, 1997, Neural Mechanisms of Spatial Selective Attention in Areas V1, V2, and V4 of Macaque Visual Cortex. *J. Neurophysiol.* **77**: 24 - 42

Lueck CJ *et al,* 1989, The colour centre in the cerebral cortex of man. *Nature* **340**: 386 - 389

Lumer ED, Edelman GM, Tononi G, 1997, Neural Dynamics in a model of the thalamocortical System I. Layers, Loops and the Emergence of Fast Synchronous Rhythms, *Cerebral Cortex* **7**:207 - 227

Lumer ED, Edelman GM, Tononi G, 1997, Neural Dynamics in a model of the thalamocortical System II. The role of neural synchrony tested through perturbations of spike timing., *Cerebral Cortex* **7**:228 - 236

Magleby, K. M., In: Edelman *et al*,Synaptic Function (Wiley Interscience 1987): 21-57

Mainen ZF and Sejnowski TJ, 1995, Reliability of spike timing in neocortical neurons. *Science* **258**: 1503 - 6

Mangun GR, 1994, Orienting attention in the visual fields: an electrophysiological analysis. In Cognitive electrophysiology (Heinze HJ, Munte TF, Mangun GR, eds), Boston, Birkhauser: 1 - 101

Markram H, Lubke J, Frotcher M, Sakmann B, 1997, Regulation of synaptic efficacy by coincidence of postsynaptic APs and EPSPs. *Science* **275**: 213 - 5

Mathiesen C, Caesar K, Akgoren N, Lauritzen M, 1998, Modification of activity-dependent increases of cerebral blood flow by excitatory synaptic activity and spikes in rat cerebellar cortex. *J. Physiol.* **512**: 555 - 566

McAdams C. J. & Maunsell J. H. R., 1999, Effects of Attention on Orientation -Tuning Functions of Single Neurons in Macaque Cortical Area V4. *J. Neurosci.* **19(1)**: 431 - 441

Mesulam MM, 1981, A cortical network for directed attention and unilateral neglect. A*nn. Neurol.* **10**: 309 - 25

Meredith M and Moulton DG, 1978, Patterned response to odor in single neurones of goldfish olfactory bulb: influence of odor quality and other stimulus parameters. *J. Gen. Physiol.* **71**: 615 - 43

Mikami A, Newsome WT, Wurtz RH, 1986, Motion Selectivity in macaque visual cortex II: Spatiotemporal range of directional interactions in MT and V1. *J. Neurophys.* vol **55(6)**: 1328 - 39

Milner PM, 1974, A model for visual shape recognition. *Psychological Review* **81(6)**: 521-535

Mistlin AJ & Perret DI, 1990, Visual and somatosensory processing in the macaque temporal cortex: the role of 'expectation'. *Exp. Brain. Res.* **82**: 427 - 450

Morecraft RJ, Geula C, Mesulam MM, 1993, Architecture of connectivity within a cingulo-fronto-parietal neurocognitive network for directed attention. *Arch. Neurol.* **50**: 279 - 84

Morgan MJ, and Ingle G, 1994, What direction of motion do we see if luminance but not colour contrast is reversed during displacement? Psychophysical evidence for a signed colour input to motion detection. *Vision Res.* **34** no. 19 2527-2535

Nicolelis MAL, Baccala LA, Lin RC, Chapin JK, 1995, Sensorimotor encoding by synchronous neural ensemble activity at multiple levels of the somatosensory system. *Science* **268**: 1353 - 58

Nicholls JG, Martin AR, Wallace BG, 1992, From Neuron to Brain, Sinauer, Massachusetts, U.S.A.

Nowak LG, Munk MH, Nelson JI, James AC, Bullier J, 1995, Structural Basis of cortical synchronization. I. Three types of Interhemispheric Coupling, *Neurophys.* **76**: 1:22

O'Craven KM, Rosen BR, Kwong KK, Treisman A, Savoy RL, 1997, Voluntary attention modulates fMRI activity in human MT-MST. *Neuron* **18**: 591 - 8

Otis T and Mody I, 1992, Differential activation of GABAa and GABAb receptors by spontaneously released transmitter. *J. Neurophysiol.* **67**: 227-235

Otis T, Konick YD, Mody I, 1993, Characterization of synaptically elicited GABAb responses using patch-clamp recordings in rat hippocampal slices. *J. Physiol. London* **463**: 391-407

Ohanion HC, Physics, W.W. Norton and Company, New York, London.

Oram MW & Perret DI, 1996, Integration of form and motion in the anterior superior temporal polysensory area (STPa) of money. *J. Neurophysiol* **76**:109 - 29

Oram MW, Perret DI, Hietanen JK, 1993, The directional tuning of motion-sensitive cells in the anterior superior temporal polysensory area. *Exp. Brain. Res.* **97**: 274 - 94

Pinksy PF& Rinzel, 1994, Intrinsic and network rhythmogenesis in a reduced Traub model for CA3 neurons. *J. Comput. Neurosci.* **1**: 39 - 60

Rall W, 1995, in The Handbook of Brain Theory and Neural Networks (Arbib, M.A., ed.), p728 - 732, *MIT Press*

Rauschecker JP, 1998, Parallel Processing in the Auditory Cortex of Primates, *Audiol. Neurootol.* **3**: 86 - 103

Rockland KS, 1996, Two types of corticopulvinar terminations: round (type 2) and elongate (type 1). *J. Comp. Neurol.* **368**: 57-87

Rodman, HR *et al.*, 1987, Coding of visual stimulus velocity in area MT of the macaque, *Vision Res.* **27(12)**: 2035 - 48

Roelfsema PR, Konig P, Engel AK, Sireteanu R and Singer W, 1994, Reduced synchronization in the visual cortex of cats with strabismic amblyopia. *Eur. Jounal Neurosci.* **6**: 1645-1655

Roelfsema PR, Engel AK, Konig P, Singer W, 1997, Visuomotor integration is associated with zero time-lag synchronization among cortical areas, *Nature* vol. **385**: 157 - 161

Rees G, Frackowiak R, Frith CD, 1997, Two modulatory effects of attention that mediate object categorization in human cortex. *Science* **275**: 835 - 8

Sandell JH and Schiller PH, 1982, Effect of cooling area 18 on striate cortex cells in the squirrel monkey. *J Neurophysiol.* **48**: 38-48

Schiller PH and Malpeli JG, 1977, The effect of striate cortex cooling on area 18 cells in the monkey. *Brain Res.* **126**: 366-369

Schiller PH & Lee K, 1991, The role of the primate extrastriate area V4 in vision. *Science* **251**: 1251 - 3

Shipp S & Zeki S, 1985, Segregation of pathways leading from area V2 to areas V4 and V5 of macaque monkey visual cortex. *Nature* **315**:322-325

Spitzer H, Desimone R and Moran J, 1988, Increased attention enhances both behavioural and neuronal performance. *Science* **240**: 338 - 40

Sporns O, Tononi G, Edelman GM, 1990, Dynamic interactions of neuronal groups and the problem of cortical integration, in Nonlinear Dynamics and Neural Networks, VCH: 205 - 240

Stern P, Edwards F, Sakmann B, 1992, Fast and slow components of unitary epscs on stellate cells elicited by focal stimulation in slices of rat visual cortex. *J. Physiol. London* **449**: 247-278

Sukov W & Barth DS, 1998, Three-dimensional analysis of spontaneous and thalamically evoked gamma oscillations in auditory cortex. *J. Neurophysiol.* **79(6)**: 2875 - 84

Talairach & Tournoux, 1988, coplanar stereotaxic atlas of the human brain. Thieme Medical Publishers Inc. New York

Tanaka K *et al*, 1986, Analysis of local and wide field movements in the superior temporal visual areas of the macaque monkey. *J. Neurosc.* **6**: 134 - 144

Tanaka K, 1996, Inferotemporal Cortex and Object Vision. *Annu. Rev. Neurosci.* **19**: 109 - 39

Tootell RBH, Reppas JB, Kwong KK, Malach R, Born RT, Brady TJ, Rosen BR, Belliveau JW, 1995, Functional analysis of human MT and related visual cortical areas using magnetic reonance imaging. *J. Neurosci* **15(4)**: 3215-3230

Tootell RBH, Mendola JD, Hadjikhani NK, Ledden PJ, Liu AK, Reppas JB, Sereno MI, Dale AM, 1997, Functional Analysis of V3a and Related Areas in Human Visual Cortex. *J. Neurosci* **17(18)**: 7060 - 7078

Traub RD, Wong RK, Miles R, Michelson H, 1991, A model of a CA3 hippocampal pyramidal neuron incorporating voltage-clamp data on intrinsic conductances, *J Neurophysiol.* **66**: 635:650 Eckhorn R Bauer R

Treue S & Maunsell JH, 1996, Attentional modulation of visual motion processing in cortical areas MT and MST. *Nature* **382**: 539 - 41

Ungerleider LG and Desimone R, 1986, Cortical connections of visual area MT in the macaque. **248**: 190 - 222

Vaadia E, Haalman I, Abeles M, Bergman H, Prut Y, Slovin H, Aertsen A, 1995, Dynamics of neuronal interactions in monkey cortex in relation to behavioural events. *Nature* **373**, 515-

Van Essen & Gallant JL, 1994, Neural mechanisms of form and motion processing in the preimate visual system. *Neuron* **13**: 1 -1 0

von der Malsburg C, 1981, The correlation theory of the brain. Internal report Max Planck Institute for Biophysical Chemistry Gottingen West Germany.

Wachsmuth E, Oram MW, Perret DI, 1994, Recognition of objects and their component parts: responses of single units in the temporal cortex of the macaque. *Cereb. Cortex* **5**: 509 - 522

Watson JD, Myers R, Frackowiak RS, Hajnal JV, Woods RP, Mazziotta JC, Shipp S, Zeki S, 1993, Area V5 of the human brain: evidence from a combined study using positron emission tomography and magnetic resonance imaging. *Cereb Cortex* **3(2)**: 79 - 94

Wiesenfeld K & Moss F, 1995, Stochastic resonance and the benefits of noise: from ice ages to crayfish and SQUIDs. *Nature*, **373**: 33-36

Worsley KJ & Friston KJ, 1995, Analysis of fMRI time-series revisited - again. *NeuroImage* **2**: 173-181.

Yamada WM, Koch C and Adams PR, 1989, Multiple Channels and Calcium Dynamics, in Methods in Neuronal Modeling, The MIT Press: 97-134

Zeki S, 1983, Colour coding in the cerebral cortex: The reaction of cells in monkey visual cortex to wavelengths and colours. *Neuroscience* **9**: 741 - 56

Zeki S, 1985, Colour pathways and hierarchies in the cerebral cortex. In Central and Peripheral Mechanisms of Colour Vision, edited by D. Ottoson and S. Zeki, pp. 19 - 44. Macmillan, London

Zeki S, 1990, The motion pathways of the visual cortex in "Vision: coding and efficiency" (C. Blakemore ed.), Cambridge University Press, UK p.321-345

Zeki S, Watson J, Lueck C, Friston KJ, Kennard,C Frackowiak RSJ, 1991, A direct demonstration of functional specialisation in the human visual cortex. *J. Neurosci.* **11** 641-649.

Zeki S, 1993, A Vision of the Brain, *Blackwell Science Ltd.*

Appendices

A1 PET

Radionuclides that could be used in PET are ^{15}O (which has a half life of 2 minutes and 4 seconds), ^{13}N (which has a half life of 9 minutes and 58 seconds), ^{11}C (which has a life of 20 minutes and 18 seconds) and ^{18}F (which has a life of 109 minutes and 42 seconds). ^{15}O is used as it has the shortest half life and so the body is exposed to the radioactivity for the least amount of time.

^{15}O is unstable and decays via positron emission. In this process, a proton, p becomes a neutron, n plus a positron, e^+ plus a neutrino, ν_e: $p \Rightarrow n + e^+ + \nu_e$. ^{15}O decays via the following reaction: $^{15}_{8}O \Rightarrow {}^{15}_{7}N + e^+ + \nu_e$

Such unstable proton rich ^{15}O nuclei are produced in a cyclotron. This device accelerates protons (to 10 - 18 MeV), deuterons (to 5 - 9 MeV) or other charged particles (such as alpha-particles etc.). It consists of a flat metallic can that is cut into two D-shaped pieces called dees and which are placed between the poles of a large electromagnet. A voltage generator, connected to the dees, creates an oscillating electric field in the gap between the dees. The frequency of the voltage generator is equal to the cyclotron frequency of the charged particle. *i.e.* frequency, $\nu = qB/2\pi\mu$ where q = charge of the particle, B = magnetic field strength and m = mass of the particle.

Fig. A1.1

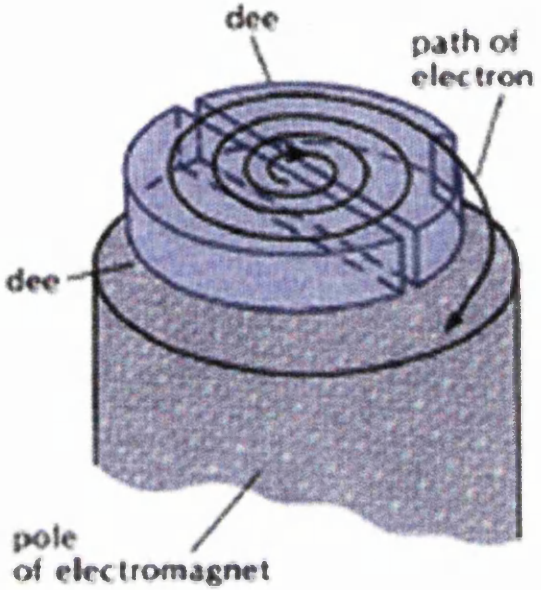

Fig. A1.1 Trajectory of a particle within the dees of the cyclotron. (Taken from Ohanion HC, Physics, p761.)

Fig. A1.2

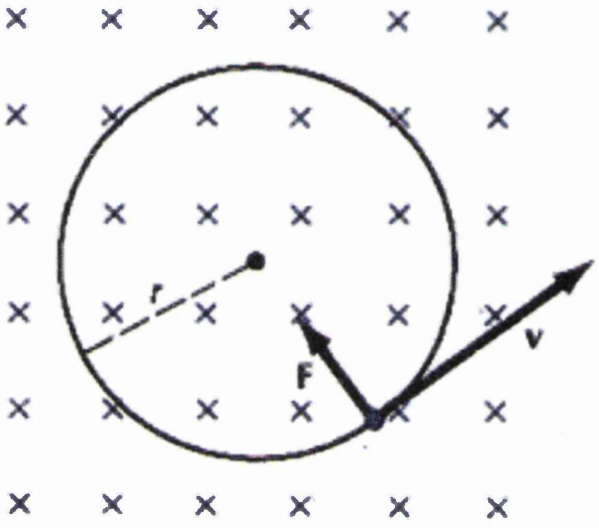

Fig. A1.2 Positively charged particle with uniform circular motion in a uniform magnetic field. The magnetic field points perpendicularly into the plane of the page. (Taken from Ohanion HC, Physics, p760.)

The force on the charged particle, $F = -q(v \times B)$
The centripetal force on the particle, $F = qvB = mv^2/r$
The radius of the circular motion of the charged particle, $r = mv/qB$
The time period of the particle's orbit, $T = 2\pi r/v = 2\pi m/qB$
The frequency of the particle's orbit, $v = 1/T = gB/2\pi m$
where v = velocity of particle.

There is an ion source at the centre of the cyclotron which releases the charged particles. The electric field in the gap between the dees accelerates the particles and the uniform magnetic field in the cyclotron makes the particles travel in a semi-circle inside the first dee. When the particles return to the gap after half a period, the high voltage generator, having reversed the electric field in the gap due to the radio frequency across the dees (which controls the polarity), pushes the particle around the second dee. This time it travels a slightly larger semi-circle as it has more energy. The increase in the energy, E of each particle per acceleration is $E = (4/1.42)qV$, where V = maximum accelerating voltage between the electrodes and the factor 4/1.42 takes account of the acceleration occurring at 45° to the dee and not 90°. The motion of the particle carries on in this way until it reaches the outer edge of the dees and leaves the cyclotron as a high energy beam. This beam is then deflected at the target material by a deflector, such as carbon foil, placed in the outer particle orbit in the cyclotron. The beam is collimated before reaching the target. The reaction occurring in ^{15}O production within the cyclotron is either:

$$^{14}_{7}N + ^{2}_{1}H \Rightarrow ^{15}_{8}O + ^{1}_{0}n + 7.82\ MeV \quad \text{or} \quad ^{15}_{7}N + ^{1}_{1}p + 3.54\ MeV \Rightarrow ^{15}_{8}O + ^{1}_{0}n$$

The next stage is for the positron emitter to be separated from the target mixture and converted into the appropriate form for administration. This is done rapidly due to the short half lives of these isotopes. The radio-nuclide is then administered to the subject. The positron emitting ^{15}O accumulates in the brain by diffusing as radiolabelled water, according to first order kinetics. The local concentration is proportional to the regional cerebral blood flow (rCBF) delivering the tracer to that part of the brain. Positrons have a short range in soft tissue. After travelling a few millimetres, as a result of losing energy in particle interactions, they slow down and either stop or annihilate with an electron to produce two 0.511 MeV gamma photons (as this is the rest mass of both the positron and the electron). These gamma photons are then detected by an array of scintillation detectors. The detectors are in a coincidence circuit so that events are only registered if the two photons are emitted at around

180° to each other, thus reflecting the nature of positron-electron annihilations. Scintillation detectors consist of materials (usually bismuth germanate (BGO) crystals) whose nuclei are excited by ionising radiation. The gamma photons excite electrons, in these nuclei, which subsequently de-excite to their original energy level and emit visible photons. Due to the scintillation materials optical transparency, these photons travel through the material to a photomultiplier tube, where they produce a detectable current pulse.

A2 MRI

A proton has spin, I = 1/2. Under normal conditions, the direction of the proton spins are isotropically directed.

Fig. A2.1

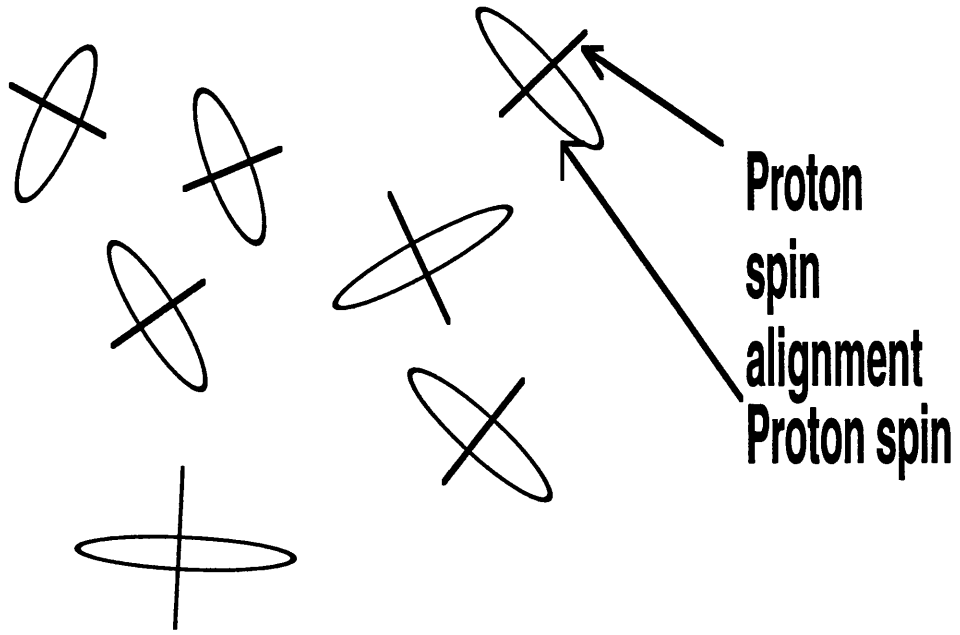

Fig. A2.1 Diagram showing isotropically oriented spins of protons under normal conditions

Under an applied magnetic field, B_0, the spinning electric charge of the proton generates a magnetic moment, $\mu = (\gamma h/2\pi)\ (I\ (\ I + 1))^{1/2}$, where γ is the gyromagnetic ratio of the particle = e/2m where e = charge of proton and m = mass of proton. This causes the protons to align in B_0.

Fig. A2.2

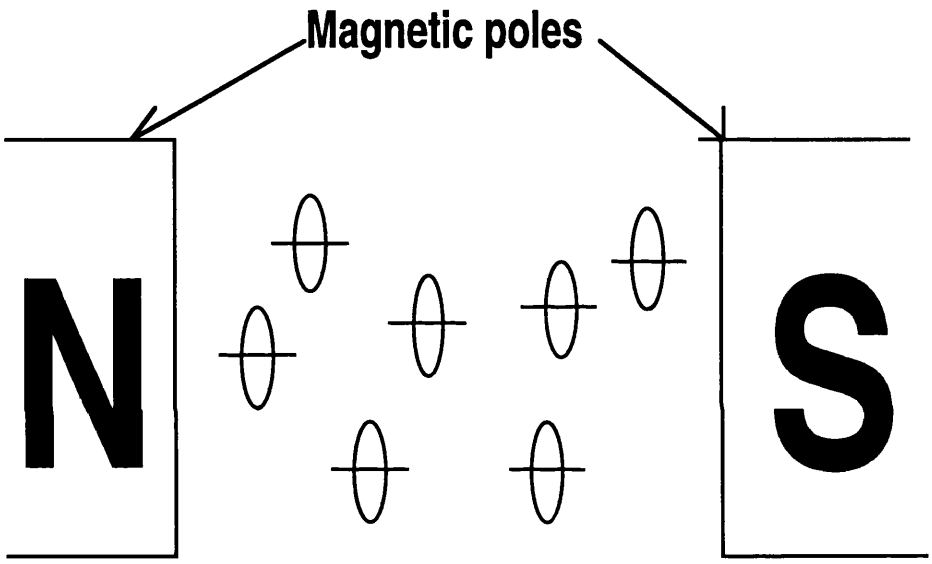

Fig. A2.2 Diagram showing proton alignments under application of a static magnetic field.

The frequency of the protons precession in the magnetic field is $\nu = \mu B_0/hI$ where h = Planck's constant. Next, a radio frequency pulse is applied perpendicularly to the protons, during the static magnetic field. This excites the protons and tips their spins.

Fig. A2.3

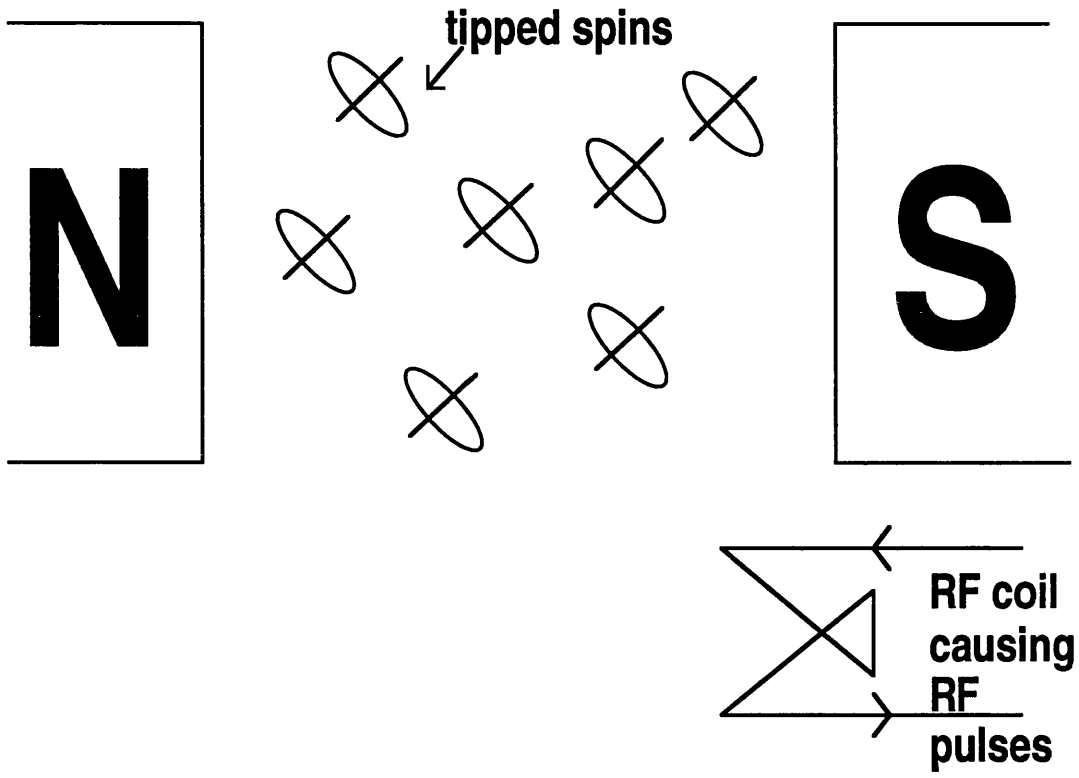

Fig. A2.3 Diagram showing proton orientation under radio pulses.

During the applied radio-pulses, a magnetic field, of flux density, B1, which is rotating at the Lamour frequency, is applied. The proton now experiences a second torque. Between the pulses, the spins relax to their original state. On de-excitation, the protons emit a radio frequency signal which is then measured. The radio frequency is equal to the energy difference between the proton spin states, $\Delta E/h_{bar}$ (where $h_{bar} = h/2\pi$), so resonant absorption occurs. As $\Delta E = \mu B_0/I$, the RF frequency, $\nu = \mu B_o/h_{bar}I$.

The rate of recovery of the protons is described by a 'longitudinal relaxation time', T1. This depends on the type of tissue containing the relevant water molecules.

In MRI, the maximum signal is obtained if the phase angle of the perturbed protons magnetization vector is constant across all protons. However, small differences in the

magnetic environment of each spin causes them to precess at slightly different frequencies, resulting in a dispersion of phase angles and, consequently, a signal which decreases with time. This signal decay is roughly exponential and is characterized by a time constant, T2 (the transverse relaxation time). As mentioned in the preface, the fMRI BOLD signal relies on the fact that deoxygenated haemoglobin is much more paramagnetic than oxygenated haemoglobin. This means that the protons of deoxygenated haemoglobin have a greater propensity to uniformly align in the presence of a magnetic field. This causes additional magnetic field variations amongst the protons and thus a further phase dispersion causing a more rapid decay of the signal. This additional relaxation is denoted by T2'. Together, the two effects result in a signal decaying with a time constant, T2*, where $1/T2^* = 1/T2 + 1/T2'$.

A3 Measuring the Effective Connectivity

Consider two cells; the first, cell i being some neuron in population one and the second, cell j, being in population two, that receives an input from cell i. The number of times cell j fires in a time window of 10ms immediately following an event in cell i is n_j. The total number of spikes from cell i is n_i. n_j/n_i is an estimate of the conditional probability that cell j fires in a time interval after cell i. To discount the effect of incidental firing in cell j, we subtracted the probability that cell j would fire spontaneously in this interval (p) when cell i had not previously fired. This was calculated as the total number of spikes from cell j divided by the total number of 10ms intervals comprising the time series (having discounted intervals following an input from cell i). The resulting estimate can be construed as an index of effective connectivity, $E = n_j/n_i - p$.

A4 Determining the Effective Membrane Time Constant

The effective membrane time constant was determined as follows: $\tau_{mem} = R_m C_m$, where R_m is the membrane resistance and:

$$C_m \, dV/dt = g_l(V - V_l) + g_{AMPA}(V - V_{AMPA}) + g_{GABA}(V - V_{GABA}) + \text{sodium and potassium currents}$$

Discounting the internal sodium and potassium channel dynamics that generate the action potentials, the last equation can be rearranged in the following way;

$$C_m dV/dt = (g_l + g_{AMPA} + g_{GABA})(V - V_0) + g_{AMPA}(V_0 - V_{AMPA}) + g_{GABA}(V_0 - V_{GABA}) + g_l(V_0 - V_l)$$

V_0 denotes the resting membrane potential. Over time, the average currents (inhibitory, excitatory and leakage) cancel each other out. Therefore, $g_{AMPA}(V_0 - V_{AMPA}) + g_{GABA}(V_0 - V_{GABA}) + g_l(V_0 - V_l)$ is negligable compared to $(g_l + g_{AMPA} + g_{GABA})(V - V_0)$ and, thus approximately, $\tau_{mem} = C_m / (g_l + g_{AMPA} + g_{GABA})$ at any given time for any particular cell. In this chapter, we take the average value of τ_{mem} over time and units.

A5 How to Read J-PSTHs

The J-PSTH is a raster plot of the two PSTHs plotted against each other and as such coincident firings are shown along the leading diagonal of the J-PSTH. Time lagged synchronised firings are shown as diagonal bands that are shifted relative to this diagonal. The displacement of the band is therefore a measure of the latency of phase-locking. The width and structure of the band depends on the details of the coherent interactions. Direct synaptic connections from population one to population two will produce a 45° band of differing density lying below the principal diagonal at a distance proportional to the latency of the interaction. Connections from population two to one will produce a similar band lying above the principal diagonal. If the interactions between the two populations are affected by the stimulus, then the diagonal band will show changes in density along it's length, evidencing dynamic correlations or coherence modulation as a function of peri-stimulus time. Correlations due purely to rate modulation evoked by the stimulus are removed by subtracting the cross product matrix of the individual PSTHs from the 'raw' J-PSTH, and then dividing the resulting difference matrix (bin by bin) by the cross product matrix of the standard deviations of the PSTHs. This is mathematically the same as computing the cross-correlation matrix between the binned activities from both populations over stimulus epochs.

A6 Explanation of Mutual Information

Our measure of mutual information is equivalent to testing the null hypothesis that all the elements of the J-PSTH are jointly zero. The mutual information can be thought of as the generalization of a correlation for multivariate data (in this case the activity over different peri-stimulus times). As such it serves as a measure of functional connectivity. The critical

idea, in this instance, is that by predicating our measure of functional connectivity on the J-PSTH we properly include dynamic correlations that would otherwise be missed if we simply looked at average correlations as implicit in the cross correlogram. The importance of using the J-PSTH in the context of this chapter is discussed fully in Aertsen *et al* (1994). A simple example makes the distinction between these two approaches clear: Imagine that a stimulus induced strong positive correlations for 100 milliseconds followed, systematically, by equally strong negative correlations for the subsequent 100 milliseconds. The average correlation over all peri-stimulus times, as measured by the cross correlogram, would be zero. However, the mutual information mediated by the dynamic correlations in the J-PSTH would be extremely significant.

The reason that the mutual information is an implicit test of the null hypothesis that the dynamic correlations are jointly zero, follows from the fact that the maximum likelihood statistic for the latter test is Wilks' Lambda. Under Gaussian assumptions, the log of this statistic is proportional to the mutual information between the stimulus induced transients that produce the dynamic correlations. In this chapter we restricted ourselves to using the mutual information and refer the interested reader to Chatfield and Collins (1982) for a discussion of Wilks' Lambda in the context of multi-variate analysis of covariance (ManCova).

A7 Mutual Information and Wilk's Lambda

The J-PSTH is given by X^TY (^{T} denotes transposition) where X is a mean corrected and normalised data matrix from unit or population one with a row for every stimulus epoch and a column for every peri-stimulus time bin. Y is the corresponding matrix from the second population. The mutual information between X and Y is given by:

$$I(X,Y) = H(X) + H(Y) - H(X \cap Y)$$

where H(X) is the entropy of X, H(Y) is the entropy of Y and $H(X \cap Y)$ is the entropy of X and Y considered jointly. Under Gaussian assumptions:

$$H(X) = \ln (2 \pi e^n |X^TX|) / 2$$

where $|X^TX|$ is the determinant of X^TX (*i.e.* the auto-covariance matrix of X) and n is the number of columns.
Let:

$$A = [X\ Y]^T [X\ Y] = \begin{bmatrix} X^TX & X^TY \\ Y^TX & Y^TY \end{bmatrix}$$

then,

$$| A | = | X^TX | \ | Y^TY - Y^TX (X^TX)^{-1} X^TY |$$

giving,

$$I(X,Y) = \ln (| Y^TY | / | Y^TY - Y^TX (X^TX)^{-1} X^TY |)$$

An alternative (statistical) perspective, that is mathematically equivalent to testing for dynamic correlations is to test the null hypothesis that $X^TY = 0$. This can be effected in the context of multivariate analysis using Wilks' maximum liklihood-ratio or Wilks' lambda, $\lambda = | R | / | R_0 |$, where R and R_0 are the residual sum of squares and products under the alternate and null hypotheses respectively. In this instance, we treat the test for statistical dependencies between X and Y as a multiple regression problem under the general linear model:

$$Y = X\beta + \varepsilon$$

where β are the regression coefficients and ε are errors with a multi-normal distribution. The parameter estimates are given by:

$$\beta = (X^TX)^{-1} X^TY$$

$Y^* = X\beta$, where Y^* is the fitted data. Under the null hypothesis, $\beta = 0$ and therefore, $R_0 = Y^TY$. Similarly, under the null hypothesis:

$$R = [Y - Y^*]^T [Y - Y^*]$$
$$= Y^TY - Y^TY^*$$

therefore:

$$\lambda = |R| / |R_0| = |Y^TY - Y^TX (X^TX)^{-1} X^TY| / |Y^TY|$$

and:

$$I(X,Y) = -\ln (\lambda)$$

i.e. The negative log of Wilks' Lambda is the mutual information.

Under the null hypothesis of no dynamic correlations, $\ln(\lambda)$ has approximately a Chi-squared distribution where $-(r - 1/2) \ln(\lambda) \sim \chi^2 (n^2)$ where r are the residual degrees of freedom (number of epochs minus time bins) (Chatfield and Collins, p145). In practice the number of time bins may exceed the number of epochs. In this instance, one generally reduces the dimensionality of the data X (and Y) using singular value decomposition.